Galyna Shul

Electrogenerated Ion Transfer
Across Liquid / Liquid Interface Supported
by Composite Ceramic Carbon Material

Advisor: prof. dr hab. Marcin Opałło,
Department of Electrode Processes

IChF

This present dissertation was prepared within

the International Ph.D. in Chemistry Studies

at Institute of Physical Chemistry of the Polish Academy of Sciences

Warsaw 2006

Contents

Introduction

The electrochemical reactions occurring at interface between two immiscible liquids are interesting from fundamental and practical point of view. Ion transfer across liquid / liquid interface is their most characteristic step. This is one of key chemical reactions in biological systems. It is also important in some areas of chemical technology like separation, extraction or organic synthesis. Obviously the prospective applications of interfacial ion transfer require new materials supporting liquid / liquid interface.

For over 30 years it is known that ion transfer between immiscible liquid phases can be driven by polarization of liquid / liquid interface. This can be done by applying potential difference to electrodes present in two immiscible electrolyte solutions. These experiments require sophisticated setup involving in most cases carefully placed four electrodes and bipotentiostat. Both phases have to be ionically conductive.

In 1997 Frank Marken introduced the three-phase electrode based approach. This technique employs oil droplet(s) deposited on the surface of electrode where three-phase junction - electrode / organic phase / aqueous phase is formed. The transfer of ion across liquid / liquid interface is driven by electrogeneration of charge in the organic phase. This can be done by electrooxidation or electroreduction of the redox probe dissolved in the organic phase. Contrary to traditional approach the experimental setup is much simpler and requires three-electrode potentiostat. Moreover, the presence of electrolyte in the organic phase is not indispensable. This makes possible to study the transfer of almost any type of ion and experiments with non-polar organic phase are possible. The three-phase electrodes have already found application in the determination of Gibbs free energies of ion transfer as proposed by Fritz Scholz. Their prospective application in electroanalysis, electrocatalysis, electroorganic synthesis, electrochemically driven extraction and separation can be also envisioned.

For the development of this methodology the novel electrode materials with appropriate design to extend the three-phase interface were recently created and applied. Among them there are electrodes based on hydrophobic porous silicate matrix and homogeneously dispersed electrode conductor (graphite particles). These so-called carbon ceramic electrodes were easily impregnated with hydrophobic organic non-polar solvent. In the experiments described in this PhD thesis non-polar solvents were

replaced with polar ones. In this case the electrogenerated insertion of ion into organic phase is possible. This thesis is oriented mainly towards this process.

Literature review

Chapter 1.   Electrochemistry at liquid / liquid interface

Electrochemistry at the interface between two immiscible electrolyte solutions (ITIES) gains more and more interest due to its relevance to biological systems and prospective wide range of applications. This relatively new topic of electrochemistry has been present at every meeting of the *International Society of Electrochemistry* for the last two decades. Recently, the *129 Faraday Discussions* meeting was focused on "The Dynamics and Structure of the Liquid / Liquid Interface" [1]. The relevance of this type of molecular interfaces expanding from fundamental charge transfer at interfaces to drug delivery in biological systems, ion-selective electrodes, sensors, artificial photosynthesis was addressed in a few review articles and books [2-5]. The present chapter encompasses the theoretical background of electrochemistry at liquid / liquid interfaces: the thermodynamics, the polarization of liquid interfaces and the various domains of charge transfer reactions in biphasic systems.

1.1   Thermodynamics of liquid / liquid interface

When two electrically conducting phases (α and β) are brought into contact, the charge carriers (i.e. ions and/or electrons) partition between the two adjacent phases because of the difference in their energy in both phases. This generates an interfacial region, where the electrical field gradient differs from zero, so that an electrical Galvani potential difference, $\Delta_{\beta}^{\alpha}\varphi$, is established [2-4, 6]:

$$\Delta_{\beta}^{\alpha}\varphi = \varphi^{\alpha} - \varphi^{\beta} \tag{1.1}$$

where φ represents the Galvani (or inner) potential of the respective phases.

At constant pressure and temperature, after the building up of the interface, the thermodynamic equilibrium is reached, when the molar Gibbs energy is equal in both phases. Consequently, the Gibbs energy difference for partitioning, ΔG, is zero and, in terms of electrochemical potential, $\tilde{\mu}_i$, it thus comes:

$$\tilde{\mu}_i^{\beta} = \tilde{\mu}_i^{\alpha} \tag{1.2}$$

The electrochemical potential represents the work required to transfer the ion i from the vacuum into a phase α and it can be divided into a chemical and an electrical part as:

3

$$\tilde{\mu}_i^{\alpha} = \mu_i^{\alpha} + z_i F \varphi^{\alpha} \tag{1.3}$$

where z_i is the charge of the ion, F is the Faraday constant, φ^{α} is the bulk electrical potential of the phase α, and μ_i^{α} is its chemical potential defined as:

$$\mu_i^{\alpha} = \mu_i^{0,\alpha} + RT \ln a_i^{\alpha} \tag{1.4}$$

with $\mu_i^{0,\alpha}$ and a_i^{α} represents the standard chemical potential the activity of ion i in the phase α, respectively.

At equilibrium, the distribution of an ion i between two phases can be directly deduced from (1.2). By substituting (1.3) and (1.4) into the equilibrium condition, the standard Gibbs energy of transfer of the ion between the bulk α and β can be derived:

$$\Delta G_{tr,i}^{0,\alpha \rightarrow \beta} = \mu_i^{0,\beta} - \mu_i^{0,\alpha} = RT \ln\left(\frac{\alpha_i^{\alpha}}{\alpha_i^{\beta}}\right) + z_i F (\varphi^{\alpha} - \varphi^{\beta}) \tag{1.5}$$

This quantity is effectively the difference between the standard Gibbs energy of solvation of the ion in the respective phases. Rewriting (1.5) in terms of the Galvani potential difference yields:

$$\Delta_{\beta}^{\alpha} \varphi = \frac{\Delta G_{tr,i}^{0,\alpha \rightarrow \beta}}{z_i F} + \frac{RT}{z_i F} \ln\left(\frac{\alpha_i^{\beta}}{\alpha_i^{\alpha}}\right) \tag{1.6}$$

Defining the standard transfer potential for i as:

$$\Delta_{\beta}^{\alpha} \varphi_i^0 = \frac{\Delta G_{tr,i}^{0,\alpha \rightarrow \beta}}{z_i F} \tag{1.7}$$

the following relationship is obtained:

$$\Delta_{\beta}^{\alpha} \varphi = \Delta_{\beta}^{\alpha} \varphi_i^0 + \frac{RT}{z_i F} \ln\left(\frac{\alpha_i^{\beta}}{\alpha_i^{\alpha}}\right) \tag{1.8}$$

It is analogous to the Nernst equation for the potential applied at a metal / electrolyte solution interface. It is often convenient for practical purpose to use this expression in terms of concentrations instead of activities. With this aim, the standard potential is replaced by the formal potential of transfer the ion i from α to β phase, $\Delta_{\beta}^{\alpha} \varphi_i^{0'}$, in which the activity coefficients of ions in both phases, γ_i^{α} and γ_i^{β}, are included:

4

$$\Delta_{\beta}^{\alpha} \varphi = \Delta_{\beta}^{\alpha} \varphi_i^{0'} + \frac{RT}{z_iF} \ln\left(\frac{c_i^{\beta}}{c_i^{\alpha}} \right) \qquad (1.9)$$

where:

$$\Delta_{\beta}^{\alpha} \varphi_i^{0'} = \Delta_{\beta}^{\alpha} \varphi_i^{0} + \frac{RT}{z_iF} \ln\left(\frac{\gamma_i^{\beta}}{\gamma_i^{\alpha}} \right) \qquad (1.10)$$

It should be noticed that the standard Gibbs energy of transfer corresponds to the transfer from pure α to pure β. Therefore it is different from the Gibbs energy of partition, which refers to the transfer between mutually saturated solvents. Nevertheless, in the case of low miscible solvents such as water / nitrobenzene, the transferred ion is practically not hydrated by water present in the organic phase, so that the ionic standard Gibbs free energy of transfer can be regarded equal to the ionic standard Gibbs free energy of partition [7].

1.2   Polarisable and non-polarisable interfaces

When a current is passed through a liquid / liquid interface or a potential difference is applied across it, two extreme behaviors may be distinguished, namely that of the ideally polarisable and non-polarisable interfaces. This classification has also been established by analogy with that used for a metal / electrolyte solution interface. For ideally polarisable ITIES, a small current forced across the interface gives rise to a large change in the potential difference across it and vice versa. On the other hand, a non-polarisable interface is characterized by the fact that a relatively high current can be passed with little change in the potential. At metal / electrolyte solution interface, the degree to which the interface is polarisable depends on the specific rate constants for the electrochemical reactions. Similarly, the polarisability of an ITIES will be determined by the ion activities and by the electrical charge in the double layer [6, 8].

When ITIES is formed in the presence of a single binary electrolyte RX, which is completely dissociated into ions R^+ and X^- in each phase, it represents the case of a non-polarisable liquid / liquid interface (Fig. 1.1).

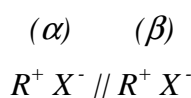$$(\alpha) \qquad (\beta)$$
$$R^+ \ X^- \ // \ R^+ \ X^-$$

Figure 1.1.   *Scheme of a non-polarisable liquid / liquid interface.*

The Nernst equation for ion transfer (1.8) derived in the previous section holds true for both ions. Considering that the concentrations of R^+ and X^- are equal in each phase, the potential difference established at equilibrium becomes:

$$\Delta_\beta^\alpha \varphi_{R^+}^0 = \frac{\Delta_\beta^\alpha \varphi_{R^+}^0 + \Delta_\beta^\alpha \varphi_{X^-}^0}{2} + \frac{RT}{F}\ln\left(\frac{\gamma_{R^+}^\beta \gamma_{X^-}^\alpha}{\gamma_{R^+}^\alpha \gamma_{X^-}^\beta}\right) \tag{1.11}$$

where $\gamma_{R^+}^\beta$, $\gamma_{R^+}^\alpha$, $\gamma_{X^-}^\beta$ and $\gamma_{X^-}^\alpha$ are the activity coefficients of ions R^+ and X^- in α and β phases, correspondingly; $\Delta_\beta^\alpha \varphi_{R^+}^0$ and $\Delta_\beta^\alpha \varphi_{X^-}^0$ are standard transfer potentials of the ions R^+ and X^- from α to β phases, correspondingly.

Hence, the Galvani potential difference between the two phases is independent of the electrolyte concentration, and is entirely controlled by the difference in solvation energy of the partitioning ions in both solvents.

Koryta *et al*. [9, 10] have shown that a system composed of two different electrolytes RX and TY dissolved in hydrophilic α and hydrophobic β phases, respectively, (Fig. 1.2) can have the properties of an ideally polarisable interface, providing that the ions R^+ and X^- are both very hydrophilic and T^+ and Y^- are both very hydrophobic.

$$(\alpha) \quad (\beta)$$
$$R^+\ X^-\ //\ T^+\ Y^-$$
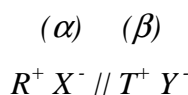
Figure 1.2.   Scheme of a polarisable liquid / liquid interface.

In terms of ion transfer potentials this system can be represented by the inequality

$$\Delta_\beta^\alpha \varphi_{R^+}^0 ,\ \Delta_\beta^\alpha \varphi_{Y^-}^0 >> \Delta_\beta^\alpha \varphi_{T^+}^0 ,\ \Delta_\beta^\alpha \varphi_{X^-}^0 \tag{1.12}$$

Under these conditions, $\Delta_\beta^\alpha \varphi$ is controlled by the electrical charge at the interfacial region, which can be supplied from an external source. The term "ideally polarisable" refers only to an electrostatic equilibrium where the constituents of each phase have infinite Gibbs energies of transfer, so that no faradaic process occurs at any potential of the polarization range. However, it is obvious that real ionic species have a limited solubility in any solvent. In practice, the interface can only be polarized within a certain potential window, which is limited by the transfer of the ions. Therefore, the potentiostatic control of polarisable liquid / liquid interfaces allows tailoring the driving

forces associated with heterogeneous charge transfer reactions by changing the Galvani potential difference between the two phases.

1.3 Charge transfer reactions at the interface between two immiscible electrolyte solutions

1.3.1 Ion transfer

From a practical point of view, the kinetics of ion transfer reactions can be regarded as very fast that it can be assumed that the surface concentrations of ions always follow the Nernst equation (1.8) [2]. In electrochemical nomenclature such reaction is called reversible. As for a reversible redox reaction on an electrode with rate limited by the mass transfer of the substrate to the electrode or by that of the products away from the electrode, the rate of an ion transfer reaction across ITIES is limited by the mass transfer of ions to or from the interface. Hence, the mass transport differential equations and the boundary conditions are similar in both cases. Thus, the whole electroanalytical studies of redox reactions at the metal / electrolyte interface can be transposed to the study of ion transfer reactions at ITIES [6]. Fig. 1.3 shows a semi-infinite linear nature of the diffusion process for the macroscopic ITIES that is considered as planar.
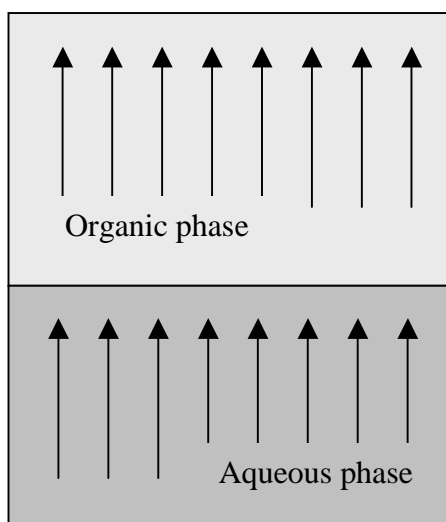
Figure 1.3.   Simplified diagram of the linear flux across a planar ITIES.

Therefore Fick's laws of diffusion describe the transport of ions at this planar interface:

$$-J_{i(x,t)} = D_i \frac{\partial c_{i(x,t)}}{\partial x} \tag{1.13}$$

7

where J represents the flux of the species i, and its concentration as a function of position and time (x, t). On the other hand, Fick's second law of diffusion describes the variation of concentration of the species, i, at a location, x, with respect to time, t, as:

$$\frac{\partial c_{i(x,t)}}{\partial t} = D_i \frac{\partial^2 c_{i(x,t)}}{\partial x^2} \tag{1.14}$$

As in classical amperometry, the response of the system stems from the solution of the diffusion equations for the same ion in the two adjacent phases, α and β:

$$\frac{\partial c_i^{\alpha}}{\partial t} = D_i^{\alpha} \frac{\partial^2 c_i^{\alpha}}{\partial x^2} \qquad \text{and} \qquad \frac{\partial c_i^{\beta}}{\partial t} = D_i^{\beta} \frac{\partial^2 c_i^{\beta}}{\partial x^2} \tag{1.15}$$

By taking the interface as the origin, the current is then simply given by the flux of ion i across the interface of area A:

$$I = z_i A F D_i^{\alpha} \left(\frac{\partial c_i^{\alpha}}{\partial x} \right)_{x=0} \tag{1.16}$$

where the boundary conditions are described by the Nernst equation (1.8) and the equality of the fluxes:

$$D_i^{\alpha} \left(\frac{\partial c_i^{\alpha}}{\partial x} \right)_{x=0} + D_i^{\beta} \left(\frac{\partial c_i^{\beta}}{\partial x} \right)_{x=0} = 0 \tag{1.17}$$

In the case of cyclic voltammetry that will be widely used throughout this work, the forward peak current for a diffusion limited ion transfer is given by the Randles-Sevcik equation [6, 11]:

$$I_p = 0.4463 \, z_i F A c_i^b \left(\frac{z_i F}{RT} \right)^{1/2} D_i^{1/2} v^{1/2} \tag{1.18}$$

where I_p corresponds to the peak current in amperes, A is the interfacial area in m^2, v is the scan rate in V s^{-1}, c_i^b is the bulk concentration of the ion i in mol m^{-3} and D_i is its diffusion coefficient in m^2 s^{-1}.

Below, the two other charge transfer processes, facilitated ion transfer and electron transfer, not connected directly to scope of this work, will be described very briefly.

8

1.3.2   Facilitated ion transfer

When metal ions form a complex with an ionophore dissolved in the organic phase, their Gibbs energies of transfer from water to an organic solvent are lower than strongly hydrated metal ions. A decrease in the Gibbs energy of transfer is equal to $RTlnK_c$, where K_c is the complexation constant in the organic phase. In this way, the transfer of many ions being too hydrophilic to be studied by voltammetry becomes amenable to electrochemical measurements. Such a transfer is named an *assisted* or a *facilitated ion transfer* [8]. Its schematic representation is shown on Fig. 1.4. The ion moves from the bulk of phase 1 towards the interface with phase 2, in which it is poorly soluble. At interface it reacts with an ionophore from phase 2, and then the complexed ion is transported towards the bulk of phase 2.
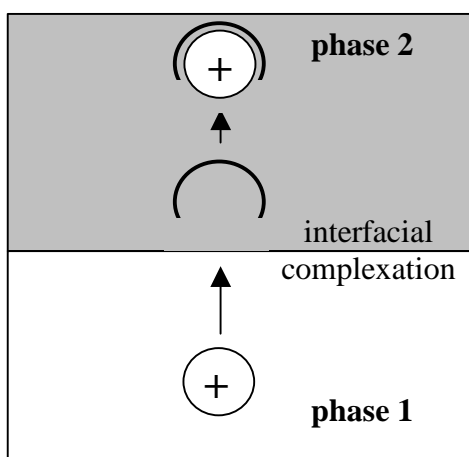
Figure 1.4.   Schematic representation of ion transfer across liquid / liquid interface assisted by interfacial complexation [8].

1.3.2   Electron transfer

Electron transfer reactions are important part of many chemical and biochemical processes. Liquid / liquid interfaces have been proposed as one of the simplest approaches to the modeling of membrane chemistry since electron transfer reactions often occur in living organisms between redox centers placed in media of different polarity [8]. The studies of electron transfer link the two areas of homogeneous and heterogeneous electron transfer, in first case redox centers exist in one phase, in second case they are present in two distinct phases (Fig. 1.5) [2].

The reduction of the species in phase α by the redox couple in phase β requires the approach of both species to the interfacial reaction planes *a* and *b*, respectively.

9
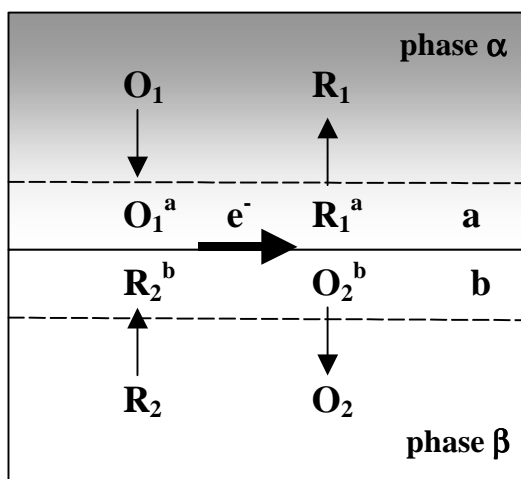
Figure 1.5.   Schematic representation of a heterogeneous electron transfer reaction at ITIES. The dashed lines represent the reaction planes located at a distance **a** *and* **b** *from the liquid / liquid junction [2].*

It should be reminded that the driving force for charge species is a potential difference applied across liquid / liquid interface.

The specific class of heterogeneous electron transfer at ITIES involves photo-excitable dye molecules adsorbed at liquid / liquid interfaces. These molecules exchange electron with redox active molecules present at the other side of the junction only via the excited state [2, 3, 8].

10

Chapter 2.   Electrochemistry at three-phase electrode

In this chapter an important type of interface, triple interface on three-phase electrode will be described. The electrochemical processes at this type of interface will be presented and compared with those occurring at two-phase interface. In the latter arrangement both phases are in contact and they form surface interface, whereas the triple interface is a line interface. It is formed by three immiscible phases that are in direct contact [12, 13]. The condition for the existence of triple interface is that each of the three interfacial tensions is smaller than the sum of the other two [14]. Fig. 2.1 shows the schematic view of three-phase electrode cell where particle or droplet is attached to the surface of the electrode.
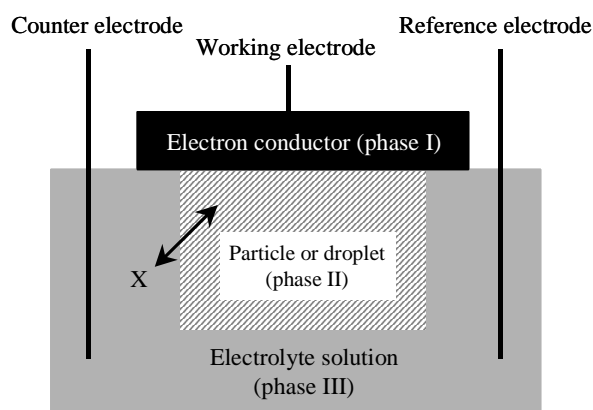
Figure 2.1.   Schematic drawing of a three-phase electrode cell with a particle or a droplet attached to the surface of the electrode immersed into electrolyte solution [13].

The phase I is a source or sink of electrons and touches phase II and phase III. The total charge of the particle or droplet is equal zero. Therefore any electron transfer between phase I and phase II enforces ion X transfer across phases II / phase III interface to maintain the electroneutrality of phase II [12, 13, 15, 16]. The both processes can take place simultaneously.

Below, the triple interface and the electrochemical processes at different type of three-phase electrodes with attached droplet(s) of redox liquid will be discussed in detail. The electrode modified with solid particles will be not discussed because they are not within the scope of this work.

11

2.1   Introduction to electrochemistry at solid electrode / redox liquid / aqueous electrolyte interface

At first the term *redox liquid* should be defined. It can be accepted that redox liquid is a pure redox probe that is liquid at room temperature. Such compounds as *n*-butylferrocene, *tert*-butylferrocene or *N,N,N',N'*-tetrahexylphenylenediamine are the examples. The solution of the redox probe in organic solvent, like solution of decamethylferrocene in nitrobenzene or solutions of *tert*-butylferrocene in *n*-alkane or room-temperature ionic liquids, RTILs, represents other examples of redox liquid. These two groups will be called pure or diluted redox liquid, respectively. Some authors call redox liquid only a pure liquid redox probe [13]. Here this term will be used also for diluted redox liquids, because this thesis is devoted to such systems.

The three-phase electrode, where redox liquid microdroplets are immobilized on the basal plane pyrolytic graphite, bppg, electrode, was pioneered by Marken and co-workers [17]. In that work the redox liquid was spread in a form of femtolitre volume droplets and multiple three-phase junctions are created at their circumference. The subsequent work on large volume drops of redox liquid on a paraffin impregnated graphite, pig, was developed by Scholz group [18]. Aoki group used glassy carbon support for the same purpose [19]. Later in order to extend three-phase junction Opallo and Saczek-Maj have modified heterogeneous electrode, namely carbon ceramic electrode, with redox liquid [20, 21]. In this system the line interface is formed by the boundary of carbon grains, silicate matrix impregnated with redox liquid and the aqueous phase. Recently, Niedziolka et. al proposed another silicate based three-phase electrode obtained with imperfect hydrophobic silicate film [22, 23]. Nakatani [24-28] used laser trapping and micromanipulating techniques to deposit a single oil microdroplet onto working ultramicroelectrode from a emulsion. Another important system consisting of the three-phase junction was recently proposed by Stojek group [29]. In their experiment a cylindrical microelectrode was immersed into the two immiscible liquid system in such a way that a part of wire was located in one liquid and the other part resided in the second liquid. Schroder et. al investigated and compared neutral and ionic redox liquids deposited on bppg in electrochemically driven process across liquid / liquid interface [30].

As it was said above the three-phase reaction system is based on the concept that the creation of charge in one phase requires counterions supply from the other phase. When electrolyte is absent in organic phase the current is expected to be proportional to

12

the length of the three-phase boundary for example the length of circumference of the droplet(s) of organic phase. According to the theoretical analysis of diffusion at a thin band electrode, the diffusion-controlled limiting current is given by [19, 31]:

$$I_p = 4\pi\theta nFc^*Dr \, / \, [ln \, (8.6RTD/nFvw^2)+3] \qquad\qquad (2.1)$$

where w < 17 μm and $2\pi r$ are width and length of a thin band electrode, correspondingly; D is diffusion coefficient of redox probe in the organic phase; c^* is its bulk concentration; θ is the contact angle between droplet and electrode surface; v is potential scan rate. For the three-phase junction w corresponds to the thickness of the reaction layer [31]. Chen group has estimated its thickness on the basis of visual observation and investigated the reasons of extending the three-phase boundary [31]. They claimed, that besides the effect of the electrode surface roughness, there is an effect of diffusion electrogenerated ion towards the bulk of the organic phase. Stojek group has shown that the value w depends on the type of anion present in the aqueous phase [29]. Earlier, the same group directly proved that the oxidation reaction at the three-phase electrode with organic phase starts at the three-phase junction [32].

To clarify all processes, which take place at the three-phase electrode, the electrode modified with single droplet of redox liquid can be examined. The triple interface (Fig. 2.2) is located at the electrode / redox liquid / electrolyte solution – three-phase junction, namely at the circumference of the droplet.

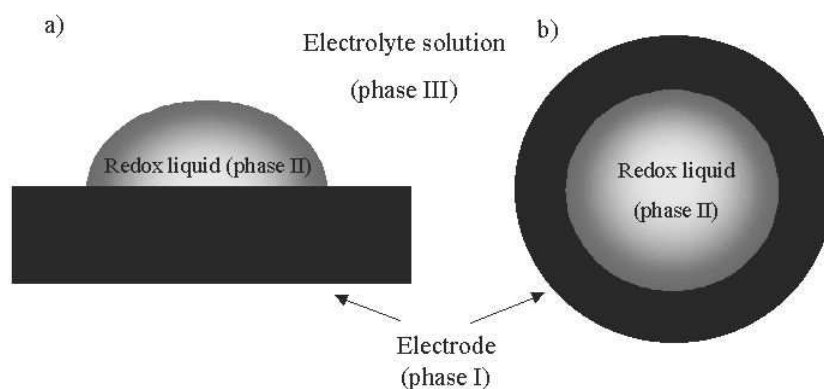*Figure 2.2.   Schematic view from the side (a) and the upper side (b) of an oil droplet forming a three-phase junction with the aqueous phase and the electrode.*

Typically, the ion transfer reactions across the liquid / liquid interface are driven by potential difference between two phases (Chapter 1). The liquid / liquid interface of the three-phase electrode is not polarized, so the ion transfer process is driven by

13

electron transfer reaction across the redox liquid / solid interface. Each electron transfer between electrode (phase I) and redox liquid (phase II) enforces the ion transfer between redox liquid (phase II) and aqueous electrolyte solution (R^+X^-) (phase III) to compensate the newly formed charge at the three-phase boundary (Fig. 2.3).
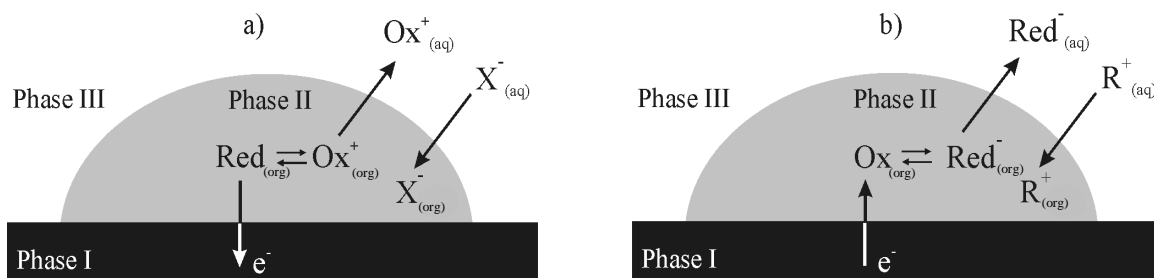
Figure 2.3. *Schematic drawing of redox liquid droplet on the electrode surface and possible processes in the presence of oxidizable compound Red (a), or reducible compound Ox (b) in phase II. Phase II is does not contain electrolyte. This drawing is not to scale; all processes start at the line interface.*

Table 2.1 summarizes some observed reaction mechanisms at the three-phase electrodes with immobilized droplet(s) [13].

Table 2.1. *Overview of already recognized reaction mechanisms at three-phase electrodes with immobilized organic droplets. Catalytic [33] or photochemical [34, 33, 35] reactions are not included.*

Phase II	Phase III	Mechanism	Ref.
Polar organic solvent Org with dissolved non-ionic oxidizable compound Red	Aqueous electrolyte R^+X^-	(1a) $Red_{org} + X^-_{aq} \leftrightarrow Ox^+_{org} + X^-_{org} + e^-$ (1b) $Red_{org} \leftrightarrow Ox^+_{aq} + e^-$	18,19 36-40
Non-polar organic solvent Org with dissolved non-ionic oxidizable compound Red	Aqueous electrolyte R^+X^-	(2) $Red_{org} \leftrightarrow Ox^+_{aq} + e^-$	18,30 41,42
Polar organic solvent Org with dissolved non-ionic reducible compound Ox	Aqueous electrolyte R^+X^-	(3a) $Ox_{org} + e^- + R^+_{aq} \leftrightarrow Red^-_{org} + R^+_{org}$ (3b) $Ox_{org} + e^- \leftrightarrow Red^-_{aq}$	40,42 -44

14

Non-polar organic solvent Org with dissolved non-ionic reducible compound Ox	Aqueous electrolyte R^+X^-	(4) $Ox_{org} + e^- \leftrightarrow Red^-_{aq}$	13
Organic oxidizable liquid Red	Aqueous electrolyte R^+X^-	(5a) $Red_{org} + X^-_{aq} \leftrightarrow Ox^+_{org} + X^-_{org} + e^-$ (Ox^+_{org} and X^-_{org} form an ionic pair) (5b) $Red_{org} \leftrightarrow Ox^+_{aq} + e^-$ (follow-up precipitation of $[Ox^+X^-]$ is possible)	17,45 -47
Organic reducible liquid Ox	Aqueous electrolyte R^+X^-	(6) $Ox_{org} + e^- + H^+_{aq} \leftrightarrow OxH_{org}$ (the organic liquid remains non-ionic)	48,49

Electrooxidation of Red to Ox^+ in a polar organic solvent droplet(s) may be accompanied by the transfer of anion X^- from the aqueous to the organic phase (1a). This happens if the free energy of that reaction is smaller than free energy for the transfer of Ox^+ to the aqueous phase (1b) [13]. For a non-polar solvent the ejection of electrogenerated cation Ox^+ to the aqueous phase is the most preferred reaction. The reduction non-ionic compound Ox to Red^- may be followed by the transfer of counter cation R^+ from the aqueous to the organic phase (3a) or the escape of Red^- to the aqueous phase (3b). The latter reaction is more preferred for non-polar organic solvent. The dominant role of one of these processes depends on the relationship between the free energies of the transfer Red^- to the aqueous phase and R^+ to the organic solvent. For pure redox liquid modified electrode the situation different. Other reactions as formation ionic pair between Ox^+_{org} and X^-_{org} in droplet (5a) or a precipitation of the salt $[Ox^+X^-]_{aq}$ (5b) are quite probable. Obviously anion insertion from the aqueous phase and cation ejection to this phase can also take place for the organic oxidizable liquid Red. In the case of the reduction of pure redox liquid the electron transfer can be also accompanied by a proton insertion to phase II (6).

2.2 Electrochemistry at three-phase electrode with pure redox liquid

Here, some important examples of immobilized pure redox liquid and their electrochemistry will be exhibited. Table 2.2 shows the list of the most often investigated redox liquids.

Table 2.2.   Liquid redox compounds studied voltammetrically as microdroplets immobilized on a bppg or other* electrodes.

Pure redox liquid	Ref.
$N,N,N^{'},N^{'}$-Tetrabutyl-1,4-phenylenediamine	33,50,51
$N,N,N^{'},N^{'}$-Tetrahexyl-1,3-phenylenediamine	46
$N,N,N^{'},N^{'}$-Tetrahexyl-1,4-phenylenediamine	17,30,33-35,45, 46,50-55
$N,N,N^{'},N^{'}$-Tetraheptyl-1,4-phenylenediamine	33,50,51
$N,N,N^{'},N^{'}$-Tetraoctyl-1,4-phenylenediamine	51,56,57
$N,N,N^{'},N^{'}$-Tetranonyl-1,4-phenylenediamine	33,50,51
$N,N,$-Dibutyl-$N^{'},N^{'}$-diethyl-1,4-phenylenediamine	33
$N,N,$-Diethyl-$N^{'},N^{'}$-dihexyl-1,4-phenylenediamine	33
$N,N,$-Diethyl-$N^{'},N^{'}$-diheptyl-1,4-phenylenediamine	33
$N,N,N^{'}$-*Trihexyl*-1,4-phenylenediamine	30
$N,N,N^{'},N^{'}$-Tetrakis(6-methoxyhexyl)-1,4-phenylenediamine	46
$N^{'}$-[4-(Dihexylamino)phenyl]-N^{1},N^{4}, N^{4}-trihexyl-1,4- phenylene-diamine	58
3-methylthiophene (as millimetric drop immobilized on pig electrode)*	59
n-Butylferrocene	47
tert-Butylferrocene (immobilized in ceramic carbon electrode or in thin film of hydrophobic silicate matrix on gold impregnated with redox liquid)*	21-23,60,61
4-Nitrophenylnonyl ether	48,62
Vitamin K_1 (2-methyl-3-phytyl-1, 4-naphthoquinone	49
Vitamin E (*dl*-α-tocopherol)	63

These compounds are almost insoluble in water. In most cases the long alkyl chains ensure their highly hydrophobic character resulting in low solubility. They also disturb regular packing of the molecules and thus prevent crystallization. As one can see from Table 2.2 family of $N,N,N^{'},N^{'}$-tetraalkyl-1,4-phenylenediamines was the most often studied. Its representative - $N,N,N^{'},N^{'}$-tetrahexyl-1,4-phenylenediamine, THPD, is shown on Fig. 2.4.
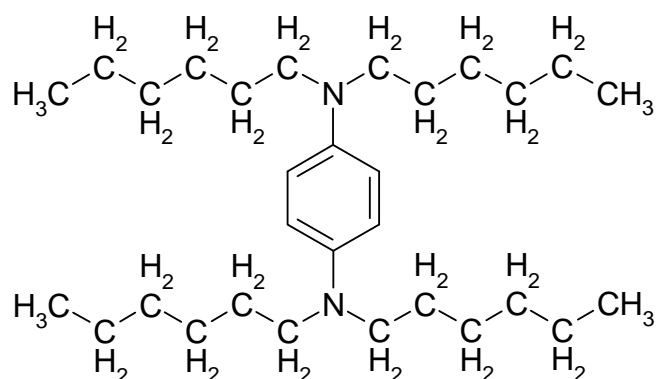
Figure 2.4.   Structure of the N,N,N$^{'}$,N$^{'}$-tetrahexyl-1,4-phenylenediamine [17].

It is required that redox process of these compounds occurs within the potential window of the electrolyte solution into which the modified electrode is placed. The electrooxidation of THPD in non-aqueous solution is characterized by two subsequent reversible one-electron processes (Fig. 2.5). However, the second oxidation process, which occurs at the more positive potentials, can be followed by irreversible chemical reaction.
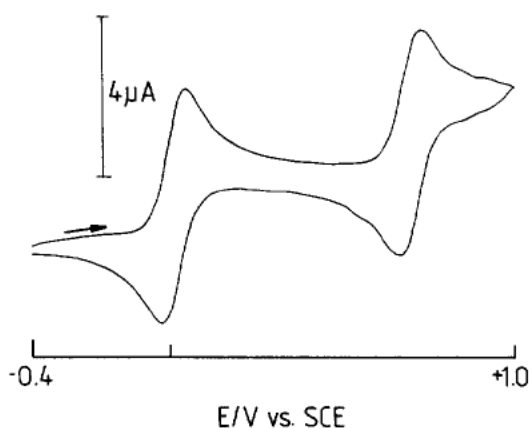
Figure 2.5.   Cyclic voltammogram for the oxidation of 0.6 mM THPD dissolved in acetonitrile (0.1 mol dm^{-3} NBu$_4$PF$_6$) at a 3-mm diameter glassy carbon disk electrode (22 °C, scan rate 10 mVs^{-1}) [17].

These processes are described by the following equation [43].

$$(2.2)$$
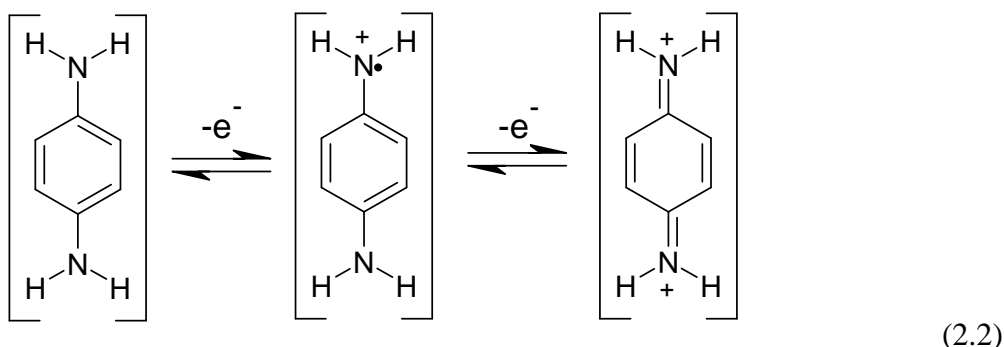
The product of first oxidation step is the blue radical cation, $THPD^{•+}$. It was detected by in-situ electrolysis of THPD in acetonitrile in cavity of an electron spin resonance spectrometer [17]. The yellow droplets of THPD deposited on ITO also turn blue during switching the potential from E = -0.1 to +0.4 V vs. saturated calomel electrode, SCE. The blue ring appears close to the three-phase boundary and slowly expands to the center of the large droplets [17].

The electrooxidation of THPD immobilized in form of microdroplets on bppg surface immersed to the aqueous solution is connected with the uptake of anions from the surrounding electrolyte solution to preserve electroneutrality of the organic phase (2.3) [17, 52]:

$$THPD_{(org)} + X^-_{(aq)} \leftrightarrow THPD^+_{(org)} + X^-_{(org)} + e^- \qquad (2.3)$$
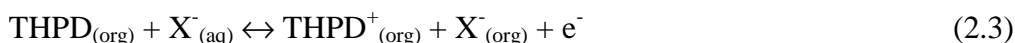
It was observed that the mid-peak potential and the shape of the voltammetric curves depend on the type of electrolyte anion, whereas the influence of cation is insignificant [17]. Fig. 2.6 shows subsequent voltammetric cycles for the oxidation THPD deposited on bppg and immersed in different aqueous electrolyte solutions.

The change of magnitude of the current in subsequent cycles depends on anions present in the aqueous phase. For such hydrophobic anions as ClO_4^- and PF_6^- the current magnitude remains almost stable. For these anions transfer of hydrophobic anions into the organic phase (2.3) is preferred. For Cl^- the current magnitude slightly decreases, whereas for the most hydrophilic anions I^- and OH^- the current magnitude gradually falls down in the subsequent cycles. This decrease is explained by a loss of electroactive compound. The reason of this effect is described below.
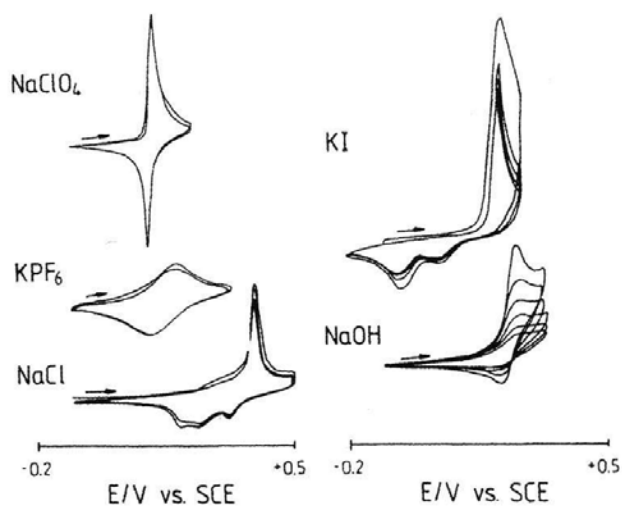
Figure 2.6.   Multicycle voltammograms for the oxidation of 1.24 μg THPD deposited on a 4.9-mm diameter bppg electrode and immersed in aqueous solutions of different electrolyte salts (electrolyte concentration 0.1 mol dm^{-3}, 6 cycles, 22 °C, scan rate 10 mV s^{-1}) [17].

It was expected that the formal potentials could be determined by specific ion-pairing interactions between the THPD cations and the transferred anions, because of the high concentration of redox centres in the organic phase and their strong intermolecular interactions [51]. Schroder and co-workers observed a strong linear relationship between the mid-peak potential and the reciprocal radii of the hydrated electrolyte anion (Fig. 2.7). For data analysis it was assumed that the formal potential, $E^{0'}$, is equal to the mid-peak potential, E_{mid}.
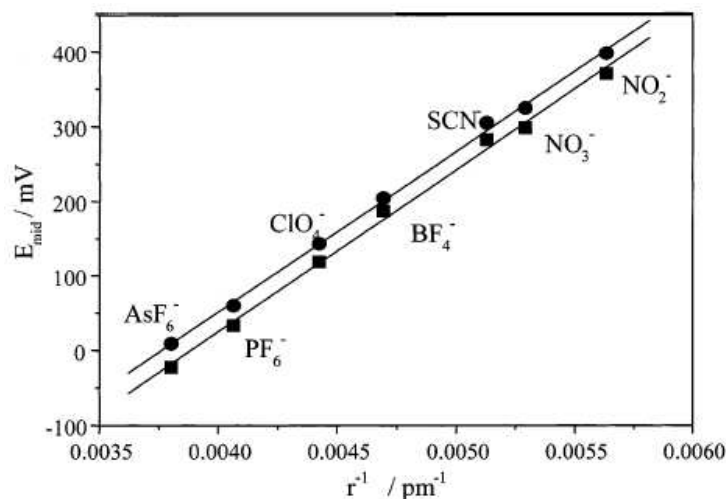
Figure 2.7.   Plot of the mid-peak potential (E_{mid}) of microdroplets of THPD (■) and N,N,N$^{'}$,N$^{'}$-tetraoctyl-1,4-phenylenediamine (●) vs. the reciprocal of the radii of the electrolyte anions (r^{-1}) measured in 0.1 mol dm^{-3} electrolyte solutions at pH 8 [51].

This relationship was considered as a proof of the anion insertion to the organic phase (2.3). According to approach based on Born theory [51, 64], the free Gibbs energy of the transfer of the anions between the aqueous and the organic phase, $\Delta G_{tr,i}^{0,org \rightarrow aq}$, depends on the hydrated anion radius, r, (2.4) and has a dominant influence on the formal potential. It can be described by following equation:

$$\Delta G_{tr,i}^{0,org \rightarrow aq} = -\frac{N_A z^2 e^2}{8\pi\varepsilon_0 r}\left(\frac{1}{\varepsilon^{org}} - \frac{1}{\varepsilon^{aq}}\right) \tag{2.4}$$

where e represents the elementary charge; N_A is the Avogadro constant; ε_0 is the permittivity of vacuum; ε^{org} and ε^{aq} are the relative permittivities of the organic and the aqueous phase, correspondingly. Because of the lack of the data for the anion transfer across water / THPD interface, the use of Gibbs free energy for anion transfer across water / organic solvent (nitrobenzene, NB) was proposed [33, 50]. Corresponding plot of the mid-peak potential as a function of the standard transfer potential, $\Delta_{aq}^{NB}\varphi_{X^-}^0$ (see 1.7) of a number of different electrolyte anions across water / NB interface is presented on Fig. 2.8.
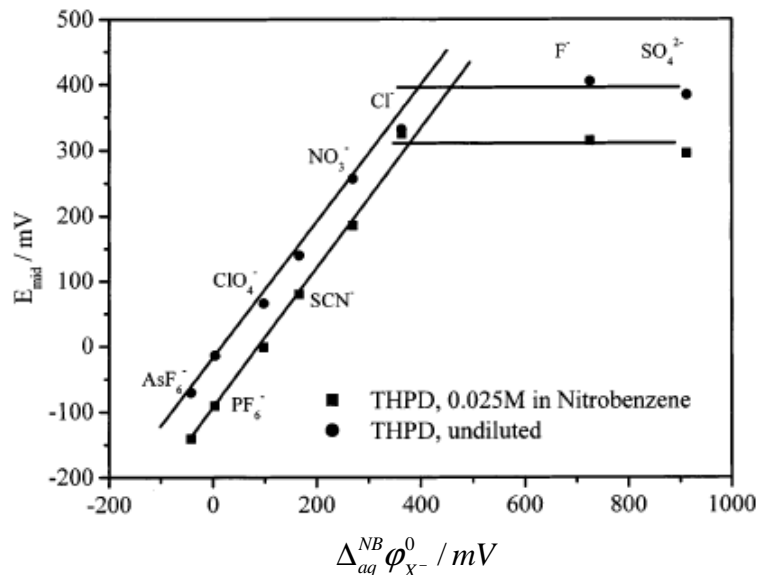
Figure 2.8. *Plot of the mid-peak potential (E_{mid}) of the first oxidation step for droplets of THPD dissolved in nitrobenzene and pure THPD measured in the presence of different electrolyte anions vs. the standard transfer potential of the electrolyte anions at the water / NB interface, $\Delta_{aq}^{NB}\varphi_{X^-}^0$, at pH 9 [51].*

The features of both plots made for the droplets of pure THPD and diluted with NB are very similar, and two different sections are visible. First one corresponds to

hydrophobic anions, such as PF_6^- or NO_3^-. In their presence the formal potential of reaction (2.3) is strongly correlated with the standard potential transfer anions across water / NB interface, $\Delta_{aq}^{NB}\varphi_{X^-}^0$. The Nernst type equation for the reaction (2.2) was formulated as follows [51]:

$$E = E^0 + \Delta_{aq}^{NB}\varphi_{X^-}^0 - \frac{RT}{F}\ln a_{X_{aq}^-} + \frac{RT}{F}\ln\frac{a_{THPD_{org}^+} a_{X_{org}^-}}{a_{THPD_{org}}} \tag{2.5}$$

where E^0 is standard potential of THPD/THPD$^+$ couple. According to the electroneutrality condition $a_{THPD_{org}^+} = a_{X_{org}^-}$ and taking into account that $a_{THPD_{org}^+} = a_{THPD_{org}}$, the equation 2.5 was rewritten to that defining formal potential, $E^{0'}$:

$$E^{0'} = E^0 + \Delta_{aq}^{NB}\varphi_{X^-}^0 - \frac{RT}{F}\ln a_{X_{aq}^-} + \frac{RT}{F}\ln\frac{a_{THPD_{0,abs}}}{2} \tag{2.6}$$

where $a_{THPD_{0,abs}}$ is the total THPD activity in NB phase. This type of reaction is characterized by a high chemical reversibility of the voltammetric oxidation and rereduction [51]. According to equation (2.6) when electron transfer is followed by anion insertion into organic phase the slope of dependence $E^{0'}$ vs. $\Delta_{aq}^{NB}\varphi_{X^-}^0$ has to be equal unity. The deviation from such behavior indicates that apart from the anion insertion the electrogenerated cation ejection takes place. The considerable contribution of the latter reaction can be judged from the second section of the plot on Fig. 2.8. It corresponds to extremely hydrophilic anions (characterized by highly positive Gibbs free energy of transfer across water / NB interface), such as F^- and SO_4^{2-}. For these anions the correlation between $E^{0'}$ and $\Delta_{aq}^{NB}\varphi_{X^-}^0$ is absent. The transfer of these ions to the organic phase is energetically unfavorable. In this case electrogenerated cation THPD$^+$ transfers to the aqueous solution follows electron transfer reaction:

$$\text{THPD}_{(org)} \leftrightarrow \text{THPD}^+_{(aq)} + e^- \tag{2.7}$$

Then, the Nernst type equation can be exhibited as follows:

$$E = E^0 - \Delta_{aq}^{NB}\varphi_{THPD^+}^0 + \frac{RT}{F}\ln\frac{a_{THPD_{aq}^+}}{a_{THPD_{org}}} \tag{2.8}$$

Under condition $a_{THPD_{aq}^+} = a_{THPD_{org}}$, the formal potential becomes:

21

$$E^{0'} = E^0 - \Delta_{aq}^{NB}\varphi_{THPD^+}^0 \qquad\qquad (2.9)$$

This type of reaction is chemically irreversible and leads to the dissolution of the redox liquid. Recently, Marken and co-workers have claimed the insertion of sulfate into droplets of *N,N,N',N'*-tetrakis(6-methoxyhexyl)-1,4-phenylenediamine [46] or insertion of phosphate and arsenate into microdroplets of TOPD [56]. This is accompanied by dimerization and oligomerization of radical cation or precipitation of redox liquid, respectively.

Due to basicity of some tetra-*N*-alkylated phenylenediamines [30, 52, 56] and 4-nitrophenyl nonyl ether [48], they can be protonated if the pH of the aqueous phase is smaller than their pK_a. In order to maintain charge neutrality within microdroplets the protonation is accompanied with anion insertion [52]:

$$THPD_{(org)} + H^+_{(aq)} + ClO_4^-{}_{(aq)} \leftrightarrow [THPDH^+ClO_4^-]_{(org)} \qquad (2.10)$$

Obviously, the protonation process has considerable effect on electrochemical process. Indeed, the proton concentration affects shape and position of voltammetric curves (Fig. 2.9).
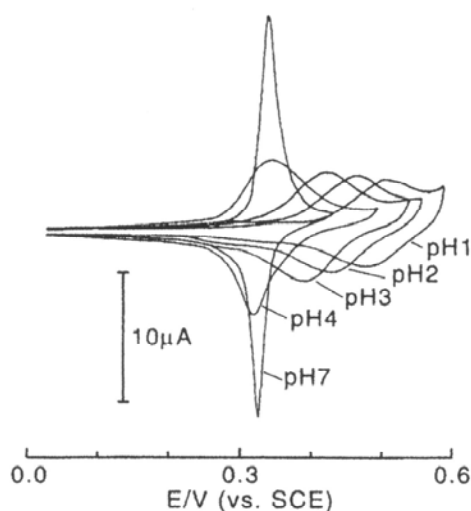
Figure 2.9.   The influence of pH on cyclic voltammograms for the oxidation and rereduction of 0.5μg THPD deposited onto a 4.9 mm diameter bppg electrode and immersed in aqueous 0.1 mol dm⁻³ KNO₃ solution. The pH of the solution was adjusted by addition of aqueous HNO₃. Scan rate 10 mV s⁻¹ [52].

The oxidation of the protonated redox liquid is associated with proton expulsion into the aqueous phase under low pH conditions:

$$[THPDH^+ClO_4^-]_{(org)} \leftrightarrow [THPD^+ClO_4^-]_{(org)} + H^+_{(aq)} + e^- \qquad (2.10)$$

22
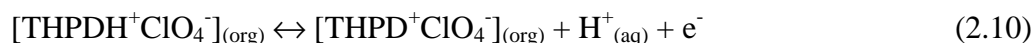
In the case of neutral and high pH electrolyte the formal potential is independent of pH (Fig. 2.10). In these conditions electrode reaction can be described by equation (2.3).
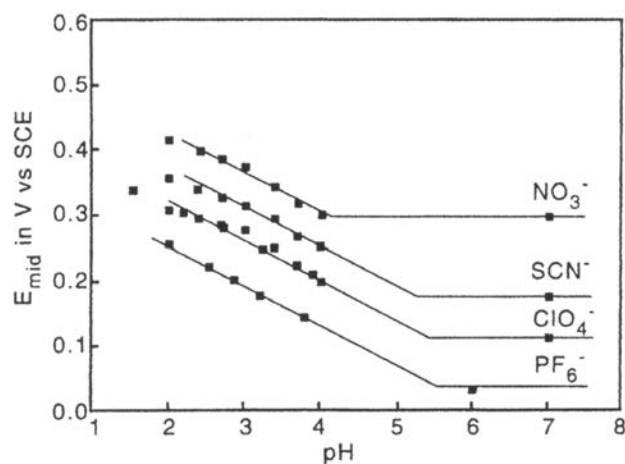
Figure 2.10.   Plot of the mid-peak potential, E_{mid}, for the oxidation and rereduction of 0.5 μg THPD deposited onto a 4.9 mm diameter bppg electrode immersed in aqueous 0.1 mol dm^{-3} KNO$_3$ (pH adjusted with HNO$_3$), 0.1 mol dm^{-3} KSCN (pH adjusted with HNO$_3$), 0.1 mol dm^{-3} NaClO$_4$ (pH adjusted with HClO$_4$), 0.1 mol dm^{-3} KPF$_6$ (pH adjusted with HNO$_3$) as a function of pH [52].

It has been also proven that in the case of the oxidation of the protonated redox liquid in the presence of an acidic aqueous solution phase the electron transfer takes place at the entire droplet / electrode interface (Fig. 2.11, b).
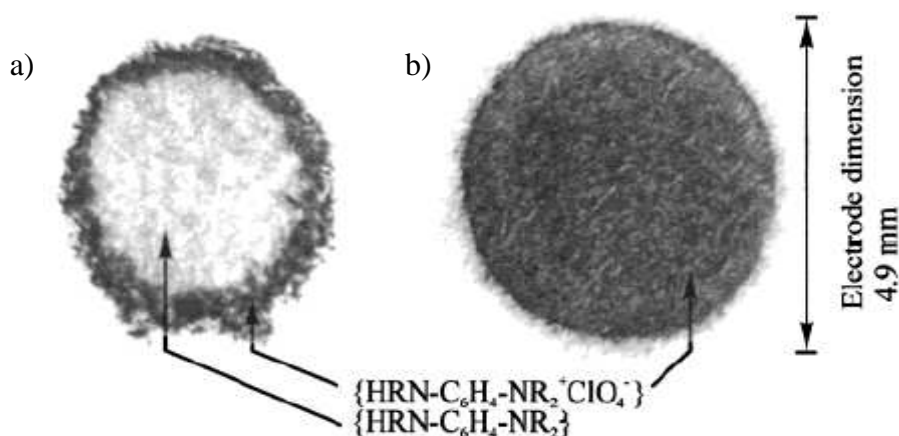
Figure 2.11.   Photographic image of a stamp imprint of the interface layer of N,N,N'-trihexyl-1,4-phenylenediamine at a graphite electrode. The electrode was modified with a closed layer of the redox liquid and electrolyzed at a potential of +0.5 V vs. SCE for 60 s in order to form the colored radical cation. The neutral redox liquid (a) and the protonated, ionic liquid (b) [30].

The arrows show light and dark areas corresponding to unreacted and reacted compound, respectively. The product of electrooxidation of protonated *N,N,N'*-trihexyl-1,4-phenylenediamine, TriHPD, is formed at the entire electrode surface, leaving a homogeneous film of the reaction product [30]. This probably results from some ionic conductivity of the redox liquid deposit. On the other hand for non-protonated TriHPD reaction occurs only at circumference of the droplet (Fig. 2.11, a).

2.3   Electrochemistry at three-phase electrode with diluted redox liquid

The previous chapter concerned the electrodes modified with pure redox liquid without organic solvents added to the organic phase. Here, the experiments with electrodes modified with redox liquid consisting of redox probe solution in organic hydrophobic solvent are reviewed. This approach allows to study the electrochemical behavior of solid redox probes as solutes in the organic media at three-phase electrodes. Tables 2.3 and 2.4 include selected redox probes and organic solvents used for modification of the three-phase electrodes, correspondingly.

Table 2.3.   Redox probes that have been dissolved in hydrophobic solvents and studied voltammetrically at the three-phase electrodes.

Electroactive probe	Ref.
Bis(cyclopentadienyl)iron (ferrocene, Fc)	18,19,32,36
tert-Butylcyclopentadienylcyclopentadienyl iron (*tert*-butylferrocene, *t*BuFc)	60
Bis(pentamethylcyclopentadienyl) iron (decamethylferrocene, DMFc)	18,20,29,32,37-41, 44,65-72
2,3,5,6-tetrachloro-1,4-benzoquinone (*p*-chloranil)	73
Iron (III) tetraphenylporphyrin chloride	66,74
Iodine	42,75
Lutetium bis(tetra-*tert*-butylphthalocyaninato)	68
Lutetium bis(phthalocyaninato)	68
Lutetium (tetra-*tert*-butylphthalocyaninato hexadecachlorphthalocyaninato)	68
Cobalt tetraphenylporphyrin	76

These solid redox probes are soluble in the organic solvents. On the other hand, their both neutral and charged forms are poorly soluble or insoluble in water. Therefore the escape of electrogenerated ion to the aqueous phase is almost avoided.

Table 2.4.   Hydrophobic solvents that have been used for the preparation of three-phase electrodes.

	Hydrophobic solvent	Ref.
Polar solvents	Nitrobenzene, NB	18,19,20,29,32,36-39,42,44,51,66-70, 72,74,75
	2-Nitrophenyloctyl ether. NPOE	69
	1-Octanol	41,69,71
	4-(3-phenylpropyl)-pyridine	76
	1,2-Dichloroethane	37,67
	D- and L-2-octanol	77
	D- and L-menthol	78
RTILs	1-decyl-3-methylimidazolium bis(trifluoromethylsulfonyl)imide	79
	1-butyl-3-methylimidazolium bis(trifluoromethylsulfonyl)imide	79
	1-butyl-3-methylimidazolium hexafluorophosphate	79
Non-polar solvents	Toluene	20
	Hexane	40
	Decane	40
	Hexadecane	17,20,40,60
	Nujol	18

The organic solvents used in the studies of electrogenerated ion transfer through the redox liquid / water interface can be divided into two groups: polar and non-polar. This list includes RTILs recently used for preparation of the three-phase electrode [79]. The solvents used for preparation of the three-phase electrode should be electrochemically inert and insoluble in water. The use of aqueous electrolyte solutions saturated with the

25

organic solvent together with organic phase saturated with water is often practiced. In this way the dissolution of organic solvents in water diminishes, and as consequence the concentration of redox probe in the organic phase remains unchanged. As it was presented in Table 2.1 the mechanism of the electrode process depends on the polarity of the organic solvent. Below, two principally different situations are described: electrodes modified with organic and salt containing organic phases.

2.3.1   Electrodes modified with organic phase

The electrochemical behavior of the redox probe dissolved in inert solvent and that of pure redox liquid is in many respects identical. Nevertheless, there are some differences. Due to the low concentration of electroactive species within the droplet, interactions between them are insignificant. Then, the insertion or expulsion of ions to/from the organic phase does not change the physicochemical properties of the organic phase during oxidation or reduction processes. However the ionic conductivity of the organic phase still can be changed.

Most reports about these systems came from Scholz group [16]. In the majority of their studies DMFc solution in NB was used as organic phase. This is because DMFc is neutral lipophilic compound, soluble in various organic solvents. Its both neutral and positively charged forms are almost insoluble in water [80]. The stable voltammogram corresponding to electrochemically reversible one electron redox reaction can be obtained with droplets DMFc solution in NB deposited on electrode immersed into aqueous solution [70] (Fig. 2.12).

The oxidation of DMFc in NB can be described as follows [18]:

$$DMFc_{(NB)} \leftrightarrow DMFc^+_{(NB)} + e^- \qquad\qquad (2.11)$$

The square-wave voltammetric technique is often applied to obtain well-defined voltammograms with the peak potential, E_p, approximately equal to $E_{Red/Ox}$ of reaction [81].

As in the case of undiluted redox liquids, $E_{Red/Ox}$ of diluted redox liquids is sensitive to the nature and concentration of anion present in the aqueous solutions (Fig. 2.13).
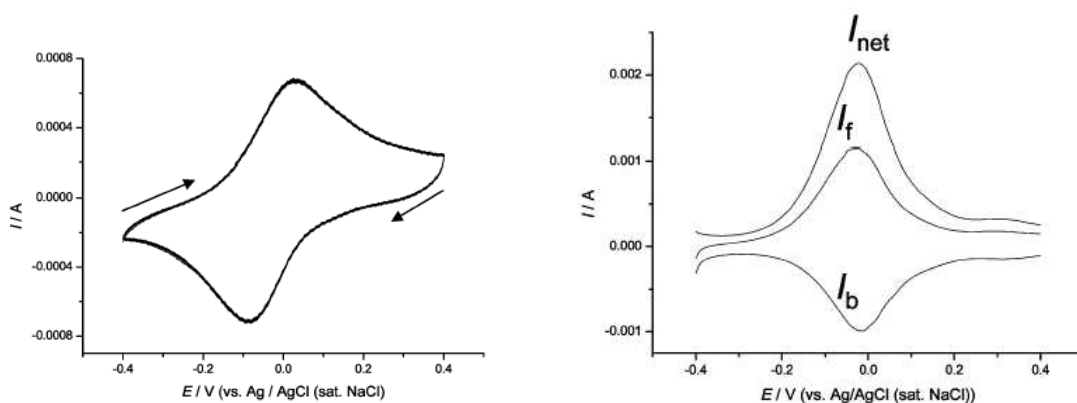
Figure 2.12. *Typical cyclic (10 scans) and square-wave voltammograms (forward (I_f), backward (I_b) and net (I_{net}) components) of a NB droplet containing 0.1 mol dm^{-3} DMFc attached to a graphite electrode and immersed in aqueous solutions containing 1 mol dm^{-3} NaClO$_4$. The other conditions were: SW frequency f = 100 Hz, SW amplitude E_{sw} = 50 mV, potential scan increment dE = 1 mV and scan rate = 100 mV s^{-1} [70].*
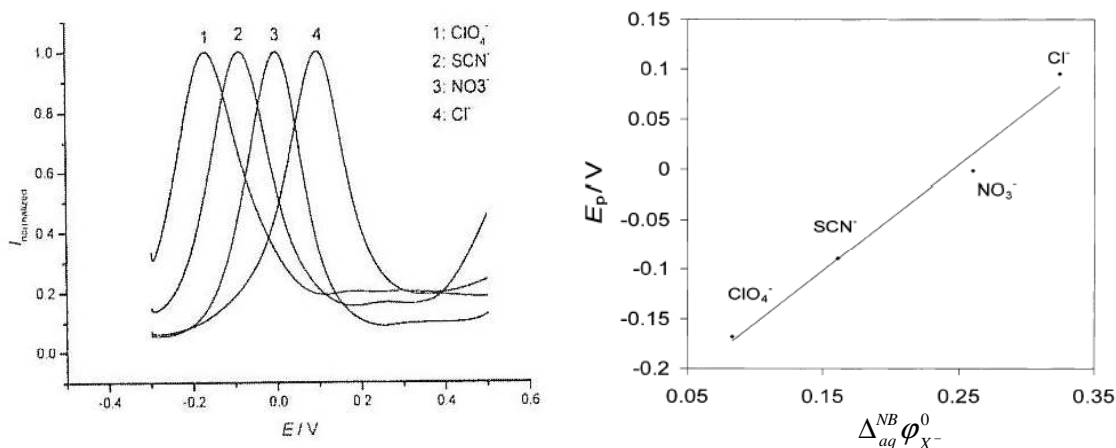
Figure 2.13. *Normalized square-wave voltammograms [13] and dependence of the peak potentials (E_p) on standard potentials of transfer of anions across the water / NB phase, ($\Delta_{aq}^{NB}\varphi_{X^-}^0$) [38] recorded at electrodes modified with droplets of a DMFc solution in NB (0.1 mol dm^{-3}) and immersed in 1 mol dm^{-3} aqueous solutions of different sodium salts. The instrumental parameters are the same as on Fig.2.12.*

Similarly to (2.3) the overall electrode process can be written as follows:

$$DMFc_{(NB)} + X^-_{(aq)} \leftrightarrow DMFc^+_{(NB)} + X^-_{(NB)} + e^- \tag{2.12}$$
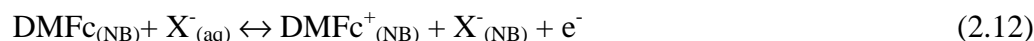
The slope of linear dependence E_p on $\Delta_{aq}^{NB}\varphi_{X^-}^0$ is close to that predicted by (2.6) [38].

Knowing the value of the standard potential of DMFc/DMFc$^+$ couple in NB, $E^0_{DMFc/DMFc^+}$, and studying the reaction (2.12) at a droplet-modified electrode immersed to aqueous solution Scholz group proposed to determine $\Delta_{aq}^{org}\varphi_{X^-}^0$ with three-phase

electrode potentiostatic measurements [18]. The use of the different redox probes and solvents allowed to study both cations and anions transfer across water / organic solvent interface. The advantages of the three-phase electrodes is that (i) no additional electrolytes are necessary in the organic and aqueous phases; (ii) only very tiny amounts of the organic solutions are necessary; (iii) the measurements can be routinely performed with any voltammetric technique and three-electrode potentiostat. These experiments are much simpler than that for four-electrode technique [4]. The values of $\Delta_{aq}^{org}\varphi_{X^-}^0$ determined by the three-phase electrode technique are in good agreement with the classical four-electrode technique data [16].

Apart from the fact that the three-phase electrodes based on drop or droplets immobilized on electrode surface have a lot of advantages, their stability is a weak point. Even in the case of the most hydrophobic redox probe it is hard to avoid the ejection of charged product to the aqueous phase, because of the large difference of volume of both phases. As a consequence, the concentration of redox probe within small volume of organic phase decreases during the electrochemical experiment. In order to avoid or diminish these effects one may use porous hydrophobic electrode material acting as reservoir of the organic phase. For this purpose the use of carbon ceramic electrode (CCE) were recently proposed [20, 21, 40, 60, 61]. The aim of these PhD theses is actually to study electrogenerated ion transfer across hydrophobic polar solvent / water interface supported by electroactive CCE.

2.3.2 Electrodes modified with salt containing organic phase

Another type of diluted redox liquid as the modifier of the electrode is presented in this chapter. This is organic phase containing added electrolyte or ionically conductive organic phase itself. Both of them are called here *salt containing organic phase*.

This type of redox liquid was studied as deposit on edge plane pyrolytic graphite (eppg) electrode modified with thin film (thickness 25-50 µm) and subsequently immersed into the aqueous solution, by Anson and co-workers [82-84]. The surface of electrode was completely covered by the liquid thin film. Therefore only when salt like tetraalkylamonium perchlorate was dissolved in organic phase the electrode process could be observed. It has been also observed that ionically conductive organic phase can be produced when pure NB layer acquires about 2 mmol dm^{-3} sodium perchlorate from

the aqueous phase [83]. In the case of salt containing organic droplet or film with electroactive compound the oxidation of redox species is controlled by their diffusion in the organic phase [83].

Scholz claimed that electrolyte dissolved in the organic phase besides increasing the conductivity, narrows the potential window, what in not desirable [37]. Moreover, the ejection of electrolyte cation may compete with counterion insertion organic phase.

Koval group using the same electrode system has examined the electron transfer reactions between aquo and amine transition metal based redox couples present in the aqueous phase and hydrophobic alkylferrocenes present in a thin organic liquid film deposited on electrode surface [85]. The electron transfer reaction occurs at liquid / liquid interface involving solvents of different polarities. They have claimed that the ability to retain the ionic forms of hydrophobic redox couples in the organic phases is affected by the structure of the redox species, the polarity of the organic solvent and the electrolytes present in both phases [85].

Aoki and Chen have studied the electrochemical coalescence of NB / water emulsions [86, 87]. The NB phase containing Fc and salt was deposited on the electrode surface in the form of emulsion. The generation of ions by electrode reaction is responsible for the coalescence. This is because it makes the organic droplets more hydrophilic and reduces the surface tension. On the other hand the increase of the salt concentration in oil droplet deposited on the electrode surface leads to a decrease of the contact angle. The salt containing organic phase is more hydrophilic than pure organic one and thus has a larger interfacial energy between the organic and aqueous phase [36].

Recently, the electrochemical studies of analogue electrodes modified with the room-temperature ionic liquids (RTILs) were also reported [79, 88]. RTILs, as alternative green solvents, are recently very often used in electrochemistry [88]. They are room-temperature molten salts, with unique chemical and physical properties, such as high thermal stability, negligible vapor pressure, low toxicity, low melting temperature, and good electrochemical stability [88, 89]. A typical RTIL is based on the combination of bulky substituted *N*-alkylpyridinium or *N,N'*-dialkylimidazolium cations with a variety of inorganic anions. The electrochemical studies of the three-phase electrode, composed of RTIL film deposited on the electrode surface and exhibiting extraction of ionic redox probe from the aqueous solution, were reported by Dupont and co-workers [90]. Recently Niedziolka et al. have studied the ion transfer across the boundary formed at an ionic liquid drop deposited on the electrode immersed in the

29

aqueous solution, generated by electrooxidation redox probe dissolved in RTIL [79]. For most hydrophobic RTIL the ability of anions to be transferred into a RTILs phase was claimed. Due to the enhanced conductivity of droplets of ionic liquid within redox probe in comparison to the neutral redox liquid it can be expected that the electrode process not necessary starts at the three-phase junction. The voltammetry of such systems is quite similar to the voltammetry of protonated redox liquid [30] or salt containing diluted redox liquid [36] deposited on the electrode surface.

2.4   Other important results

It has to be mentioned that a several papers were dedicated to theoretical models for the voltammetry of immobilized droplets. Myland and Oldham were the first who tried to simulate the voltammetry of redox probe at droplet-modified electrode [91]. However their model was not able to predict the shape of experimental voltammogram. Later it was improved by Scholz and Lovric [67, 92]. They included the effect of electrolyte partitioning into NB drop. Later, Komorsky-Lovric and Compton successfully simulated model of electrodes covered with random arrays of microdroplets [93-95]. It has to be emphasized that the modeling of the processes occurring at the droplet-modified electrodes is not a simple task. This is because of the complicated mechanism of mass transfer sometimes involving diffusion, migration and convection at the same time. The changes in the concentration ionic species during the experiments are also affected by Ohmic drop.

Some applications of redox liquid droplet-modified electrodes were reported. As it was previously said (Chapter 2.3.1) the electrochemistry of electroactive compounds dissolved in water immiscible solvents and attached to the surface of solid electrodes in the form of droplets offers a unique access to the standard Gibbs energy of ion transfer across a liquid / liquid interface. This approach was successfully used for determination standard Gibbs energies of transfer for number anions [38, 41, 44, 66, 69-71], cations [42, 44, 66, 74] and monoanionic forms of amino acids and peptides [33]. Moreover, the ability of the three-phase electrodes modified with chiral organic solvent to discriminate between enantiometric ionic species was shown [77, 78]. The electrocatalytic reactions at microdroplet-modified electrodes were examined by Wadhawan and co-workers [33-35, 49]. The three-phase electrodes have been used as an artificial means to study complex biochemical electron transfer process, such as photosynthesis and of new

30

concept solar cells [34]. The electropolymerization at the three-phase electrodes was reported by Marken [46] and Inzelt [59].

In future work one can expect that the three-phase approach may be used in biomimetic studies simulating ion recognition process at membranes, catalytic systems at membranes and redox-driven ion pumping at membranes. Such electrodes may find application in the study of the electrochemical reactions in complex arrangements [16].

Chapter 3.   Sol-gel materials

Sol-gel materials have been known for about 150 years. M. Ebelmen at the "Manufacture de Ceramiques de Sevres" in France created the first silica gels [96]. Since that time, especially during the three last decades, the sol-gel processing has been developed intensively and wide range of new materials were created. So, how have sol-gel materials been made?
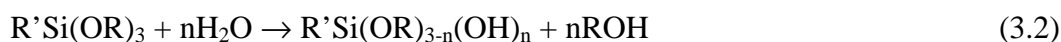
3.1   Sol-gel process

Sol-gel materials involve a wide range of inorganic and organic-inorganic composite materials. Their name results from the common strategy of preparation – sol-gel processing. Among its definitions, the general one is: "a sol-gel process is colloidal route used to synthesize ceramics with an intermediate stage including a sol and/or a gel state" [96]. From the same source, a sol is defined as **"**a stable suspension of colloidal solid particles within a liquid" [96, 97]. The solid particles of sol have to be small enough (a size between 2 nm and 2 μm) to compensate the gravity forces by the dispersion ones. The solvents used to disperse the colloidal particles of a sol are often water, alcohol or their mixtures. After some time a sol is transformed into gel namely sol-gel transition occurs. A gel is defined as "a porous 3-dimensionally interconnected solid network that expands in stable fashion throughout a liquid medium and is only limited by the size of container" [96, 97]. It should be mentioned, that the gel is not the same as polymer. This is because, gel cannot be defined as a group of molecules whose structure can be generated trough "repetition of one or few elementary units" [96, 98]. Silicon alkoxides and metal (e.g. Al, Ti, V, Zr) alkoxides are the most popular precursors of sol-gel process [99]. The use of the former compounds results in creation of silicates used as principal component of the electrodes used in research presented in this thesis. Therefore this chapter will be focused on formation of silica sol-gel materials and their applications.

There are common six steps of sol-gel process: hydrolysis (acid or base catalyzed), condensation (acid or base catalyzed), gelation, ageing, drying and densification [97].
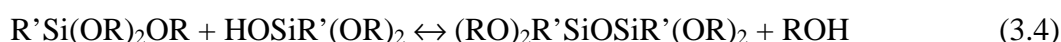
1) <u>Hydrolysis</u> (in the presence of H^+ or OH^- catalyst) can be described by following equations:

$$Si(OR)_4 + nH_2O \rightarrow Si(OR)_{4-n}(OH)_n + nROH \qquad (3.1)$$

$$R'Si(OR)_3 + nH_2O \rightarrow R'Si(OR)_{3-n}(OH)_n + nROH \tag{3.2}$$

where R and R'- are alkyl group such as $-CH_3$, $-C_2H_5$, C_6H_5 and RO– is alkoxy group. Unmodified and organically modified silicon alkoxide precursors participate in reaction (3.1) and (3.2), respectively. The Si-C bond is very stable and it does not hydrolyze during sol-gel processing. Therefore silicate materials with desired non-hydrolyzed functional groups can be obtained.

2) <u>Condensation</u> (in the presence of H^+ or OH^- catalyst) can be described by following equations:

$$Si(OR)_3OR + HOSi(OR)_3 \leftrightarrow (RO)_3SiOSi(OR)_3 + ROH \tag{3.3}$$

$$R'Si(OR)_2OR + HOSiR'(OR)_2 \leftrightarrow (RO)_2R'SiOSiR'(OR)_2 + ROH \tag{3.4}$$

Hydrolysis and condensation occur simultaneously.

3)   <u>Gelation</u>. During this step links between the sol particles producing 3-dimensional solid network that entraps the remaining solution are established (Fig. 3.1).
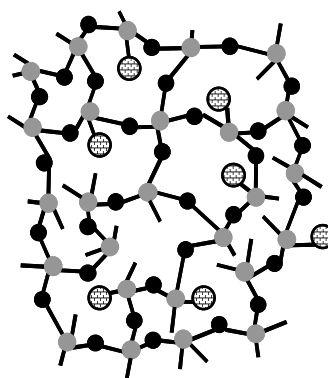
Figure 3.1.   Scheme of 3-dimensional silicate gel structure. Where • is Si atom, • - O atom, ⊖ - functional group.

In this structure Si atom is joined to neighboring Si atoms by oxygen bridges. To some silicon atoms hydroxide or functional group is attached.

The choice of acid or base catalyst substantially influences on the rate of hydrolysis and condensation reactions. Thus the newly formed gel structure depends on the selected catalyst. For acid catalyzed reactions after the first hydrolysis step the intermediate can undergo the condensation reaction. Initially an open network structure is formed, followed by further hydrolysis and cross-condensation reactions. On the other hand, for base catalyzed reactions only the fully hydrolyzed species undergoes the

33

condensation reaction. Hence highly cross-linked large sol particles are initially formed, which later link to gel with large pores between interconnected particles (Fig. 3.2).
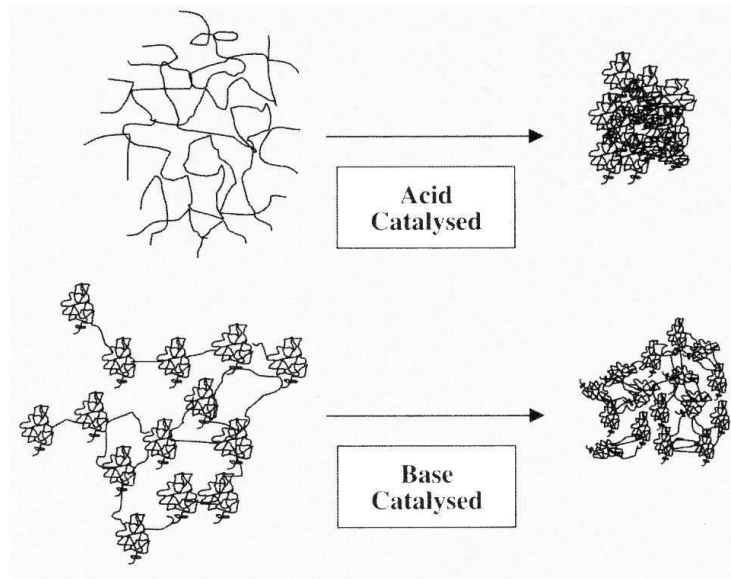

Figure 3.2.   Scheme of gel structure for acid and base catalyzed reactions [97].

4) <u>Ageing</u>. It involves further condensation, dissolution and repricipitation of precursor molecules within the solid or liquid phases. It results in changing structure and properties of gel after sol-gel transition. In this step the pore size, which is under the stress, is changed.

5) <u>Drying</u>. At first the evaporation of water, alcohol and other volatile components, as consequence the shrinkage of gels occurs. It is followed by evaporation of liquid from within the pore structure with associated development of capillary stress. The latter effect frequently leads to cracking.

6) <u>Densification</u>. Thermal treatment at above 500° C, which lead to collapse of the open structure and formation of dense ceramics.

The preparation method has tremendous influence on the properties of sol-gel materials. It means that transparency, porosity, pore size distribution, surface functionality, strongly depend on the choice of precursors, solvents and catalysts; the conditions of hydrolysis, condensation, ageing and drying. It is the most important advantage of sol-gel process that the desired characteristics of the resulting materials can be obtained by the change of the preparation procedure. Moreover, non-reactive particles can be inserted in gel by sol doping. The other advantage of sol-gel materials is its relatively simple preparation. Typically, the synthesis takes place at room

temperature (except densification stage) and under mild chemical conditions (extreme pH conditions can be avoided). The precursors are easily purified to very high levels and many of them mix easily, therefore the resulting material may contain both inorganic and organic networks. Various forms of sol-gel materials like powders, thin films, fibers or monoliths can be produced without the need for machining or melting. As it was said above the pore size and shape can be controlled. However, there are some disadvantages of sol-gel process. These are sensitivity of precursors to moisture, time-consuming processing, dimensional change on densification, shrinkage, and stress cracking on drying [96, 97, 100].

3.2   Applications of silicate sol-gel materials

Sol-gel processes are interesting from a scientific point of view as well as for new or potential industrial applications [96, 97, 100]. A sol-gel fabrication process makes the convenient way to produce coating, films, fibers, monoliths, hybrid organic-inorganic materials and high specific surface area products such as membranes and catalyst. Applying the sol-gel process enables one to make ceramic materials in different forms (Fig. 3.3).
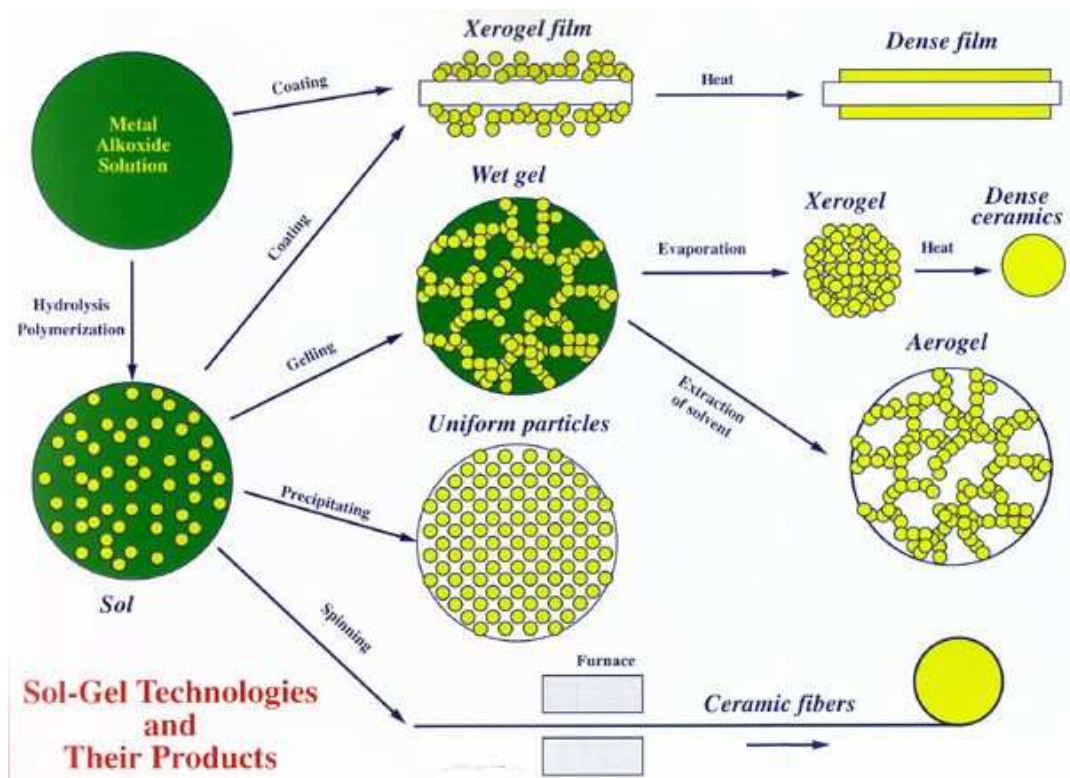

Figure 3.3.   Scheme of sol-gel fabrication [101].

35

Thin films can be produced on a substrate by sol drop deposition, spin-coating or dip-coating. After further drying and heat-treatment the "wet" gel, which still consist solvent, is converted into dense ceramics or glass materials. If the "wet" gel is dried under a supercritical conditions, the highly porous and extremely low density materials (aerogels) are obtained. The uniform ceramic powders are created directly from the sol by precipitation. Continuous fibers may be drawn from sol and converted to glass fibers by heating.

Applications of sol-gel materials derive from the various special shapes obtained directly from sol-gel processing [100]. The Table 3.1 presents the different shapes of sol-gel materials and forms in which they are used in technology.

Table 3.1.   *The applications of sol-gel materials of different shape and composites.*

Shape of sol-gel materials	Are applied …	Ref.
Thin films and coatings	…as optical, electronic, protective and porous thin films or coating.	99,102 -104
Monoliths (cast bulk shapes)	…as optical components, lenses, transparent superinsulation and ultralow-expansion glasses.	105, 106
Powders, grains and spheres	…as catalysts, pigments, fillers and abrasive grains. …as porous beads in chromatography, hollow ceramic spheres as targets in inertial confinement fusion. … in nuclear fuels.	107, 108
Fibers	…for reinforcement or fabrication of refractory textiles.	109
Porous gel and membranes	…for filtration, separations, catalysis and chromatography. …as thin free-standing membranes. …as bulk xerogels or aerogels.	107, 110, 111
Composites	…for gels as matrices for fiber-, whisker- or particle-reinforced composites. …as host for organic, ceramic or metallic phases.	110, 112

The sol-gel materials, as well as sol-gel technology are used in variety of fields of chemistry, physics, medicine and others. In order to be within scope of this study, the selected applications of sol-gel materials in electrochemistry are presented below [113].

36

1) <u>Modified electrodes and electrochemical sensors.</u> The production of sol-gel modified electrodes includes the ways to obtain novel surface and bulk modified electrodes, containing different functional group as for example redox active groups. Their possible use in electrochemical sensing was often proposed [101, 102, 113-117]. Among them are working and reference electrodes, amperometric and potentiometric sensors, biosensors. The Chapter 3.3 will focus on ceramic carbon electrodes (CCE) belonging to this group.

2) <u>Electrochemical biosensors.</u> In these devices the ability of sol-gel matrixes or silica-carbon matrixes to encapsulate enzymes, antibodies, whole cells, whole cell extracts and other active biological materials is utilized [118].

3) <u>Gas electrodes.</u> Due to porous gas permeable structure the gas feed can easily penetrate through a body of the electrode based on silicate composite and react at the solid / liquid interface [119] (see Fig. 3.10). Therefore, these electrodes can be potentially applied in fuel cells, batteries and gas sensors [120-122].

4) <u>Solid electrolytes.</u> Solid electrolytes prepared by sol-gel process are ionically conducting glasses, which are characterized by wide composition flexibility, ease fabrication, absence of grain boundaries, isotropic conduction and high ionic conductivity coupled with low electronic conductivity [123-125].

5) <u>Electrochromic devices.</u> Efficient electrochromic devices capable to change color upon electrochemical reaction, based on inorganic metal salts are constructed using sol-gel technology [126, 127].

6) <u>Supercapacitors.</u> Supercapacitors are energy-storage cells containing electrodes with very large capacitance. Twice larger capacitance of hydrous ruthenium dioxide gels ($RuO_2 \cdot xH_2O$), prepared by sol-gel technique, in comparison to that prepared by other methods because of increased specific area (porosity) of gel was reported [128].

7) <u>Sol-gel coating for corrosion protection.</u> The application of sol-gel-derived stable oxide films on metal surface protects it against corrosion. The sol-gel process is also used to manipulate both chemical and mechanical properties of metal surface. The inorganic and organically-modified silicates are used for this purpose [128].

3.3   Carbon ceramic electrode

In this chapter the physicochemical properties, voltammetric characteristic and applications of CCEs are described and compared with other classes of carbon based electrodes. These electrodes comprise of carbon powder homogeneously dispersed in

non-modified or organically modified silica matrix. For the first time they were introduced by Lev and co-workers in 1994 [114].

What are CCEs like? They are prepared by mixing carbon black or graphite powder with the sol-gel precursor and solvent. After gelation and drying the porous composite material with electron percolation pathways is formed. The choice of carbon particles and its fraction affect significantly the electrical properties of the CCE [114]. The dependence of its conductivity on type and fraction of loaded carbon is presented on Fig. 3.4.
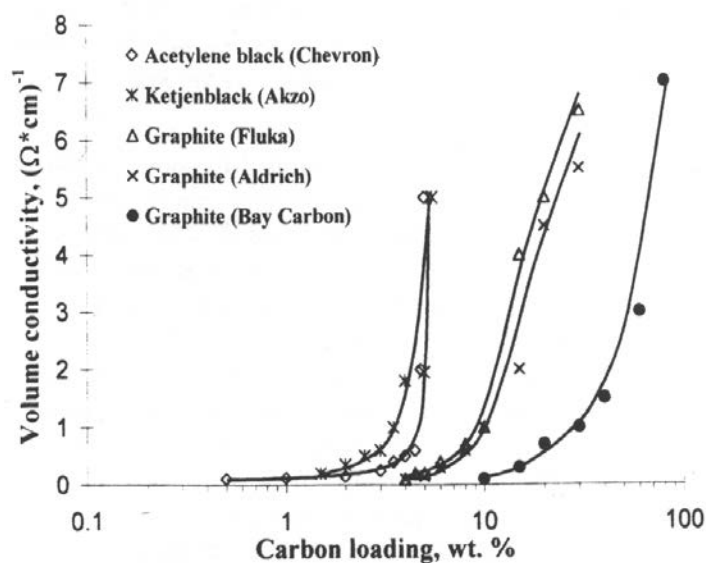

Fig. 3.4.   Dependence of the conductivity on carbon loading for different methyl-silicate CCEs [119]. The list inside presents the name of carbon powders and their producer.

Carbon particles used in experimental present on Fig. 3.4 differ in size. It increases from Acetylene black, Chevron and Ketjenblack, Akzo (30 nm) through graphite, Aldrich and Fluka (<20 µm) and Bay Carbon (40 µm). It is clearly seen, that this parameter affects both conductivity and the maximum accessible carbon loading, from 15% for carbon black (Chevron) to 90% for large size graphite powders (Bay Carbon). If CCE consists more than this limit, the rigid material cannot be formed. All types of CCE have high electrical conductivity (> 1 Ω cm^{-1}) [114]. For some carbon loading a little increase of the amount of carbon powder the conductivity of composite electrode grows up sharply. It is probably the region of percolation threshold.

The choice of sol-gel precursor also affects the physicochemical properties of CCE. So the wettability of CCEs by aqueous phase depends substantially on the

structure of selected precursors. Their appropriate choice is the simplest way to control the wettability characteristics of final material. The Table 3.2 presents the water-wetting angle of CCEs prepared with different organofunctional precursors.

Table 3.2.   The water-wetting angle of CCEs made from different precursors. A constant molar ratio C : Si = 14.7 was used for all electrodes. Bay Carbon graphite (40 μm) was used for electrode preparation [119].

Silicate precursor	Chemical formula	Molecular weight	Wetting angle,°
Methyltrimethoxysilane	$[CH_3]Si(OCH_3)_3$	136	78
Ethyltrimethoxysilane	$[CH_3CH_2]Si(OCH_3)_3$	150	72
Phenyltrimethoxysilane	$[C_6H_5]Si(OCH_3)_3$	198	76
(3-Glycidoxypropyl)trimethoxysilane	$[CH_2(O)CHCH_2O(CH_2)_3]Si(OCH_3)_3$	235	21
(3-Glycidoxypropyl)trimethoxysilane /	$[CH_2(O)CHCH_2O(CH_2)_3]Si(OCH_3)_3$	235	
methyltrimethoxysilane 1 : 1 (molar ratio)	$[CH_3]Si(OCH_3)_3$	136	45
n-Octyltrimethoxysilane	$[CH_3(CH_2)_7]Si(OCH_3)_3$	234	72
3-Methacryloxypropyl-trimethoxysilane	$[CH_2=C(CH_3)C(O)O(CH_2)_3]Si(OCH_3)_3$	248	63
Tetramethoxysilane	$Si(OCH_3)_4$	152	Totally wetted
3-Cyanopropyltriethoxysilane	$[CN(CH_2)_3]Si(OC_2H_5)_3$	231	Totally wetted

For the extremely non-wettable CCEs that are prepared with hydrophobic precursor such as methyltrimethoxysilane the water is repelled from electrode. Only segregated islands of carbon at their outer surface are in contact with the electrolyte. On the opposite side for extremely wettable CCEs prepared from tetramethoxysilane precursor the electrolyte easily penetrates inside electrode. In this case the large part of internal surface is completely wetted. These electrodes are useful, for example as a reference electrodes and for electrocatalysis [119].

There are also other ways to control the wetted section of CCEs [119]. They include incorporation hydrophilic additives, e.g. hydrophilic dopants or catalysts, into the hydrophobic precursors [121, 129]; the use of the mixture of hydrophilic and hydrophobic organofunctional precursors in appropriate ratio; and the use of the hydrophobic or hydrophilic carbon powder or modified graphite grains [130, 131].

In comparison to other carbon-based electrodes CCE exhibits good rigidity, porosity and stability. They are easily chemically modified and have a renewable external surface [114]. The wetted section of CCE is very stable and remains constant even after several months of immersion in the aqueous electrolyte [121, 129]. More differences between CCEs and other classes of graphite electrodes can be also found.

The high conductivity, relative inertness and wide potential window of graphite in an aqueous phase represent typical advantages of carbon-based electrodes. Such monolithic carbon electrodes as glassy carbon, graphite rods, carbon paste and solid

composite electrodes, where graphite powder is dispersed in organic polymers, are commonly used in electrochemistry [132-135]. Apart of advantages mentioned above these electrodes have a lot of limitations, for example the use of carbon paste electrodes is confined to aqueous solutions. Moreover, carbon paste electrodes have low operational stability and reproducibility. The voltammetric characteristics of carbon-based electrodes are also different. Fig. 3.5 presents the comparison of potential window in the aqueous solution for different classes of carbon electrodes including CCE.
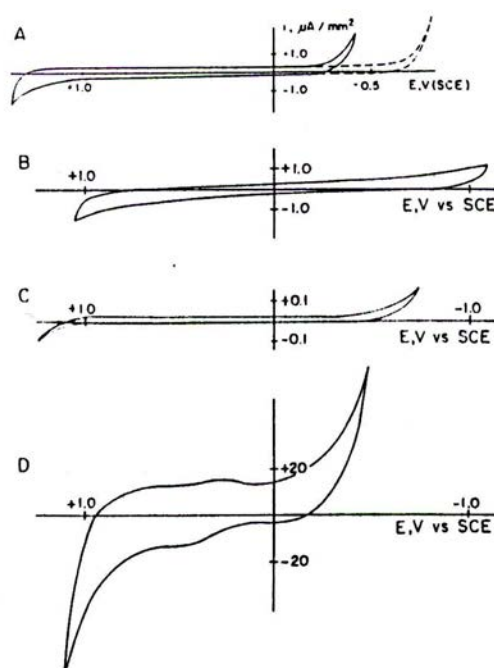

Figure 3.5.   Voltammograms of carbon electrodes in deoxygenated 1 mol dm^{-3} HCl. CCE (A, dotted line represents deoxygenated electrode body), glassy carbon (B), carbon paste (C), graphite rod (D) electrodes, scan rate 100 mV/s [136].

There are some obvious advantages of CCE. The oxygen evolution on CCE takes place at the more negative potential than on other electrodes. The cathodic overpotential of the CCE is smaller than for glassy carbon, significantly larger than for graphite rod and similar to the carbon paste electrode, CPE [136].

The magnitude of background current of carbon-based electrodes is connected with double layer charging and faradaic reactions involving surface oxide groups [137]. Despite rough surface of CCEs, the estimated capacity of these electrodes is comparable to that of the glassy carbon electrode and intermediate to that of CPE and graphite rod electrode. The edge planes of the graphite structure involve surface functional groups,

such as ketones, enols, carboxylic groups and quinones (Fig. 3.6). Especially quinone groups make substantial faradaic contribution to the background current.
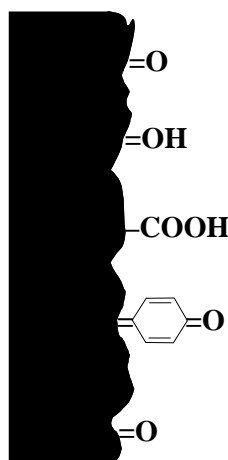

Figure 3.6.   Schematic view of the functional groups on a graphite surface.

The porous structure seems to be the most important feature of CCE. This is because of composite character of the material, which makes possible to produce large area for electron transfer. This property is also exploited in experiments described in this thesis, namely in modification procedure. Actually, CCE are more amenable to chemical modification than monolithic carbon electrodes [114]. Therefore, in order to introduce specific interactions between CCE and reactants dissolved in solution, this electrode can be modified in five routes. In particular, redox active groups can be immobilized by:

1)   doping of the redox modifier to the sol;

2)   modification of carbon particles with redox-active groups;

3)   bonding of redox-active group to silicate precursors;

4)   adsorption of the redox modifier on the electrode surface;

5)   impregnation with the redox modifier.

A number of publications were already devoted to modified CCEs [113, 114, 119, 121, 122, 138-140]. The selected examples of modified CCEs and their applications are presented below.

Doping of the modifier to the sol.

The first example is organic molecule (9,10-phenanthrenequinone) modified CCE prepared by incorporation of redox probe along with the sol-gel precursors. It can be alternatively used as voltammetric pH sensor [114]. The electrodes exhibited an

41

almost Nerstian dependence of the anodic peak current on pH, 59 mV/decade pH over a wide pH range (0-7) [114, 119]. Fig. 3.7 shows the effect of pH on the voltammograms obtained with this CCE.
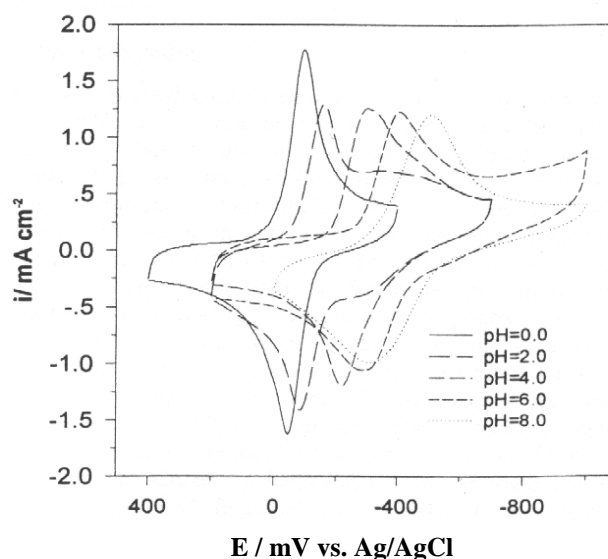

Figure 3.7.   Voltammograms of CCE modified with 9,10-phenanthrenequinone by doping. The measurements were conducted in 1 mol dm^{-3} phosphate buffer at different pH [119].

Inorganic molecule modified CCE prepared from sol doped with α-type 2:8-molybdodiphosphate (P_2Mo_{18}) represents another example. The electrode has shown catalytic activity for the electrochemical reduction of bromate in an acidic aqueous solution (Fig 3.8) [139].
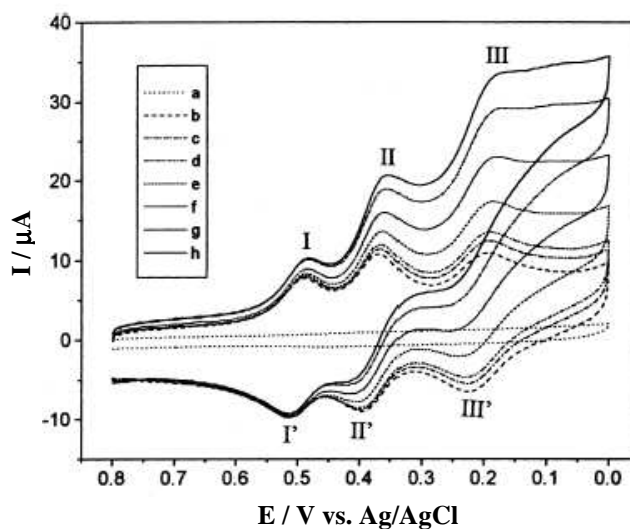
Figure 3.8.   Cyclic voltammograms of a P_2Mo_{18}-doped CCE in 0.5 mol dm^{-3} H_2SO_4 + 0.1 mol dm^{-3} Na_2SO_4 aqueous solutions containing 0 (b), 1 (c), 2 (d), 5 (e), 10 (f), 15 (g) and 20 (h) mmol dm^{-3} Na BrO$_3$, respectively, and an unmodified CCE (a) in the same solutions as (e). Scan rate is 40 mV s^{-1} [139].

42

Modification of carbon particles with redox-active groups.

There are many ways of linking redox group to carbon grains. Among them is the self-assembling method. The carbon particles are first coated with gold, material suitable to thiol adsorption [113]. Then they react subsequently with cystamine, glutaraldehyde, dialkylamine, and at the end with ferrocene acetic acid to form ferrocene appended carbon grain (Fig. 3.9).
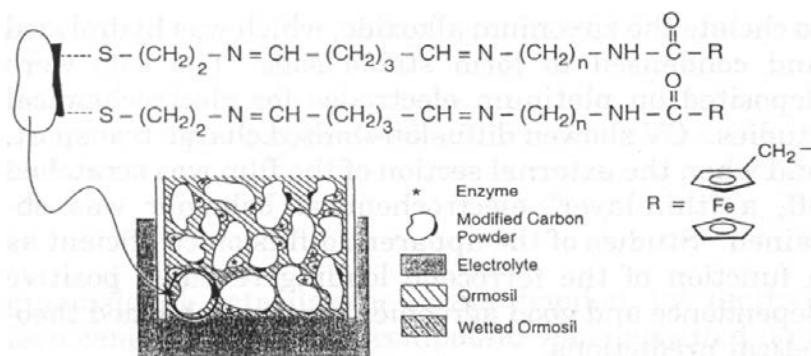

Figure 3.9.   Scheme of structure of ferrocene-modified carbon particle [113].

In this particular example ferrocene functional groups are responsible for the signal transduction from the active center of the enzyme to the electron conductive surface.

Carbon particles can be also modified by adsorption of redox active compound. The CCE made of carbon particles covered with cobalt phtalocyanine or cobalt porphyrin showed noticeable electrocatalytic activity toward the reduction of O_2 and CO and oxidation of SO_2 and H_2 [121]. The porous structure of the CCE is useful, because of its gas permeability and hydrophobicity preventing flooding electrolyte through the electrode (Fig. 3.10).
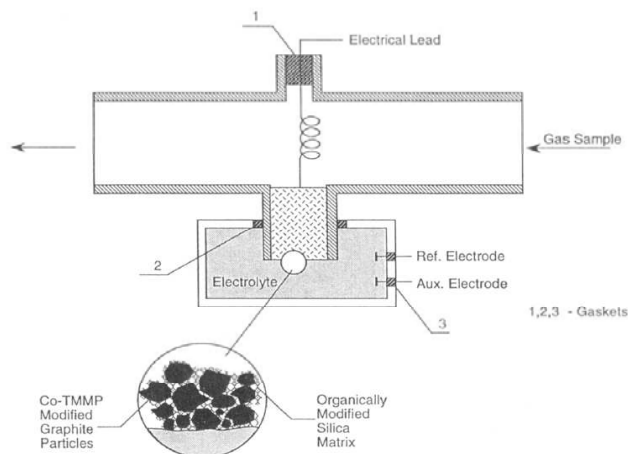

Figure 3.10.   Scheme of a CCE gas sensor [121].

43

Bonding of redox-active group to silicate precursors.

Lev and co-workers [141] proposed to use ferrocene appended precursor to immoblize ferrocene group in silicate matrix. The copolymerization of N-[3-(trimethoxysily)propyl]-ferrocenylacetamide, methyltrimethoxysilane and aminopropylsilane results in multifunctional silicate redox polymer (Fig. 3.11).
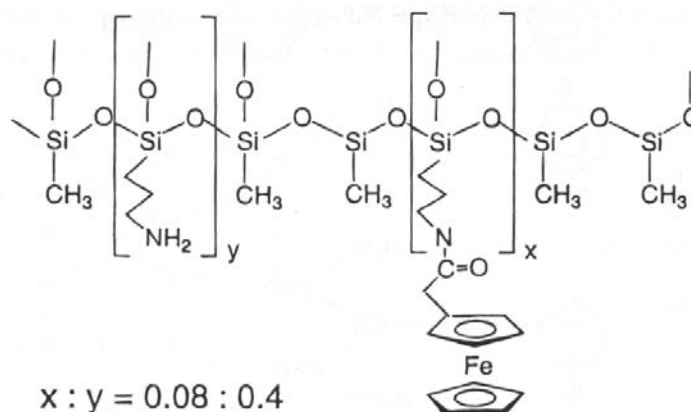

$x : y = 0.08 : 0.4$

Figure 3.11.   Scheme of structure of a ferrocenyl-modified redox silicate [113].

In this case ferrocene functional groups also were responsible for the signal transduction from the active center of the enzyme to the electron conductive surface.

Adsorption of the redox modifier on the electrode surface.

Salimi group has modified CCE with complex $[Ru(bpy)(tpy)Cl]PF_6$ or chlorogenic acid using adsorption of modifier at CCE [142, 143]. In first case a bulk-modified CCE with Nafion® was prepared, then thin film of Ru-complex was adsorbed at the electrode surface. The modified electrode has been shown to be promising for L-cysteine detection with many desirable properties including high sensitivity, low detection limit, and fast response time [142]. In the second case, bare CCE was modified with thin film of chlorogenic acid. It is adsorbed strongly and irreversible on the surface of electrode. The modified electrode showed electrocatalytic activity toward NADH (nicotinamide adenine dinucleotide) oxidation.

Impregnation with a redox modifier.

Recently Opallo and co-workers have proposed the new way of CCE modification, namely impregnation with liquid redox probe or diluted redox probe [20, 21, 40]. The modification procedure involves immersion in water-immiscible liquid redox probe or solution of redox probe in hydrophobic non-polar solvent, which easily penetrates inside a bulk of hydrophobic electrode. CCEs modified in this manner have

advantages over carbon paste electrodes, because of the CCEs can be prepared not only with very viscous binder like Nujol, silicone oil or higher liquid hydrocarbon [137, 144]. Also electrodes modified with pure redox liquid like *tert*-butylferrocene exhibits large faradaic current due to extremely large surface concentration of redox groups.

This way of modification was used in the presented study. From pure redox liquids or redox probe solutions in non-polar or polar solvent, which were proposed in earlier studies [20, 40], the latter group was selected.

Goal

The objective of this work is the understanding of the electrogenerated ion transfer reaction across liquid / liquid interface supported by carbon ceramic electrode. The redox probe solution in hydrophobic polar solvent filling the hydrophobic silicate matrix and aqueous electrolyte solution represent both sides of this interface. In principle two reactions are possible: the cation ejection to the aqueous phase or anion insertion from the aqueous to organic phase. The contribution of these reactions in whole electrode process was studied using electrochemical methods at different conditions. They were changed by appropriate selection of experimental factors. The type of redox probe, organic solvent and anion present in the aqueous phase seem to be among the most important.

Experimental results and discussions

Chapter 4.   Methods

Here, an overview of finite-current controlled-potential techniques used in these thesis, is presented. The last part deals with scanning electron microscopy that has been used to obtain images of CCEs surface.

4.1   Electrochemical techniques

The most common instrumentation required for controlled-potential experiments is an electrochemical cell connected to a potentiostat. Typical electrochemical cell consists of the three electrodes i.e. counter electrode (CE), reference electrode (RE) and working electrode (WE) all immersed into an electrolyte. The potentiostat controls potential difference between RE and WE with minimal interference from IR (ohmic) drop [81]. The basis of all controlled-potential techniques is the measurement of the current response to an applied potential [81, 145, 146].

4.1.1   Cyclic votammetry

The cyclic voltammetry (CV) provides considerable information on the thermodynamics of redox processes; the kinetics of heterogeneous electron-transfer reactions, coupled chemical reactions and adsorption processes.

CV technique is based on the use of a triangular potential waveform [81, 145, 146] (Fig. 4.1, a).
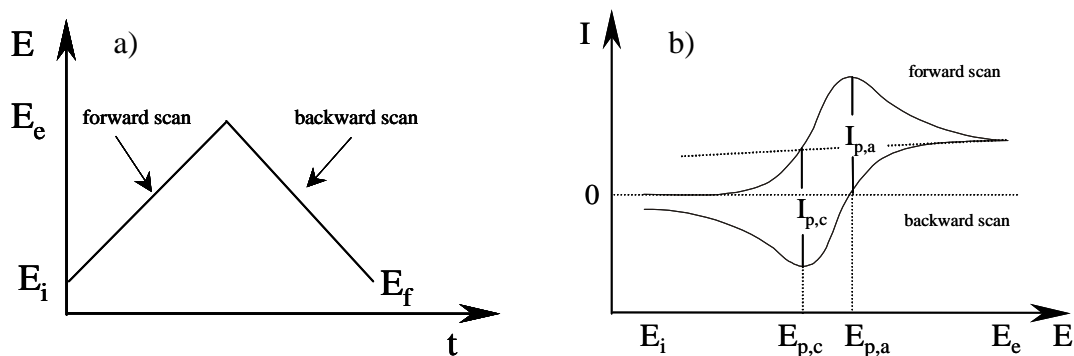

Figure 4.1.   Plots of the potential program applied in CV (a), applied potential (E) vs. time (t) and resulting current response (I) vs. E (b). Initially only Red is present in solution. Other abbreviations are described in text below.

The Fig. 4.1 (a) presents single cycle starting from initial E_i, to final potential, E_f, being equal in this case. E_e is the end potential, where the sweep is reversed. This sequence can be repeated using a repetitive triangular potential excitation. During the potential sweep, the potentiostat measures the resulting current. The plot shows expected single cyclic voltammogram for one electron reversible process (Fig. 4.2, b):

$$Ox + e^- \leftrightarrow Red \tag{4.1}$$

Such peak shaped voltammogram appears when radius of electrode is much larger than diffusion layer thickness. The $I_{p,c}$ and $I_{p,a}$ are peak currents, $E_{p,c}$ and $E_{p,a}$ are peak potentials for the cathodic and anodic processes, respectively. For process (4.1) the formal potential, $E^{0'}$, is assumed to be equal the mid-peak potential, E_{mid}, $= \frac{1}{2}(E_{p,c} + E_{p,a})$ (with acceptance the equality of diffusion coefficient of Ox and Red forms: $D_{Ox} = D_{Red}$) [81]. $E^{0'}$ in CV has the same meaning as in direct current polarography (DCP), as consequence the mid-peak potential in CV corresponds to half-wave potential in DCP. For one-electron reversible processes the ratio $I_{p,c}/I_{p,a}$ is equal unity and the peak separation, $\Delta E_p = E_{p,a} - E_{p,c}$, is 57 mV at 25 C° [81].

The shape of the voltammogram depends on the reversibility of the electrochemical reaction. In electrochemically reversible systems the electron transfer rate at all potentials is significantly greater than the rate of mass transport, and therefore Nernstian equilibrium is always maintained at the electrode surface. When the rate of electron transfer is insufficient to maintain this equilibrium, the shape of the voltammogram changes to that of an electrochemically irreversible system. The terms "reversible" and "irreversible" refer to limiting cases, where the electrode kinetics is fast or slow relative to the mass transport conditions of the electrode [147]. There is also another meaning of reversibility, namely chemical one. After an electrode reaction the product can undergo consumption, for example a further chemical reaction or transfer to other phase. In this case the most marked feature of a cyclic voltammogram of a totally irreversible system is the absence of a reverse peak.

For diffusion-controlled processes the peak current, I_p, is proportional to square root of scan rate, $v^{1/2}$, and can be calculated with Randles-Sevcik equation (1.18). Thus I_p is proportional to the concentration of electroactive species and to the square root of the sweep rate and diffusion coefficient. The reducing of size electrode (microelectrode) leads to a situation in which the radial diffusion becomes dominant. In this case current

magnitudes are independent of the scan rate and voltammograms have a sigmoidally shape.

4.1.2 Differential pulse voltammetry

Pulse voltammetric techniques originally were aimed at lowering the detection limits of voltammetric measurements [81, 145]. The introduction of potential pulse to the electrode considerably increases the ratio of the faradaic and capacitive currents in comparison to the linear scan voltammetry [81, 145, 146]. Fig. 4.2 qualitatively illustrates the currents flowing after the imposition of a potential pulse. It is clear that the capacitive current decreases much faster than the faradaic one.
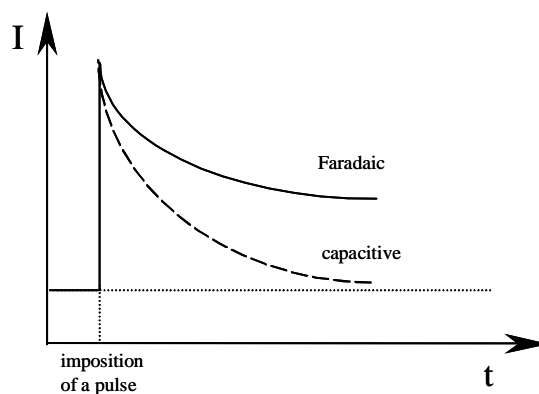

Figure 4.2.   Faradaic and capacitive current, I, flowing after the application of a potential pulse plotted vs. time, t [81]. This plot refers to reaction 4.1.

In most cases the aim of measurements is to detect the current magnitude when the influence of capacitive current is negligible. In differential pulse voltammetry method (DPV) the current is sampled twice: before pulse application and at the end of pulse (Fig. 4.3, a). In this case the large contribution of capacitive current is eliminated.

The current measured is equal the difference of the current measured before the beginning of the pulse and close to the end of the pulse. Therefore it has the largest value at potentials close to formal potential. The Fig. 4.3 (b) presents typical peak shaped DPV curve corresponding to the reaction (4.1). The E_p can be described as follows [81, 146]:

$$E_p = E^{0'} + \frac{RT}{nF} \ln \left(\frac{D_{\mathrm{Re}d}}{D_{Ox}} \right)^{1/2} - \Delta E_p/2 \qquad (4.2)$$

If $D_{Red} = D_{Ox}$ and ΔE_p is very small, the potential of maximum current is close to $E^{0'}$.
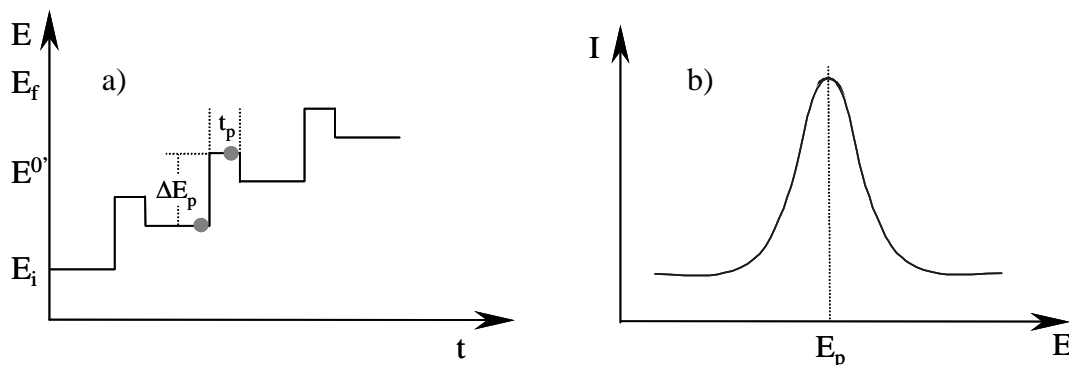
Figure 4.3.   Plots of the potential program applied in DPV (a) as a function of time, t, and resulting current response, I vs. E (b) of the process (4.1). ● is the point of current detection. ΔE_p is pulse (step) height, t_p is pulse (step) width, $E^{0'}$ corresponds standard redox potential, E_i and E_f have the same meaning as on Fig. 4.1.

4.1.3   Chronoamperometry

In chronoamperometry technique (CA) current is recorded as a function of time. The method involves stepping the potential of WE from a value at which no faradaic reaction occurs to a potential at which the surface concentration of the electroactive species approaches zero (Fig. 4.4). Most frequently double potential step chronoamperometry is used and will be described below.
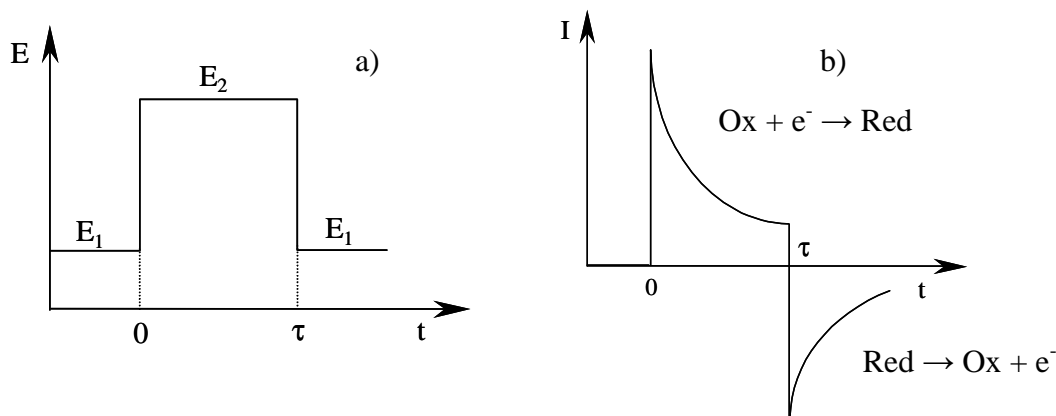

Figure 4.4.   Plots of the potential program applied in double potential step CA (a) and resulting current response, I vs. E (b) for the process (4.1). E_1 and E_2 are potentials, at which reaction (4.1) does not occur and occurs, respectively, τ - time of polarization of electrode at E_2.

E_1 is in a potential region where faradaic processes do not occur, whereas E_2 is in a potential region where the kinetics for oxidation of *Red* becomes so rapid that no *Red* is present close to the electrode surface [145]. Anodic current decreases subsequently from

large magnitude to a limiting current, where the interfacial concentration of the reactant *Red* falls to zero. After $t = \tau$ the potential is returned to E_1, where only reduced form is stable at the electrode. Again, a large cathodic current gradually flows down to fully rereduced form at the electrode (Fig. 4.4, b).

Similarly to CV and DPV the stationary WE and unstirred solution are required in CA method. If the mass transport under these conditions is solely by diffusion, thus the current-time curve is sensitive to the change in the concentration gradient in the vicinity of the electrode surface. For a planar electrode under the following boundary conditions for the concentration profile, $C_{Ox}(x,t)$:

$$C_{Ox}(x,0) = C_{Ox}^*;$$

$$\lim_{x \to \infty} C_{Ox}(x,t) = C_{Ox}^*;$$

$$C_{Ox}(0,t) = 0 \ (for \ t > 0)$$

the time dependence of diffusion-limited current is described by Cottrell equation [145, 148]:

$$I(t) = z_i AF \frac{D_{Ox}^{1/2} C_{Ox}^*}{\pi^{1/2} t^{1/2}} \tag{4.3}$$

where C_{Ox}^* is bulk concentration of species Ox, D_{Ox} – their diffusion coefficient, A – interfacial area, z_i – charge number of electrochemical reaction.

If the rate of the electrode reaction is controlled by diffusion of redox active species the linear dependence of the current on reciprocal square root of time can be observed. CA technique is used for estimation of the diffusion coefficient of electroactive species or the surface area of the WE. It is also applied to the study of mechanisms of electrode reactions.

4.2   *Scanning Electron Microscopy*

Scanning Electron Microscopy (SEM) is used for surface characterization and chemical analysis at micro-scale [149, 150]. The topics of SEM research are microelectronics, agriculture and environmental science, material preparation, optics, electrochemistry, mechanics and micro-machining, biological science, and innovative SEM methods.

Modern SEM with field emission gun (FEGSEM), used for experiments described in this thesis, is capable of resolution near 1nm on appropriate samples (conducting itself or covered with conducting material) using the scanning electron signal. FEGSEM uses a focused electron beam to scan small areas of solid samples i.e. to study surface topography. The SEM apparatus consists of a carbon cathode with a very sharp (< 100 nm) tip usually made of a wire of single-crystal tungsten filament from which electrons are emitted [149]. The small tip radius allows an electric field to be concentrated to an extreme level ($> 10^7$ V cm^{-1}) at the tip. The electric field applied at the tip forces electrons to "tunnel" directly through the potential barrier and leave the cathode without requiring any thermal energy. As the electron beam is produced by a tunneling process very high vacuum ca. 10^{-10} Torr is needed [150]. The electrons are accelerated to ca. 10 keV and targeted at the sample (Fig. 4.5).
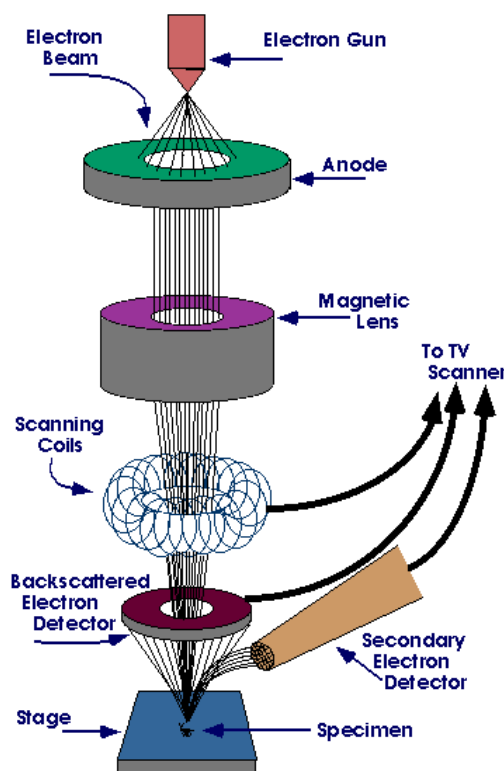

Figure 4.5.   Schematic view of SEM apparatus „heart" [151].

A beam of electrons is produced at the top of the microscope by heating of a metallic filament. The electron beam follows a vertical path through the column of the microscope. It makes its way through electromagnetic lenses that focus and direct the beam down towards the sample. Two types of electrons are produced from the

interaction of the electron beam with the sample surface, secondary electrons and backscatter electrons.

Secondary electrons are emitted from the sample and collected to create an area map of the secondary emissions. Since the intensity of secondary emission is very dependent on local morphology, the area map is a magnified image of the sample. These electrons were used for analyzing of the electrode surface concerned this paper. Typical spatial resolution of SEM is 4 nm and in FEGSEM – 1 nm [149, 150].

Backscatter electrons are high-energy electrons from the primary beam that are scattered back out of the sample by the atomic nuclei. The intensity of the signal is dependent on the mean atomic number of the area of interaction i.e. backscattered electrons tell us about surface structure and average elemental composition. The incident electrons can also generate X-rays. Energy Dispersive X-ray Spectroscopy (EDX) can utilize these signals for compositional analysis of microscopically small portions of the sample.

Chapter 5.   Equipment and chemicals

5.1   Equipment

Electrochemical experiments were performed with an Autolab (Eco Chemie, Netherlands) electrochemical system with dedicated software (GPES v.4.9) in conventional three-electrode or four-electrode cells. The start potential in CV and DPV experiments was always chosen as the most negative point in the potential window. An Ag|AgCl|KCl sat. electrode (Ag/AgCl) or saturated calomel electrode (SCE) were used as reference. A platinum wire (diameter 0.5 mm) was used as a counter electrode. Various type of CCE, carbon paste electrode (CPE) or bppg electrode was used as a working electrode. In some experiments Au disk (diameter, *d* = 2 mm) as second working electrode was also used in bipotentiostatic conditions (Fig. 5.1).
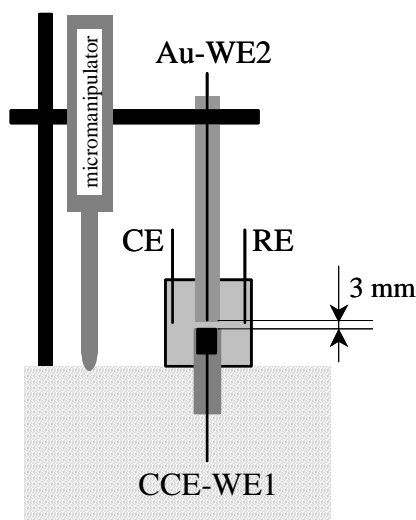

Figure 5.1.   Schematic view of the electrode cell with two working, WE, counter, CE, reference, RE, electrodes. The distance between WE1 and WE2 was controlled by micromanipulator.

Unless it is not otherwise written, a scan rate in cyclic voltammetry measurements is equal 0.01 V s^{-1}. Since electrooxidation reactions were studied voltammetric scan starts at most negative potential.

5.2   Chemicals

Electrode substrates: methyltrimethoxysilane (MTMOS) (99%, Aldrich, Strem); tetramethoxysilane (TMOS) (99+%, Aldrich); graphite powder (MP-300, average particle size 20 μm, Carbon GmbH) and graphite powder (UPC-1-M, average size 1

μm, Graphite Pold). Bppg (Le Carbone Ltd., UK) and carbon nanofibers (CNFs) (average diameter 100 nm) were obtained from Loughborough University, UK. The latter were grown by chemical vapour deposition (CVD) following a published methodology [152].

Redox probes: Substituted ferrocene derivatives (SFc): Fc (98%, Aldrich), *t*BuFc (99%, Strem), DMFc (97%, Aldrich), ferrocenedimethanol (Fc(CH$_2$OH)$_2$) (98%, Aldrich). *N,N*-didodecyl-*N',N'*-diethylphenylenediamine (DDPD) was obtained from Loughborough University, Loughborough, UK. It was synthesized and purified as described in [153].

Solvents: NB (+99%, Aldrich), NPOE (99+%, Fluka), 2-nitrophenylphenyl ether (NPPhE) (99+%, Fluka), bis-(2-ethylhexyl)hydrogen phosphate (HDOP) (97%, Aldrich), methanol (MeOH) (analytical grade, POCh), acetonitrile (ACN) (for spectroscopy, Merck). RTILs: C$_4$mim(PF)$_6$, C$_4$mimN(Tf)$_2$, C$_{10}$mimN(Tf)$_2$ were obtained form Laboratoire d'Electrochimie et Chimie Analytique University Pierre et Marie Curie, Paris, France.

Acids, Alkalines, Salts: H$_3$PO$_4$, NaF, NaCl, NaClO$_4$, NaSCN, Na$_2$SO$_4$, KBr, KNO$_3$, KOH (analytical grade) were from POCh; KPF$_6$ (98+%) was from Merck. Tetrabutylammonium perchlorate (TBAP) was prepared by metathesis of (C$_4$H$_9$)$_4$NBr (Fluka) with HClO$_4$ (Aldrich) in water. The product was recrystallized twice from water and dried under reduced pressure at 100° C for 24 h.

All chemicals were used without further purification. Water was filtered and demineralised with an ELIX system (Millipore).

55

Chapter 6.   Selection of studied systems

Although the list of chemicals used in this thesis was presented in previous chapters, the rules of the selection of redox probes, solvents and aqueous electrolytes are described below.

Special attention was paid to selection of the redox probes used in this research. They have to undergo facile one-electron reaction in appropriate potential range, where no another electrode processes are presented. Moreover, these redox probes should have good solubility in polar organic solvents and be insoluble in aqueous solution.

Ferrocene and its alkyl-substituted derivatives, SFc, seem to be good candidates for this purpose. Their structures of these redox probes are presented below (Fig. 6.1). The ferrocene is substituted with one (*tert*-butyl) or ten (methyl) groups. Therefore hydrophobicity of these compounds increases in the order Fc < *t*BuFc < DMFc and systematic study of the role of this factor in the mechanism of electrogenerated ion transfer is possible. Additional redox substrate, *N,N*-didodecyl-*N',N'*-diethylphenylenediamine, which does not belong to above group, was used in experiment with liquid acid-base complex. The presence of N-atom with electron donor properties gives possibility of such complex formation.
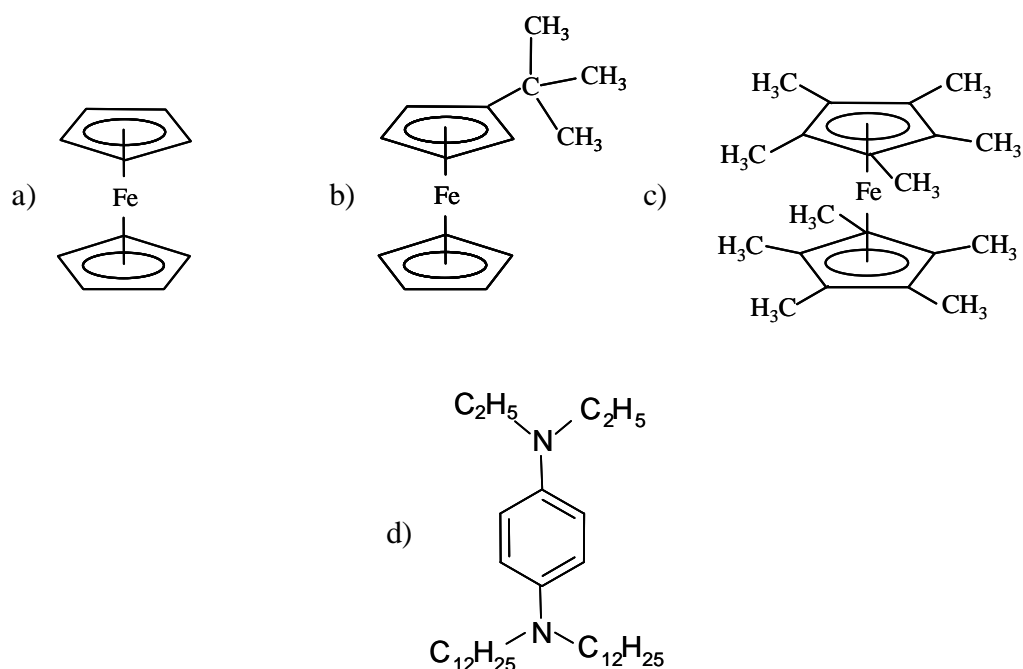

Figure 6.1.   *Structure of ferrocene (a), tert-butylferrocene (b), decamethylferrocene (c) and N,N-didodecyl-N',N'-diethylphenylenediamine (d).*

No less important concern was paid to selection of solvents. The choice obviously was restricted to polar hydrophobic solvents. According to Table 2.1 the transfer of anion from aqueous to organic phase following the electrogeneration of cation in the latter is possible only where organic phase is polar. Obviously liquid / liquid interface has to be stable. This is possible only with hydrophobic solvents. Three structurally similar hydrophobic polar solvents, NB, NPOE and NPPhE (Fig. 6.2) were employed. First two were frequently used in electrochemical studies of liquid / liquid interface [13]. The presence of alkyl or phenyl substituents connected to nitrobenzene moiety increases the hydrophobicity and viscosity of last two. The first parameter was expected to affect the stability of the electrode. Their different viscosities helped us to study the effect of reactant transport inside the organic phase. The most viscous polar solvent NPOE as well as $C_{10}mimN(Tf)_2$ were also employed for preparation of CPE used to study the effect of silicate matrix.

For experiment with liquid acid-base complex the hydrophobic acid HDOP (Fig. 6.2) was selected. As ionically conducting solvents two RTILs one relatively hydrophilic - C_4mimPF_6 and other hydrophobic - $C_{10}mimN(Tf)_2$ (Fig. 6.3) were used. The properties of all solvents used are presented in Table 6.1.

a)   b)   c)   d)
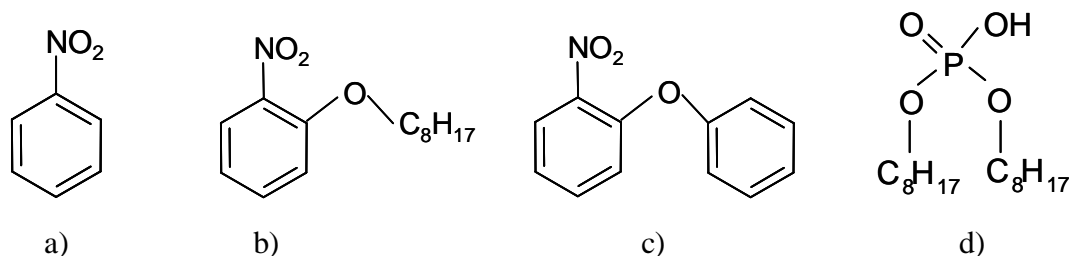
Figure 6.2.   Structure of solvents used in experiments: nitrobenzene (a), 2-nitrophenyloctyl ether (b), 2-nitrophenylphenyl ether (c) and bis-(2-ethylhexyl)hydrogen phosphate (d).
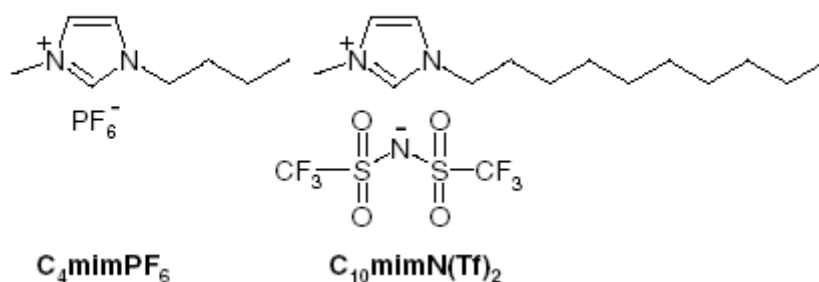

Figure 6.3.   The structural formula of ionic liquids used in the experiments.

57

Table 6.1.   Selected physicochemical properties of polar solvents and RTILs used in experiments of these theses.

Solvent [Ref.]	Boiling point, °C	Density, g/cm^{-3}	Relative dielectric permittivity	Viscosity, η, cP	Solubility in water	Solubility of water in solvent
NB [154,155]	210-211	1.196 (25 °C)	34.8	1.80	1.5×10^{-2} mol dm^{-3}	0.2 mol dm^{-3}
NPOE [154-156]	197-198	1.041 (25 °C)	24.2	12.35	2.0×10^{-6} mol dm^{-3}	4.6×10^{-2} mol dm^{-3}
NPPhE [156,157]	177-178	1.098 (20 °C)	-	7.58	-	-
HDOP [155]	-	0.965 (25 °C)	-	-	-	-
C$_4$mimPF$_6$ [158-160]	-	-	11.4	397 (25 °C)	2.4 % (30 °C)	2.7 % (30 °C)
C$_{10}$mimN(Tf)$_2$ [161]	-	-	-	152.8 (20 °C)	-	-

As the anion transfer from the aqueous to the organic phase was expected to play important role in electrochemical process, the aqueous solutions of salts of anions having different hydrophobic-hydrophilic properties were used as electrolytes. The standard transfer potential across aqueous phase / organic phase interface, $\Delta_{aq}^{org}\varphi_{X^-}^0$ (see p. 21) describes the ability of the anion to be transferred across water / organic solvent interface and therefore its hydrophobicity. Below, the anions of selected salts, their radii and standard transfer potentials from water to NB or NPOE are presented in Table 6.2.

The anions having smaller values of $\Delta_{aq}^{NB}\varphi_{X^-}^0$ or $\Delta_{aq}^{NPOE}\varphi_{X^-}^0$ are easier transferred to organic solvent. These parameters also correlate well with the radii of an anion. In the discussion of obtained results the values of $\Delta_{aq}^{NB}\varphi_{X^-}^0$ were used for all systems. This is because $\Delta_{aq}^{NPOE}\varphi_{X^-}^0$ were determined only for some anions and the transfer potentials of ion transfer across water / NPPhE interface are not reported in literature. This procedure is justified, because the order of this parameter is similar for both NB and NPOE (Table

6.2). It is also expected to be similar for NPPhE, because of similar structure of these solvents.

Table 6.2.   The anion radii, r, and the standard transfer potentials of anion transfer from the aqueous solution to NB, $\Delta_{aq}^{NB}\varphi_{X^-}^0$, and to NPOE, $\Delta_{aq}^{NPOE}\varphi_{X^-}^0$.

Anion	r, pm [Ref.]	$\Delta_{aq}^{NB}\varphi_{X^-}^0$, V [Ref.]	$\Delta_{aq}^{NPOE}\varphi_{X^-}^0$, V [Ref.]
PF_6^-	0.245 [51]	0 [50]	-
ClO_4^-	0.236 [163]	0.083 [18]	0.175 [130]
SCN^-	0.213 [163]	0.161 [18]	0.260 [130]
NO_3^-	0.189 [163]	0.270 [18]	0.372 [130]
Br^-	0.182 [163]	0.290 [18]	-
Cl^-	0.167 [163]	0.324 [18]	0.521 [130]
F^-	0.136 [164]	0.720 [18]	-
SO_4^{2-}	0.230 [164]	0.920 [18]	-

Expecting that the size of conductive particles may affect the efficiency of the electrode process [13], the different carbon based fillers were chosen for electrode preparation. There were graphite particles with average size 20 μm or 1 μm and CVD-grown CNFs with ca. 100 nm diameter. Most experiments were performed with CCE prepared with 20 μm size graphite particles; therefore, if it is not otherwise mentioned, the presented results were obtained with this type of CCE.

59

Chapter 7.   Electrode preparation and its SEM images

7.1   Electrode preparation procedure

The hydrophobic CCE was prepared as described elsewhere [114, 136]. The hydrolyzed sol was made by mixing 1.5 cm^3 of methanol, 1.0 cm^3 of MTMOS and 0.05 cm^3 of 11 mol dm^{-3} aqueous HCl as catalyst and than it was sonicated for 2 min. Next, 1.25 g of graphite powder (average size 20 μm) was added and the mixture was sonicated for another minute. The resulting mash was immediately placed into 2 mm deep cavity of 2 mm inner diameter glass tubing filled tightly with copper wire. The electrode was left for drying for at least 48 hours at room temperature (Fig. 7.1).
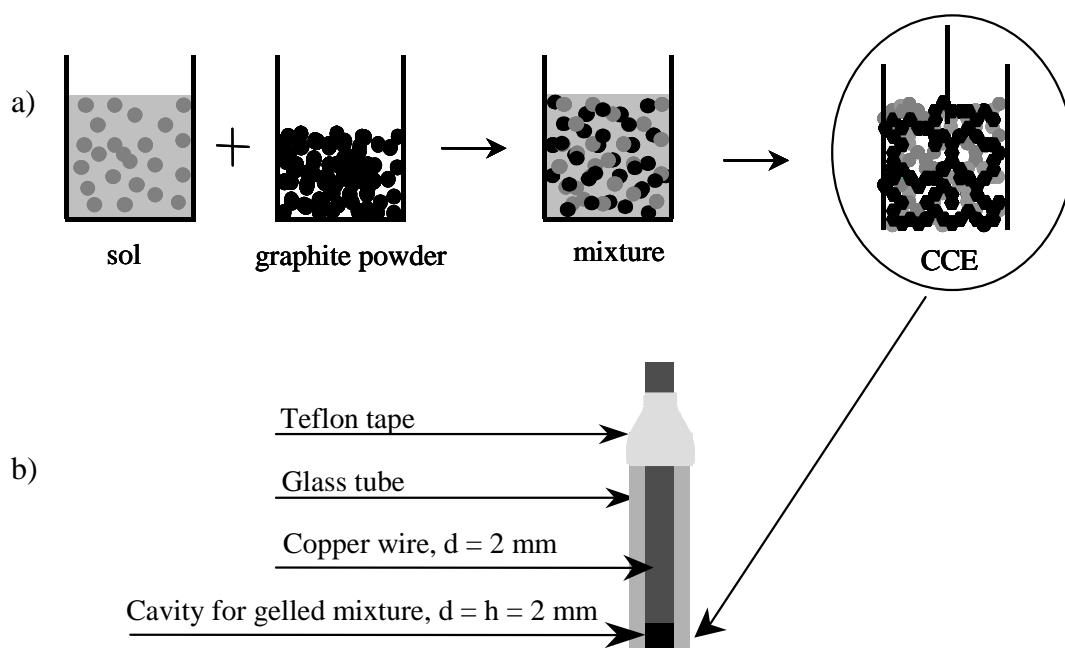

Figure 7.1.   Scheme of CCE preparation procedure (a) and sketch of CCE (b) used in the measurements (d and h are diameter and height of the cavity respectively).

First electrode was polished on emery paper (grit 800) and then with smooth paper. The geometric surface area of its intersection is equal 0.031 cm^2.

Modification of CCE was achieved by immersion to a hydrophobic redox liquid (Fig. 7.2) [20, 21]. The ingress of redox liquid into CCE can be observed even with the naked eye. The body of CCE becomes wet and the amount of the redox liquid in the beaker decreases.
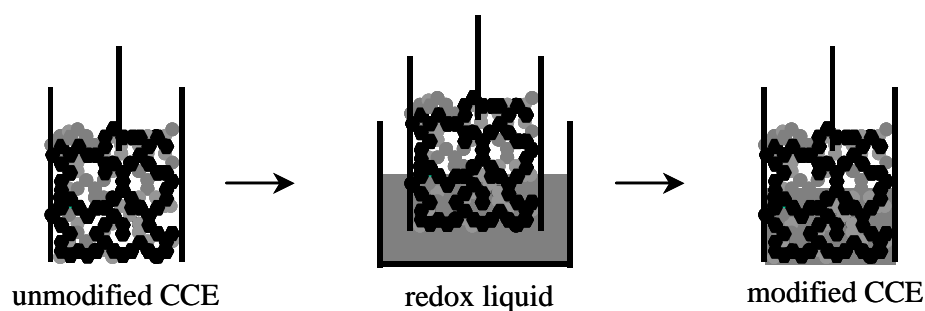
60

unmodified CCE   redox liquid   modified CCE

Figure 7.2.   Scheme of the modification of hydrophobic CCE with redox liquid.

In the studies of CCE modified with ionic liquids the sol was prepared by mixing hydrophobic (MTMOS) and hydrophilic (TMOS) precursors with different ratio. This electrode was modified by pipetting of 2 µl redox probe solution in RTIL on the top of electrode.

In some experiments a graphite powder with smaller average size of particles 1 µm, CNF, or mixture CNFs with graphite powder (20 µm) were used. For these electrodes, instead of 1.25 g the 0.17 g of graphite powder (1 µm) or CNF and graphite particles (20 µm) mixture were added to sol, in order not to lose the rigidity of the electrode body.

CPE was prepared as follows: 0.17 g of 20 µm graphite powder or CNF was mixed with 100 µm of the redox probe solution in NPOE or RTILs. The resulting mixture was placed into an electrode body used for CCE. The electrode surface was polished with a smooth paper.

Bppg embedded in Teflon holder with geometric surface area being equal 0.188 cm^2 was modified by pipetting of correspond amount of redox liquid solution in volatile solvent. After evaporation of solvent it was immersed into an aqueous solution. The surface of electrode was renewed by polishing on emery paper (grit 1000).

7.2   SEM images of CCE

All images of CCE were obtained with a Leo 1530 Field Emission Gun Scanning Electron Microscope, FEGSEM, system at Loughborough University, UK. The images of hydrophobic CCE prepared with 20 µm graphite powder and CNF are shown on Figs. 7.3 and 7.4, respectively.
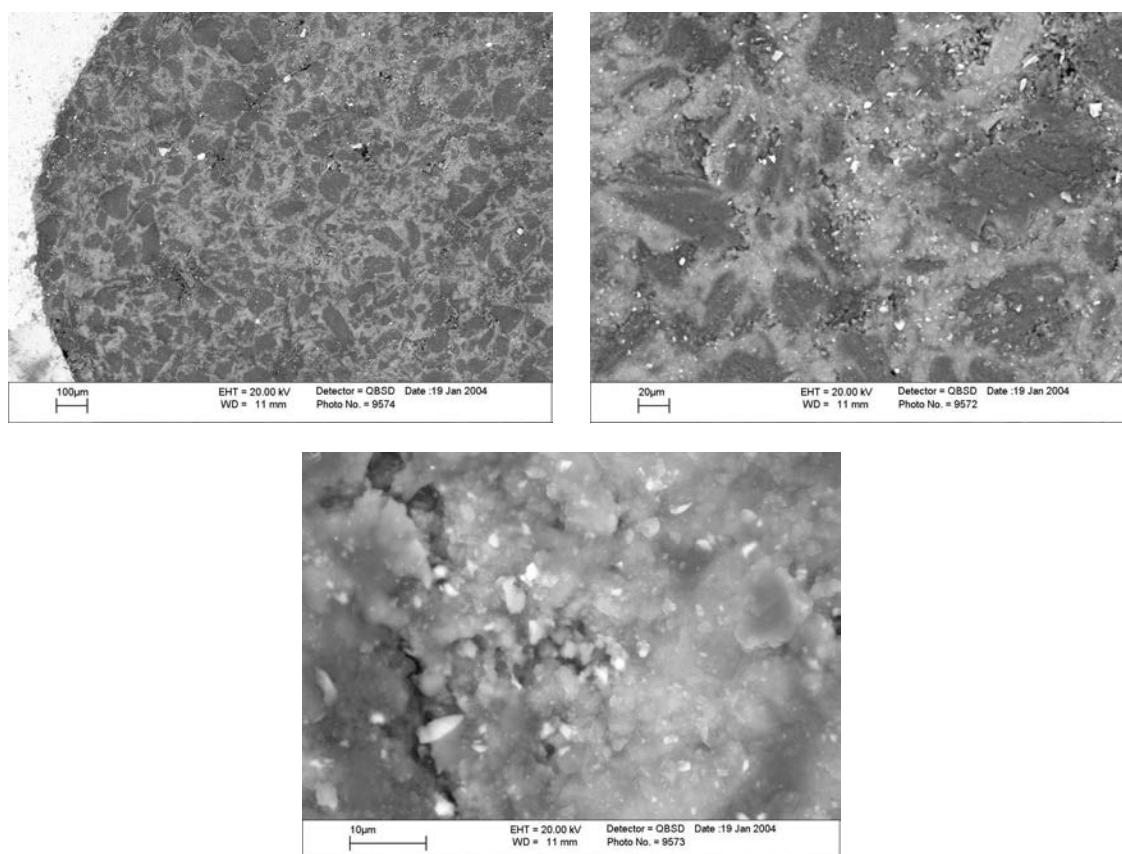
Figure 7.3. FEGSEM images of the surface of hydrophobic CCE prepared with 20 μm graphite particles at different magnification.

Similarly as it was reported in literature [130], one can observe (Fig. 7.3), that on the surface of the CCE small aggregates of graphite particles (approximate diameter = 20-40 μm [131]) (dark areas) are present within a mesoporous matrix of the hydrophobic silicate (bright areas).
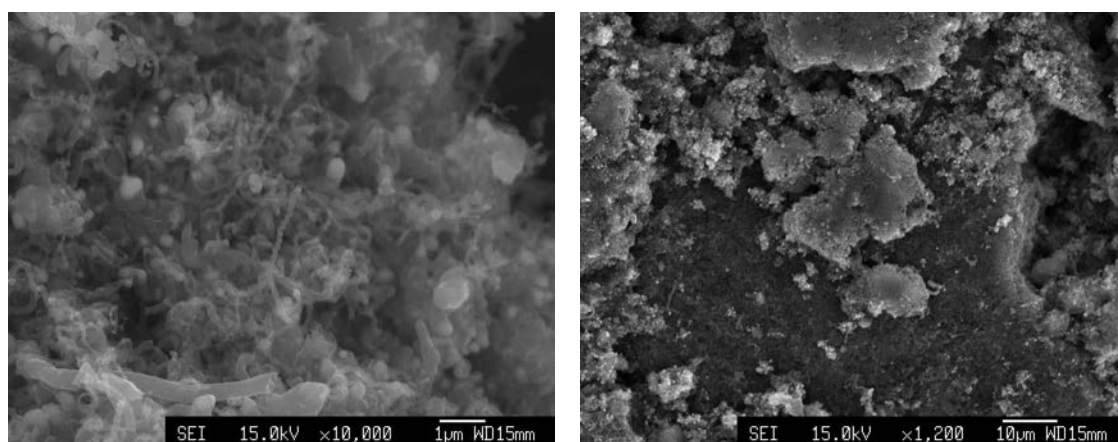

Figure 7.4. FEGSEM images of the surface of CCE composed of CNF at different magnification.

A dense network of CNF formed within silicate matrix can be seen on Fig. 7.4. Particles of hydrophobic silica appear as bright areas with typically 200-500 nm size. At larger magnification the fibers are easily visible electrode surface. In comparison to CCE based on 20 µm carbon particles (Fig. 7.3), the smaller number of cracks and less extended silica regions are formed.

63

Chapter 8.   Ion transfer across hydrophobic polar solvent / aqueous solution interface supported by carbon ceramic electrode

This chapter concerns mainly with electrochemical behavior of unmodified and modified CCEs under impact of different factors. The major attention is paid to electrogenerated ion transfer across liquid / liquid interface, because of the main goal of this PhD thesis. The composition of CCE body, the type and concentration of the redox probes, polar solvent and ions present in the aqueous solution are among studied factors influencing this process. The redox liquids used for modification of CCE do not contain any electrolyte. The studies of CCE modified with ionically conducting redox liquid are presented in Chapter 11.

8.1   Electrochemical behavior of unmodified CCE in aqueous solution

Although electrochemical behavior of CCE containing graphite particles of different size and immersed in solution of redox probes was presented in literature [103, 110], the application of CNF for CCE preparation is reported here for the first time. The material based on CVD-grown CNFs is expected to be a high surface area carbon with high porosity. Therefore the electrochemical properties of these electrodes in the absence of liquid modifier are compared below.

The cyclic voltammograms obtained during continuous scanning of the potential applied to a CCE containing mixture of CNF and graphite particles or exclusively graphite particles immersed in the aqueous solution are presented in Fig. 8.1, a.

The value of the current is approximately linearly dependent on scan rate (Fig. 8.1, b). The value of capacity calculated from capacitive current is equal 750 μF. It is consistent with 12 μg of active CNF (the capacitance of CNFs is 60 Fg^{-1} [165]). The capacitive current is by almost one order of magnitude larger than that observed at CCE prepared with 20 μm diameter particles (Fig. 8.1, a). Therefore the presence of CNFs is responsible for larger capacitive background current. These results indicate that some penetration of liquid into the porous CNF based CCE structure occurs. The electric contact in the composite materials seems to be good and that conventional voltammetric measurements are possible.
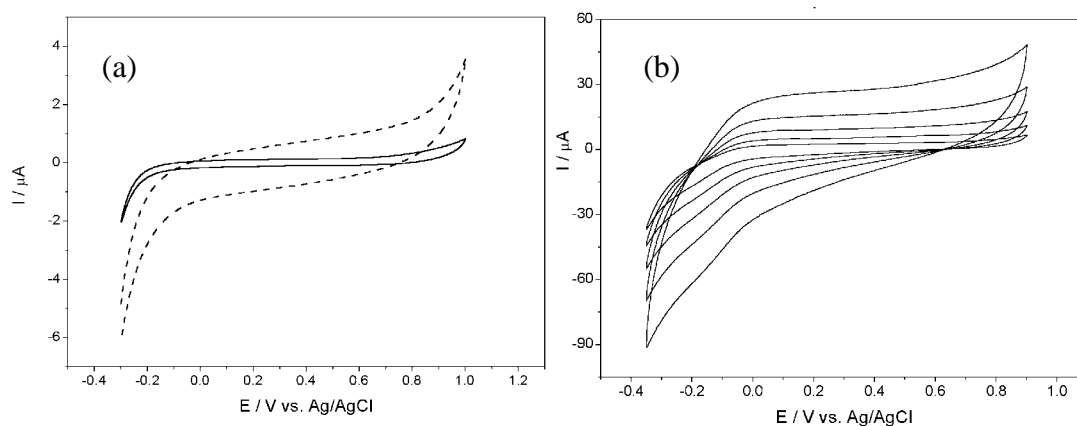
64

Figure 8.1.   *Cyclic voltammograms obtained with CCE composed of CNF and graphite particles (1:3 ratio) (dashed) and only graphite particles (solid) (a) and cyclic voltammograms (scan rate = 0.01, 0.02, 0.04, 0.08 and 0.16 V s⁻¹) obtained with CCE composed of CNF and graphite particles (1:3 ratio) (b) immersed into 0.1 mol dm⁻³ aqueous KNO₃.*

Experiments conducted with neutral redox probe - $Fc(CH_2OH)_2$ dissolved in the aqueous electrolyte solution using the same electrodes results in the well-defined nature of voltammetric responses (Fig. 8.2).
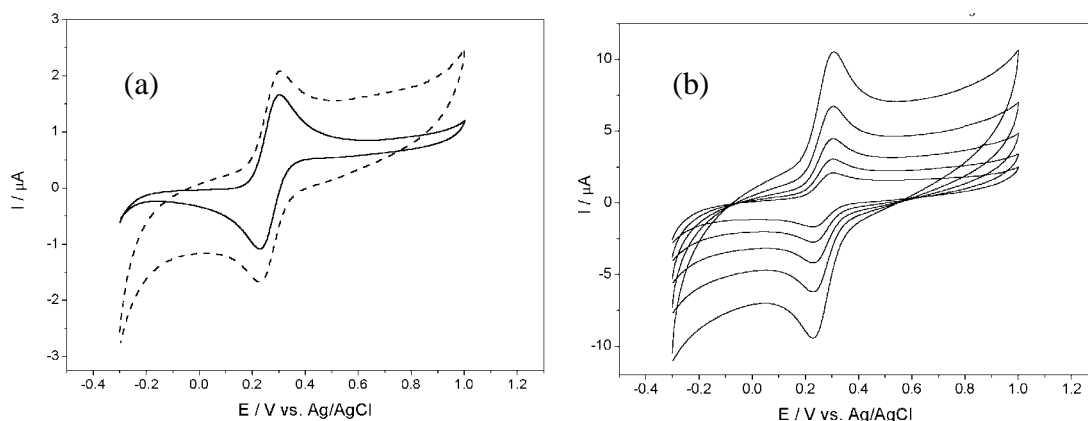

Figure 8.2.   *Cyclic voltammograms obtained with CCE composed of CNF and graphite particles (1:3 ratio) (dashed) and only graphite particles (solid) (a) and cyclic voltammograms (v = 0.01, 0.02, 0.04, 0.08 and 0.16 V s⁻¹) obtained with CCE composed of CNF and graphite particles (1:3 ratio) (b) immersed in 0.001 mol dm⁻³ Fc(CH₂OH)₂ solution in 0.1 mol dm⁻³ aqueous KNO₃.*

One can observe, that the CV curves have a well-defined peaks for both oxidation and reduction processes with a midpoint potential at 0.23 V vs. Ag/AgCl and peak-to-peak separation only 40 mV. Such behavior of voltammograms as well as non-linear dependence of peak current on square root of scan rate (not shown) can indicate partial adsorption of redox species on CNFs. The peak current for the diffusion controlled

oxidation of $Fc(CH_2OH)_2$ under these conditions ($D = 1 \times 10^{-9}$ m^2 s^{-1} [166], $v =$ 0.16 V s^{-1}) I_p, calculated from Randles-Sevcik equation (1.18), is equal 10.5 µA. It is larger than the measured peak current, $I_p = 6.6$ µA, indicating that only fraction of the geometric electrode surface is electrochemically active for this redox reaction. This is understandable because of heterogeneous structure of CCE (see Fig. 7.3). As a results only fraction of the surface is electronically conductive and accesses by the redox probe molecules present in the aqueous solution. Interestingly, the replacement of fraction of graphite particles with CNF having much larger apparent surface leads only to moderate increase of the current (Fig. 8.2, a). This indicates that electrical double layer builds up at larger surface not necessary accessible by the redox probe molecules present in solution. The further increase of CNF fraction failed because of the mechanical instability of the electrode material.

Further studies were performed with CCE modified with redox liquid. Below, the stability of cyclic voltammograms, its features and proposed mechanism of the electrode reaction are shown. At the end of this Chapter, this mechanism will be proven and the factors affecting an ion transfer across liquid / liquid interface will be presented.

8.2   Stability of cyclic voltammograms

To obtain conditions of electrode where the ion transfer across liquid / liquid interface are in dynamic equilibrium, the special attention was paid to the stability of the voltammetric response of CCE. As an example, the first few CV cycles obtained with CCE modified with tBuFc solution in NB are presented on Fig. 8.3.

The voltammogram obtained with pure solvent modified CCE is characterized by the absence of peaks. Therefore, the peak shaped form of voltammograms obtained with CCE modified tBuFc solution in NB is connected with the electrooxidation of this redox probe (8.1) [85]:

$$t\text{BuFc}_{(org)} - e \leftrightarrow t\text{BuFc}^+_{(org)} \tag{8.1}$$

The peak current gradually decreases during subsequent cycles with the largest difference between first and second cycle. A constant value is reached after 5-7 cycles. The increase of current magnitude after keeping the electrode at open circuit potential is caused by morphology of the electrode body. This effect will be described later (see p. 74).
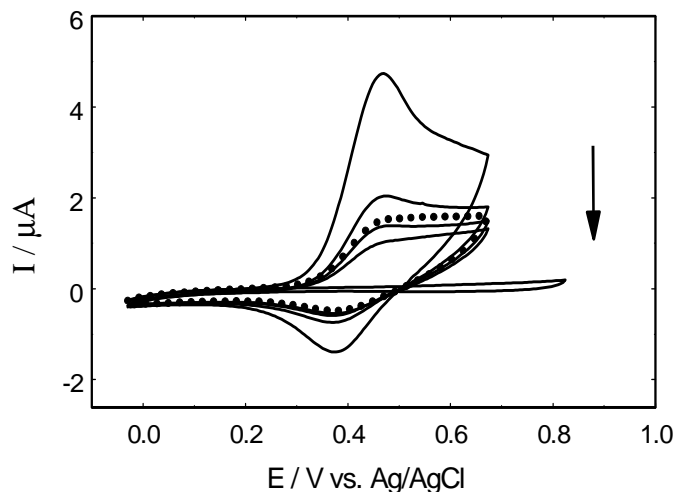
Figure 8.3.   Cyclic voltammograms obtained with CCE modified with 0.0045 mol dm⁻³ tBuFc solution in NB immersed in 0.1 mol dm⁻³ aqueous KNO₃. 1, 3, 5, 7ᵗʰ cycles are presented and the arrow shows increasing number of cycles. The flat curve with current much below 0.5 µA was obtained with CCE modified with pure NB. The dotted curve was obtained after 7ᵗʰ cycle and 15 min at open circuit potential.

It was observed that the stability of voltammograms in subsequent cycles is affected by four important factors. These are type of the redox probe, anion present in the aqueous phase and their concentration. The effects of all these factors are presented below.

Fig. 8.4 shows subsequent cyclic voltammograms obtained with CCE modified with ferrocene and its derivatives, SFc, solution in NPOE. Electrooxidation of SFc is observed in all cases. It is easily seen that the shape of the voltammetric signal depends on the type of SFc dissolved in the organic phase. The magnitude of the current decreases on repeated oxidation and reduction cycles. In the case of DMFc and *t*BuFc solution modified electrode (Fig. 8.4, b and c) a stable voltammogram is obtained after 7-10 scans. For electrode modified with Fc solution, even after 20ᵗʰ polarization cycle a further current decrease is observed.

One can analyze the stability of voltammograms in terms of the electric charges passed during the anodic, Q_a, and cathodic, Q_c, processes as well as their ratio, Q_a/Q_c. They also decrease during the first few cycles (Fig. 8.5).
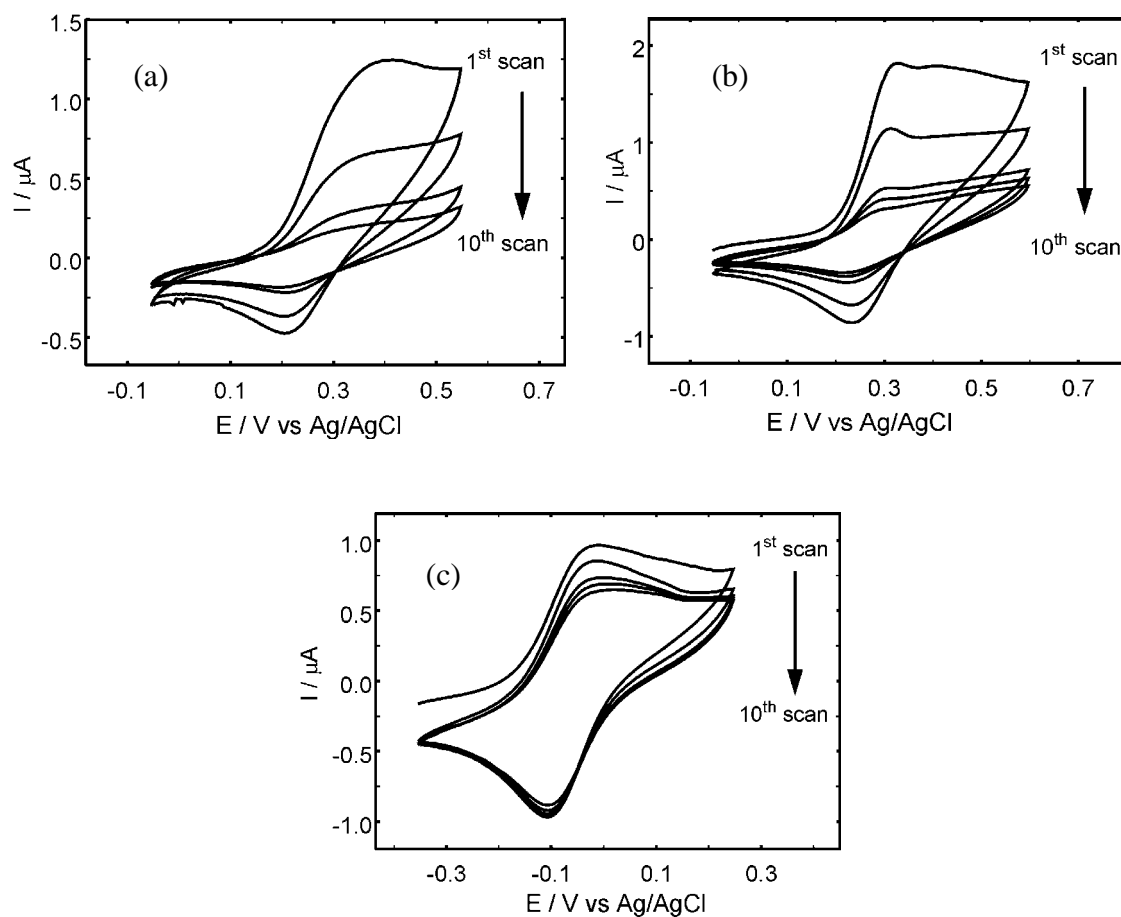
Figure 8.4.   *Cyclic voltammograms obtained with CCE modified with 0.01 mol dm^{-3} Fc (a), tBuFc (b) and DMFc (c) solution in NPOE immersed in 0.1 mol dm^{-3} aqueous KClO$_4$. 1st, 2nd, 5th, 7th and 10th cycles are presented and the arrow shows increasing number of cycles.*
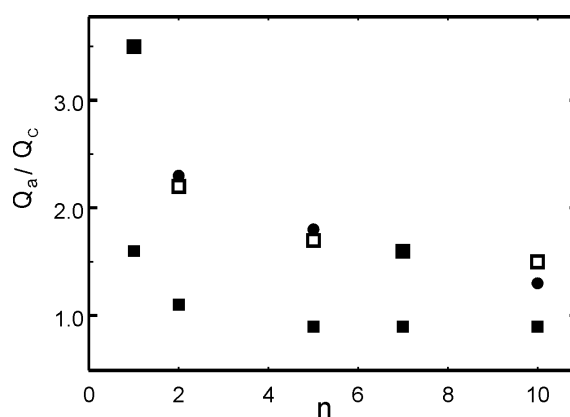

Figure 8.5.   *Plot of the ratio of anodic to cathodic charges (Q$_a$/Q$_c$) vs. number of cycle, n, for a CCE modified with 0.01 mol dm^{-3} Fc (●), tBuFc (□) and DMFc (■) solution in NPOE immersed in 0.1 mol dm^{-3} aqueous KClO$_4$ (condition as at Fig. 8.4).*

The values of Q_a, and Q_c were obtained by the integration of peak shaped responses in voltammograms. For tBuFc and Fc the values of ratio Q_a/Q_c are quite similar and always much larger than unity, whereas for DMFc starting from the second cycle this value is closed to unity. Evidently, the stability of voltammetric curves increases going from Fc and tBuFc to DMFc.

It is important, that the shape of the voltammograms and the value Q_a/Q_c may depend on the end potential, E_e, (see Fig. 4.1), which in a given experiment is arbitrarily selected. After a few cycles, when stable voltammogram was obtained, E_e was shifted by +0.05 V increment and procedure was repeated. The selection of E_e also affects the current magnitude over all potential range (Fig. 8.6).
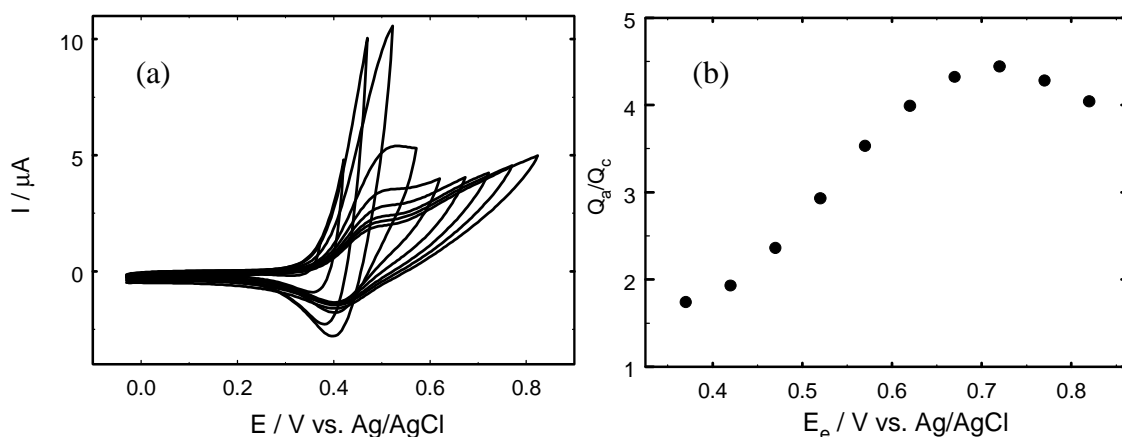

Figure 8.6.   *Cyclic voltammograms (a) with different end potential, E_e, obtained with CCE modified with 0.045 mol dm^{-3} tBuFc solution in NB immersed in 0.1 mol dm^{-3} aqueous KNO$_3$. The plot of Q_a/Q_c vs. E_e (b) was obtained from the data presented on (a).*

The ratio Q_a/Q_c intensely increases from 1.6 to 5 for E_e going from 0.3 V to 0.7 V. For E_e more positive than 0.7 this effect is reversed. Obviously, the more positive E_e the smaller fraction of tBuFc$^+$ is reduced during the backward scan.

Since there is some mutual solubility of NB in water and water in NB (see Table 6.1), the influence of the presence or absence of NB in the aqueous solution on voltammetric results was checked. This problem seems to be less important for NPOE or NPPhE modified electrodes, because of smaller solubility of these solvents in water (see Table 6.1). For this purpose, the voltammetric experiments in the aqueous solutions saturated with NB were performed. It was observed that the degree of systematic decrease of the current during first few cycles did not much differ from that obtained in

69

the absence of NB in aqueous phase. Thus, the initial decrease of the current magnitude (Fig. 8.3) is not connected with dissolution of NB in the aqueous phase or enrichment of the organic phase with water. Moreover, it seems to that despite the larger density of NB than water, the gravity force is compensated by the capillary forces and hydrophobic interactions with silicate matrix. One can conclude, that although the voltammetric response of CCE depends on its history, the conditions for stable voltammograms can be found. From these reasons in further experiments the aqueous phase was not saturated with polar organic solvent, as well as the organic phase was not saturated with water.

8.3   Features of cyclic voltammograms

To understand the nature of electrode process the experiments at different scan rates were carried out. As an example, the CV curves obtained with CCE modified with *t*BuFc in NB are presented. The shape of the voltammograms recorded at larger scan rate (Fig. 8.7, a) apparently claims that there is a quasi-reversible heterogeneous electron transfer reaction, because of the increasing difference between peak potentials, ΔE_p.
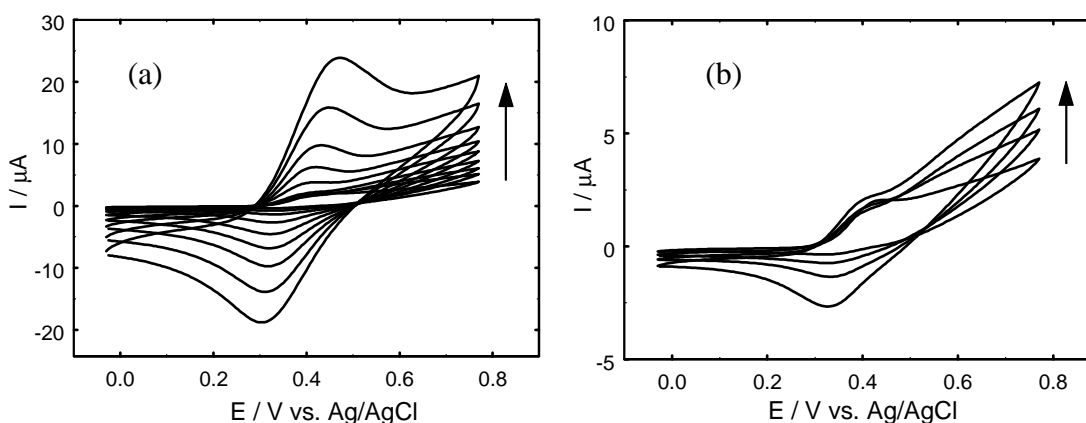

Figure 8.7.   Cyclic voltammograms obtained with CCE modified with 0.045 mol dm^{-3} tBuFc solution in NB immersed in 0.01 mol dm^{-3} aqueous KNO$_3$ for different scan rate, v: 0.00125 $\leq$ v $\leq$ 0.64 V s^{-1} (a) and 0.00125 $\leq$ v $\leq$ 0.020 V s^{-1} (b). The arrows show increasing scan rate.

At slower scan rate (Fig. 8.7, b) the anodic peak current does not significantly depends on scan rate, opposite to the cathodic peak current.

70

The linear dependence of anodic peak current, I_p, on square root of scan rate, $v^{1/2}$, (Fig. 8.8, a) indicates that electrode reaction is controlled by diffusion of reactants.
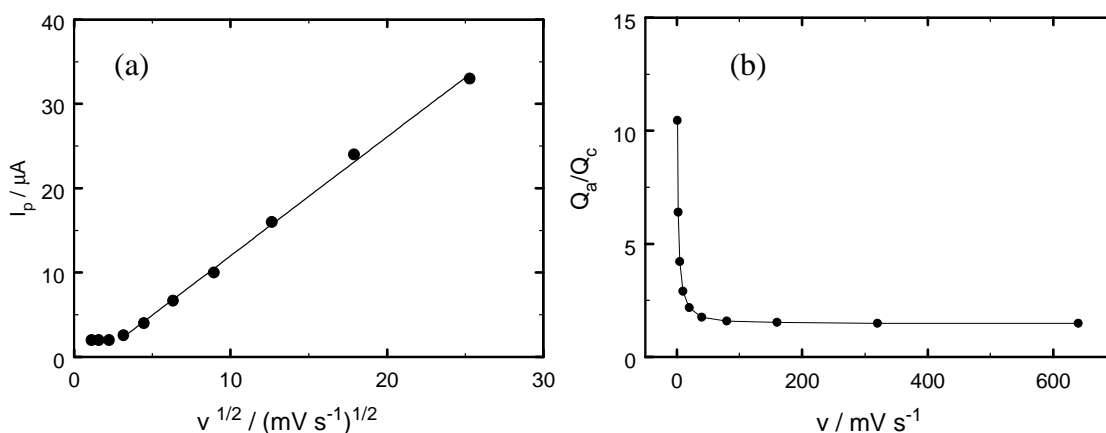

Figure 8.8.   *The plot of anodic peak current, I_p, vs. square root of scan rate, $v^{1/2}$, (a) and the plot of anodic to cathodic charge ratio, Q_a/Q_c vs. $v^{1/2}$ (b). The latter parameter was obtained from data presented on Fig. 8.7 (a).*

The noticeable deviation for anodic peak current at smallest v from linear dependence is concomitant with the appearance of poorly developed peak at more negative potentials. In the case of cathodic process this deviation does not occur. The value ΔE_p is larger than 0.059 V for $v \geq 0.01$ V s^{-1} and it is proportional to v. It indicates some kinetic control of the electrode reaction at faster scan rates. The value Q_a/Q_c is larger than unity and it depends on v indicating that the fraction of tBuFc$^+$ rereduced during reverse scan is affected by this parameter (Fig. 8.8, b). At some faster scan rate Q_a/Q_c becomes independent of v but still is larger than unity.

It is reasonable to expect that size of conductive particles and composition of CCE affect the features of cyclic voltammograms. The beneficial effect from the use of CNF can be seen after modification with redox liquid. The corresponding cyclic voltammograms are presented in Fig. 8.9. The effect of the nature of conductive particles on the efficiency of electrode process is visible. Efficiency of the electrode process is defined as the ratio of observed charge passed during the electrode process to theoretical charge calculated on base of amount of electroactive substrate. In the presence of CNFs significantly higher peak currents are observed. This can be explained with the extended length of the three phase junction electrode / organic liquid / aqueous solution present in the highly porous CNF composite material.
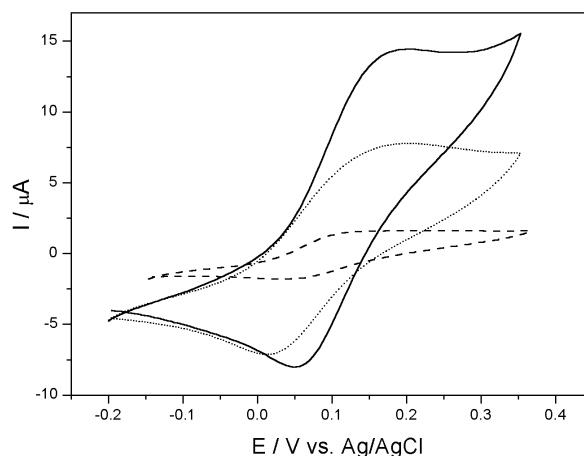
71

Figure 8.9.   Cyclic voltammograms obtained with CCE composed of CNF (solid), CNF and graphite particles (1:3 ratio) (dotted) and graphite particles (dashed), modified with 0.01 mol dm^{-3} DMFc solution in NPOE immersed into 0.1 mol dm^{-3} aqueous NaCl.

Although the highest current was detected for CNF-based CCE, we observed that addition of graphite particles improves the mechanical stability of the electrodes. Therefore for further studies the electrode prepared with CNFs and graphite particles ratio equal 1 : 3 was used.

8.4   Mechanism of the electrode reaction

It seems to that from this point the obtained results can be discussed in terms of the most possible and foreseen mechanism of the electrode reaction. It appears to be similar to that previously proposed for electrodes modified with drop or droplets of redox probe solution in polar hydrophobic solvent [15] presented in Chapter 2.

In general, the polarization of the electrode towards positive potential results in electrochemical oxidation of SFc in the organic phase:

$$SFc_{(org)} - e_{(electrode)} \leftrightarrow SFc^{+}_{(org)} \tag{8.2}$$

In order to maintain electroneutrality with organic phase, this reaction generates the transfer of the anion from the aqueous phase:

$$SFc^{+}_{(org)} + X^{-}_{(aq)} \rightarrow SFc^{+}_{(org)} + X^{-}_{(org)} \tag{8.3}$$

or/and the transfer of the electrogenerated cation to the aqueous phase:

$$SFc^{+}_{(org)} \rightarrow SFc^{+}_{(aq)} \tag{8.4}$$

The decrease of the voltammetric response with consecutive potential cycles (Fig. 8.4)

72

and large value of Q_a/Q_c (Fig. 8.5) can be attributed to the loss of SFc$^+$ from the organic to the aqueous phase (8.4). This process seems to dominate for less hydrophobic redox probes: Fc and *t*BuFc.

To confirm the significance of expulsion reaction (8.4) few experiments with the second electrode positioned close to CCE surface (Fig. 5.1) and polarized at a potential of the SFc$^+$ reduction were performed. Both CV (Fig. 8.10) and CA (Fig. 8.11) techniques were applied.
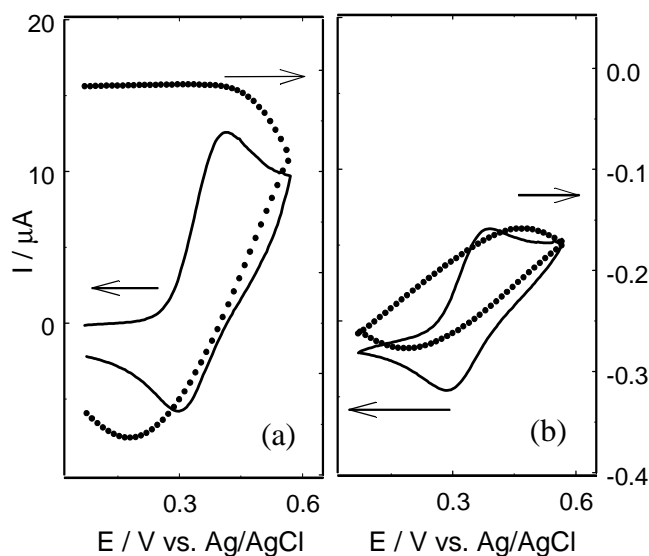

Figure 8.10. *Cyclic voltammograms obtained with CCE (solid) modified with 0.1 mol dm^{-3} tBuFc solution in NB and Au disk electrode (dotted) in 0.1 mol dm^{-3} aqueous KNO$_3$. (see Fig 5.1 for details of experimental setup). The arrows show corresponding axis. First scan (a) and stable scan (b).*

The second electrode (Au disc) was positioned in the aqueous phase 0.3 mm from CCE surface according to Fig. 5.1 and it was polarized at 0.2 V, potential enabling detection of *t*BuFc$^+$ cations in the aqueous phase. The cathodic current recorded at Au electrode follows with some delay to the voltammogram obtained on CCE. During the first cycle (Fig. 8.10, a) it starts to increase from zero at potential more positive than anodic peak potential, $E_{p,a}$, and it passes a minimum at potential more negative than cathodic peak potential, $E_{p,c}$. The observation of cathodic current indicates ejection of *t*BuFc$^+$ cations into the aqueous phase (Fig. 8.10, b). When the shape of voltammogram recorded at CCE became stable during subsequent scans it is approximately followed by curve recorded at Au electrode with maximum and minimum shifted towards more positive and negative potentials. Since, the current magnitude of the stable cycle is smaller in

73

comparison to the first cycle, smaller amount of tBuFc$^+$ escapes from the organic phase during the stable cycle. The results of CA experiments (Fig. 8.11) show the cathodic current recorded at Au electrode, which was polarized at potential of tBuFc$^+$ reduction, sharply increases when CCE is polarized at the potential corresponding to tBuFc electrooxidation.
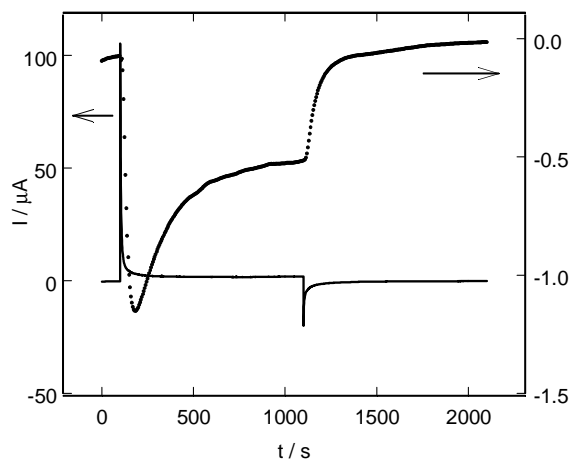

Figure 8.11.   The I vs. t plot obtained with CCE (solid) modified with 0.1 mol dm^{-3} tBuFc solution in NB and Au disk electrode (dotted) in 0.1 mol dm^{-3} aqueous KNO$_3$. The CCE was polarized steeply at 0.1, 0.6 and 0.1 V vs. Ag/AgCl during 100, 1000 and 1000 s, respectively. The arrows show corresponding axis.

One can conclude, the ejection of tBuFc$^+$ into aqueous phase at beginning of polarization is the highest, then it reaches an almost stable value. Further decrease of cathodic current after potential step back to 0.1 V vs. Ag/AgCl is connected with electrolysis of tBuFc$^+$ cations presented in the aqueous phase.

With regard to above experiments one can conclude the part of electrogenerated tBuFc$^+$ dissolves in the aqueous phase. The ejection of organic cations to the aqueous phase probably results in continuous development of tBuFc concentration gradient in the organic phase, perpendicular to the organic / aqueous interface (Fig. 8.12). The decrease of "effective" bulk concentration of neutral form of redox probe probably occurs. Therefore, the diminishing anodic current during first cycles is caused by decreasing tBuFc concentration gradient. The stable voltammogram as well as the steady state current obtained at longer time in CA experiment at CCE indicates that after a few cycles the concentration gradient of tBuFc near the liquid / liquid interface becomes constant. It means that from this moment the same amount of electrogenerated

74

cation is expelled from the organic phase during every subsequent CV cycle.

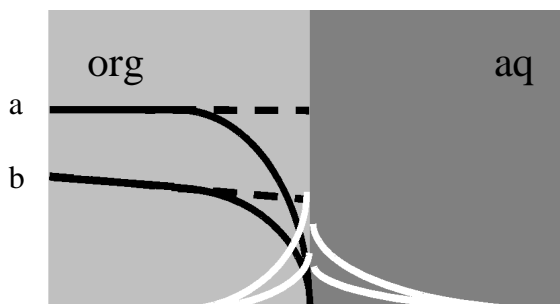*Figure 8.12.   Schematic representation of SFc (black) and SFc⁺ (white) concentration as a function of the distance from the organic / aqueous interface at CCE. The dashed and solid lines represent concentration profile at the most negative and the most positive potential, respectively. a and b correspond to first and stable voltammetric cycles, respectively.*

Interestingly when CCE is kept for some time at open circuit potential (no *t*BuFc is oxidized) the current magnitude increases (Fig. 8.3) as a consequence of the increase of *t*BuFc "effective" concentration. This result supports the evidence of a continuous supply of redox probe molecules from the CCE bulk.

As a consequence of the above conclusions, it is reasonable to assume that the redox liquid fills the opened pores of the matrix close to the electrode surface and chinks between graphite aggregates and the matrix (see Fig. 7.3). Due to attractive interaction between hydrophobic electrogenerated cations and free electron pair of oxygen atom of silicate matrix (Fig. 3.1) the stabilizing effect of the organic phase in the mesoporous silica host was previously suggested [22, 21, 61]. This can be also the case of the studied electrode.

8.5   Redox probe concentration effect

Some CV data enabling to analyse the redox probe effect has already been presented in Chapter 8.2. There is an evidential influence of SFc hydrophobicity on stability of voltammetric response obtained at CCE. The potential for the redox process (8.1), $E_{Red/Ox}$, can be determined from E_{mid} of stable cycles. From data shown on Fig. 8.4 $E_{Red/Ox}$ (Fc) = 0.30 V vs. Ag/AgCl, $E_{Red/Ox}$ (*t*BuFc) = 0.28 V vs. Ag/AgCl and $E_{Red/Ox}$ (DMFc) = -0.06 V vs. Ag/AgCl are obtained. These potential values are consistent with literature reports for the oxidation in continuous organic solvent phase [167, 168].

However, different stability of voltammograms for all three SFc indicates at least two competing reactions (8.3 and 8.4). The expulsion process (8.4) seems to dominate for the least hydrophobic redox probe, Fc. The competition between insertion (8.3) and expulsion (8.4) is most probable for *t*BuFc. Finally, the transfer of the anion from the aqueous phase seems to dominate for DMFc, the most hydrophobic redox probe.

In order to investigate the effect of the redox probe concentration in the organic phase the experiments with different concentrations of *t*BuFc in the organic phase, $c_{tBuFc(org)}$, were performed (Fig. 8.13).
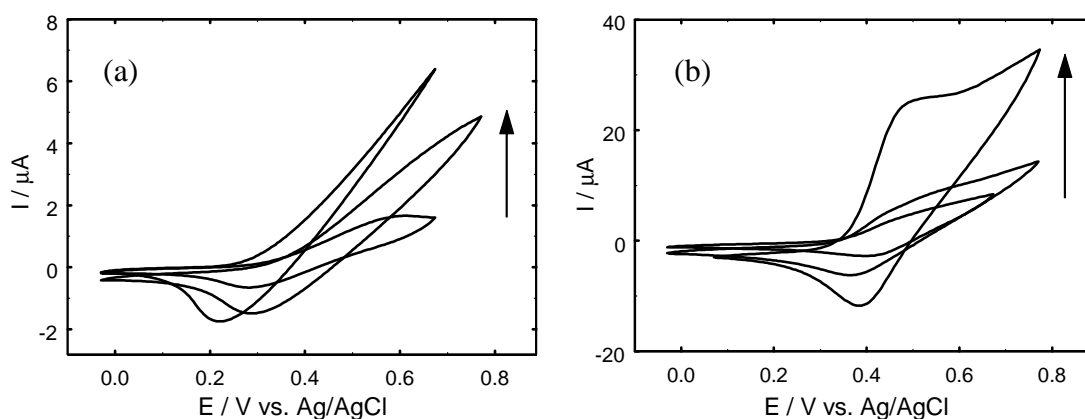

Figure 8.13.   Cyclic voltammograms obtained with CCE modified with 0.0045, 0.045, 0.45 mol dm^{-3} tBuFc solution in NB immersed in 0.001 (a) and 0.1 (b) mol dm^{-3} aqueous KNO$_3$. The arrows show increasing of tBuFc concentration.

The shape of the cyclic voltammograms and the current magnitude depend on $c_{tBuFc(org)}$. The voltammograms are peak-shaped with noticeable exception for those obtained for the largest ratio $c_{tBuFc(org)}/c_{X^-}$, where c_{X^-} is the concentration of salt in the aqueous phase. More about this phenomenon can be found in Chapter 8.7. Interestingly, no significant effect of E_{mid} on $c_{tBuFc(org)}$ is visible.

8.6   Solvent effect

It is no wonder that organic solvent affects the rate of transport of reactants, either of redox probe or counter ions within organic phase. As a consequence the current is expected to depend on the type of solvent (Fig. 8. 14).
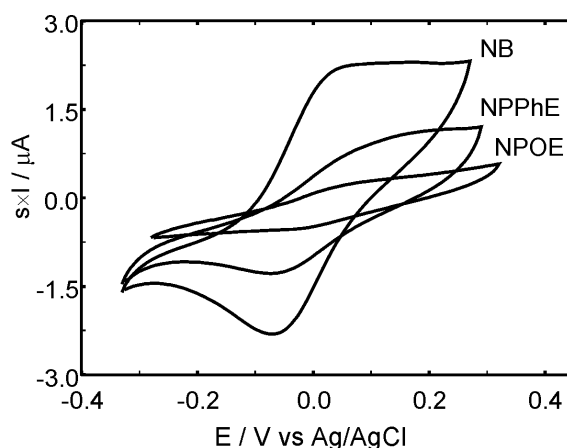
Figure 8.14.   Cyclic voltammograms (10th scan) obtained with CCE modified with 0.01 mol dm^{-3} DMFc solution in NB (s = 1), NPOE (s = 5) and NPPhE (s = 5) immersed into 0.1 mol dm^{-3} aqueous KNO$_3$.

For spherical molecule [169] its diffusion coefficient D in a solvent of viscosity, η, can be calculated from Stokes-Einstein equation [170]:

$$D = kT/6\pi\eta a \tag{8.5}$$

where k and a are Boltzman constant and radii of molecule, respectively.

The value of η of solvent influences on the value of D of species moving in this solvent. In turn the latter parameter affects magnitude of the current, thus from Randles-Sevcik equation (1.18) one would expect that the peak currents in these solvents will decrease in the order NB > NPPhE > NPOE. This trend is indeed observed (Fig. 8.14). One can conclude, the mass transport of ionic species in the organic phase affects the rate of electrode process. However, additional factors such as the mutual solubility of the solvent in aqueous environments and the interfacial tension may also affect observed dependence.

To continue the mass transport calculation it is possible to estimate diffusion coefficient of reactant in polar solvent, such as NB, using equation (8.5). The *t*BuFc radius is assumed to be 0.37 nm, value appropriate for metallocenes [171]. The value of diffusion coefficient of *t*BuFc is equal to 4.8×10^{-7} cm^2 s^{-1}. According to Randles-Sevcik equation (1.18) peak current obtained with CCE modified 0.01 mol dm^{-3} *t*BuFc solution NB is expected to be equal 5.8 μA. The estimated value is close to observed experimentally (Fig. 8.14). However, the surface of CCE is rough and real area is larger than geometric one, the observed magnitude of current is smaller than expected. The

77

reason of this effect is that, the electrode reaction occurs at only areas where three phases: graphite particle, organic and aqueous phase are in contact, namely at three-phase junction.

8.7   Anion concentration effect

The dependence of the current magnitude on concentration of the redox probe is comprehensible. However the dependence of the current magnitude on anion concentration is more surprising. If mechanism of the electrode reaction, namely the insertion of anion into the organic phase, is taken into account the influence anion concentration on the current magnitude becomes to be clear. The CV curves obtained with modified CCE immersed into the aqueous solution at different salt concentration are presented on Fig. 8.15.
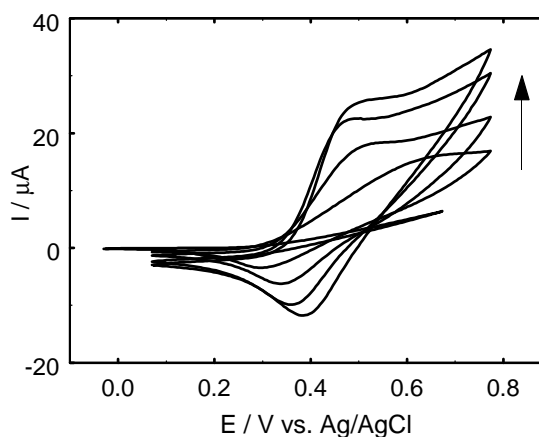

Figure 8.15.   Cyclic voltammograms obtained with CCE modified with 0.45 mol dm^{-3} tBuFc solution in NB immersed into 0.0001, 0.001, 0.01, 0.1 and 1 mol dm^{-3} aqueous KNO$_3$. The arrow shows increasing KNO$_3$ concentration.

The current magnitude is proportional to c_{X^-} and becomes larger for more concentrated SFc solution. Apparently, the ratio of anodic to cathodic peak current also depends on c_{X^-}. This effect may be discussed on the basis of Q_a/Q_c dependence on c_{X^-} for different concentration of redox probe in the organic phase (Fig. 8.16).

This plot can be analyzed in terms of the ratio of the redox probe and electrolyte concentration, $c_{tBuFc(org)}/c_{X^-}$. For largest ratio $c_{tBuFc(org)}/c_{X^-}$ the largest ratio Q_a/Q_c is observed and vice versa for the smallest $c_{tBuFc(org)}/c_{X^-}$ the smallest Q_a/Q_c is also observed.
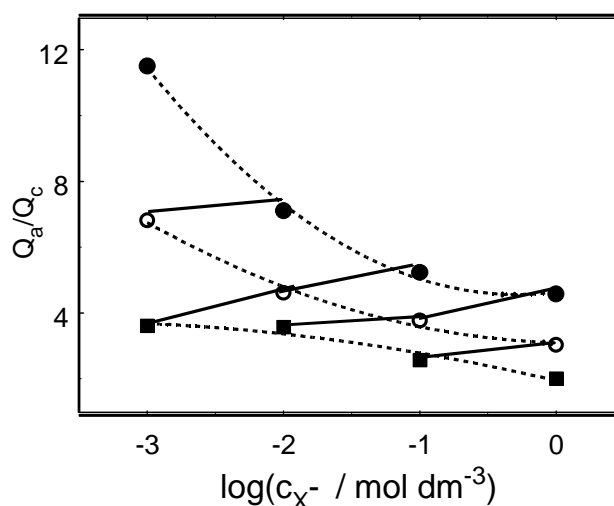
78

Figure 8.16.   *Plot of Q_a/Q_c vs. logarithm of c_{X^-}, log (c_{X^-}). Q_a/Q_c values were calculated from cyclic voltammograms obtained with CCE modified with 0.0045 (■), 0.045 (○) and 0.45 (●) mol dm^{-3} tBuFc solution in NB immersed into aqueous KNO$_3$. The solid lines connect the points for the same $c_{tBuFc(org)}/c_{X^-}$ ratio. The dashed lines connect points for the same redox probe concentration.*

The value of Q_a/Q_c ratio (Fig. 8.16) is also proportional to $c_{tBuFc(org)}$ indicating that for the larger $c_{tBuFc(org)}$ the larger fraction of tBuFc$^+$ is expelled to the aqueous phase. One can also conclude, that for the more diluted tBuFc solution and more concentrated electrolyte the smaller fraction of tBuFc$^+$ is expelled to the aqueous phase and contribution of anion insertion (8.3) in overall electrode reaction becomes more significant. This is opposite to the case of the largest $c_{tBuFc(org)}/c_{X^-}$, where the influence of the reaction (8.4) is dominating. One may conclude, in the absence of kinetic constrain for ion transfer across the liquid / liquid interface any deviation of Q_a/Q_c from unity can be explained by contribution of cation expulsion reaction (8.4).

Another way to estimate the contribution of reactions (8.3) and (8.4) in the overall electrode process can be based on thermodynamics by studying of the dependence $E_{Red/Ox}$ on c_{X^-} and $\Delta_{aq}^{NB}\varphi_{X^-}^0$ (see p. 83). For an electrode process involving the anion transfer from the aqueous to the organic phase electrogenerated by the electrooxidation of SFc in the organic phase, described by reaction (8.2) and (8.3), the $E_{Red/Ox}$ is expected to show a Nernstian dependence on the c_{X^-} described by equation similar to (2.6) [13]:

$$E_{Red/Ox} = E_{SFc_{org}^+/SFc_{org}}^0 + \Delta_{aq}^{NB}\varphi_{X^-}^0 - \frac{RT}{F}\ln c_{X^-} + \frac{RT}{F}\ln\frac{c_{SFc_{org}}^*}{2}, \qquad (8.6)$$

79

where $E^0_{SFc^+_{org}/SFc_{org}}$ is the standard redox potential of SFc/SFc$^+$ redox couple in the organic solution, c_{X^-} and $c^*_{SFc_{org}}$ are the initial concentrations of X$^-$ in the aqueous and SFc in the organic phase, respectively.

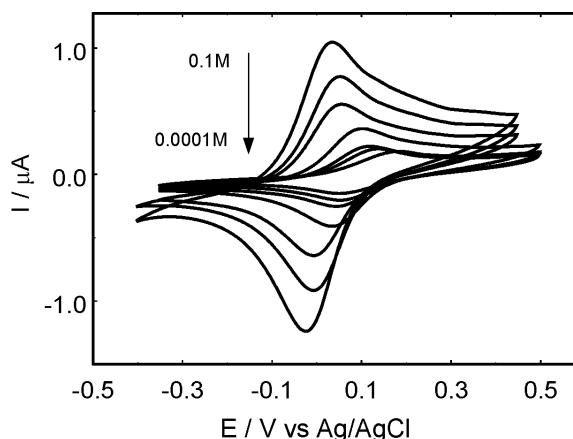The example of anion concentration effect is presented on Fig. 8.17.

Figure 8.17.   Cyclic voltammorgams obtained with CCE modified with 0.01 mol dm^{-3} DMFc solution in NPOE immersed in 0.0001, 0.0005, 0.001, 0.005, 0.01, 0.05 and 0.1 mol dm^{-3} aqueous KClO$_4$. The arrow shows decreasing KClO$_4$ concentration.

One can observe that the mid-peak potential systematically shifts towards more positive potentials as concentration of ClO$_4^-$ in the aqueous phase is decreased. This effect can be analyzed in terms of $E_{Red/Ox}$ vs. *log* c_{X^-} plot (Fig. 8.18), where the values of $E_{Red/Ox}$ were obtained from cyclic voltammograms as equal mid-peak potentials in Fig. 8.17.
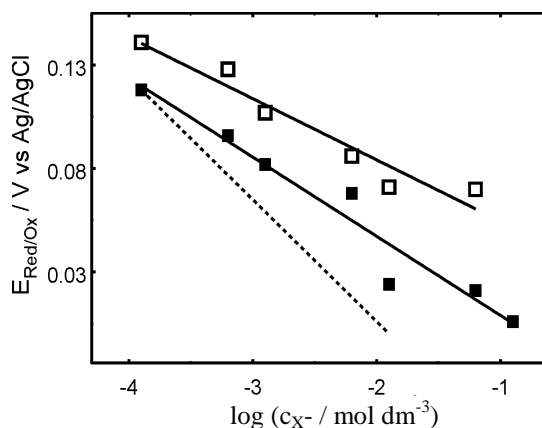

Figure 8.18.   Plot of $E_{Red/Ox}$ vs. log (c_{X^-}) for KClO$_4$ (■) and KCl (□). The straight lines were obtained by linear regression. The dotted line indicates a slope -0.059 V per decade change in concentration.

80

The approximately linear dependences are observed with sub-Nernstian slope (-0.038 V / decade) for ClO_4^- and (-0.030 V / decade) Cl^- anion. The change of $E_{Red/Ox}$ as function of c_{X^-} is more significant for more hydrophobic anion, ClO_4^-. For more hydrophilic Cl^- anion the larger deviation from Nernstian behavior is observed. Therefore, one can conclude that the larger contribution of cation expulsion reaction (8.4) is expected for anion with more hydrophilic properties. This deviation from Nernstian slope rather should not be attributed to the presence of the silicate matrix close to the liquid / liquid interface (see p. 88). The results of experiments with large number of anions with different hydrophobic-hydrophilic properties are presented in Chapter 8.8.

The electrolyte concentration also affects the peak currents, namely I_p is linearly dependent on c_{X^-} with positive slope (Fig. 8.19).
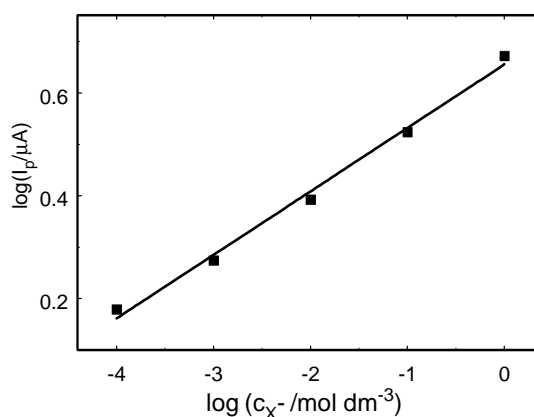

Figure 8.19.   Plot of log I_p vs. log c_{X^-} for CCE modified with 0.0045 mol dm^{-3} tBuFc solution in NB immersed into KNO$_3$ aqueous solution.

This effect was also observed for CCE impregnated with pure redox probe, *t*BuFc [40, 61]. It can be explained (at least in part) by the presence aqueous anions within the reaction zone and participation them in electrode reaction. The diffusion of the anion to the three-phase boundary becomes rate-limiting and therefore the peak currents are reduced.

8.8   Anion effect

To clarify the effect of anion on the direction of ion transfer across liquid / liquid interface, the experiments with CCE modified with SFc solution in hydrophobic polar solvent and immersed to the aqueous solution containing anions with different

81

hydrophobic-hydrophilic properties were done. The selection of anions was already presented in Table 6.2.

It was observed, that for some systems the shape of cyclic voltammograms is complex. In the presence of some anions in the aqueous phase the voltammetric peaks are not well-developed, making reliable estimation of the values $E_{Red/Ox}$ difficult. Reliable $E_{Red/Ox}$ values can be obtained from E_p [81, 145] of DPV curves, which are generally peak-shaped. Fig. 8.20 shows selected examples obtained with CCE composed of graphite particles (a) and mixture of CNF and graphite particles (b).
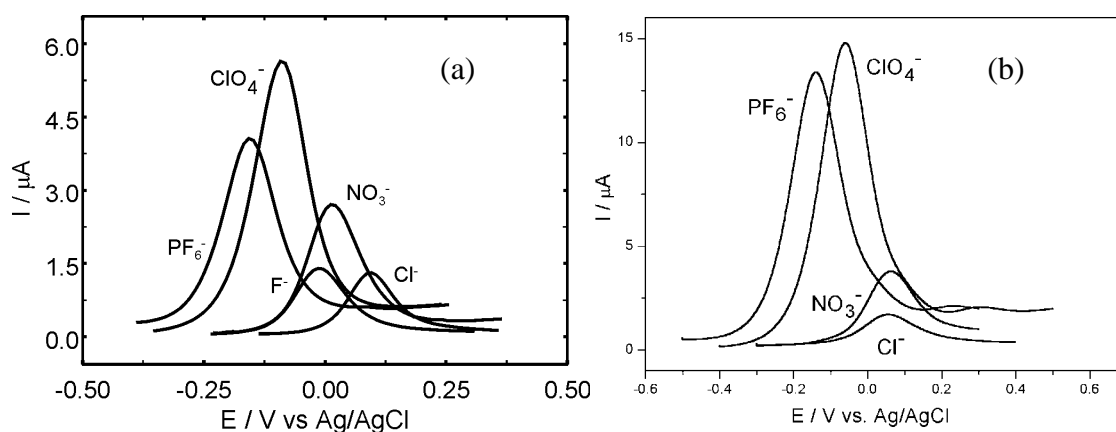

Figure 8.20.   *Differential pulse voltammograms (step potential 0.01 V, modulation amplitude 0.01 V, modulation time 0.05 s, interval time 1 s) obtained with CCE composed of graphite particles (a) and CNF with graphite particles (1:3 ratio) (b) modified with 0.01 mol dm^{-3} DMFc solution in NPOE immersed into 0.1 mol dm^{-3} aqueous solution containing: KPF$_6$, KClO$_4$, KNO$_3$, KCl or NaF.*

For both types of CCE one can observe that a shift of the voltammetric signals depends on the nature of the anions. Very similar effect is observed for other studied systems. The magnitude of the DPV peaks is larger for more hydrophobic anions. In this case the concentration of ions in the organic phase is larger and reaction zone can extend from triple-phase boundary into the organic phase. This is probably the reason that much higher current is detected. Whereas, the cation expulsion does not cause the build-up of ionic charge carries in the organic phase and voltammetric signals remain small. The similar influence of anions on the magnitude of DPV peak current was observed for cylindrical microelectrode immersed into two immiscible liquids: DMFc solution in NB and the salt aqueous solution [29].

The effect of anion on $E_{Red/Ox}$ can be analysed in terms of equation (8.6). Figs. 8.21 - 8.23 show the potential shift by plotting the measured peak potentials assumed to be equal $E_{Red/Ox}$ potential (see p. 49) as a function of $\Delta_{aq}^{NB}\varphi_{X^-}^0$ or $\Delta_{aq}^{NPOE}\varphi_{X^-}^0$.
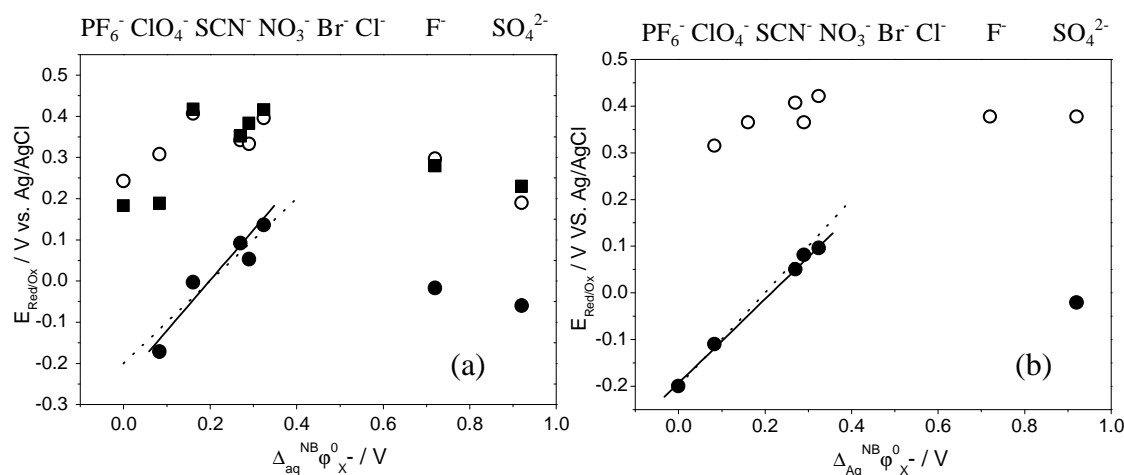

Figure 8.21.   Plot of $E_{Red/Ox}$ vs. $\Delta_{aq}^{NB}\varphi_{X^-}^0$ obtained with CCE modified with 0.01 mol dm^{-3} Fc (■), tBuFc (○) and DMFc (●) solution in NB (a) and NPPhE (b). The sequence of anions is indicated on the top of the plot. The slope of dotted line is equal unity. Solid line was obtained by linear regression.
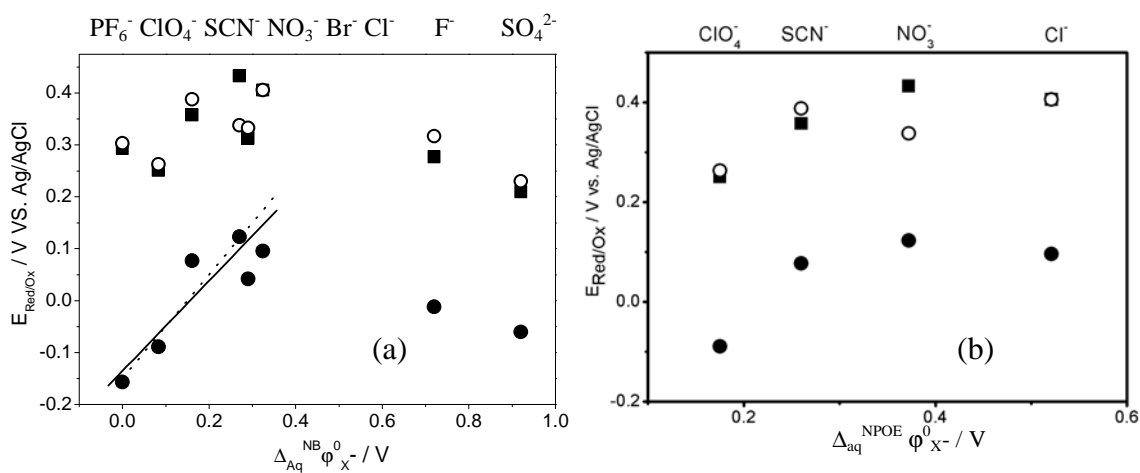
Figure 8.22.   Plots of $E_{Red/Ox}$ vs. $\Delta_{aq}^{NB}\varphi_{X^-}^0$ (a) and $\Delta_{aq}^{NPOE}\varphi_{X^-}^0$ (b) obtained with CCE modified with 0.01 mol dm^{-3} Fc (■), tBuFc (○) and DMFc (●) solution in NPOE. The sequence of anions is indicated on the top of the plot. The slope of dotted line is equal unity. Solid line was obtained by linear regression.

The points corresponding to some anions are not shown due to poor data quality.

Figure 8.23.   Plots of $E_{Red/Ox}$ vs. $\Delta_{aq}^{NB}\varphi_{X^-}^0$ (a) and $E_{Red/Ox}$ vs. $\Delta_{aq}^{NPOE}\varphi_{X^-}^0$ (b). $E_{Red/Ox}$ values were determined from DPV with CCE obtained with CNF, modified with 0.01 mol dm^{-3} DMFc solution in NPOE and immersed into 0.1 mol dm^{-3} aqueous salt solution. The sequence of anions is indicated on the top of the plot. The slope of dotted line is equal unity. Solid line was obtained by linear regression.
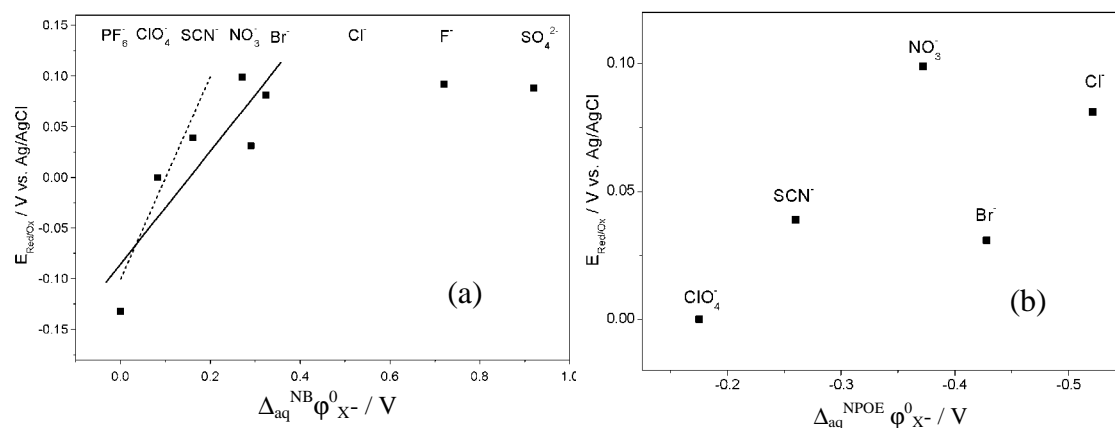
A purely thermodynamic explanation of the potential shift observed for different anions can be based on the Gibbs energy of transfer (see equation 8.6). For the coupled electron- and ion-transfer reaction steps (8.2 and 8.3) the linear dependence $E_{Red/Ox}$ vs. $\Delta_{aq}^{NB}\varphi_{X^-}^0$ is expected. Although the points in Figs. 8.21 - 8.23 are somewhat scattered, it is clear that in the presence of more hydrophobic anions, DMFc is oxidized at more negative potentials and the approximately linear dependence $\Delta_{aq}^{NB}\varphi_{X^-}^0$ with unity slope is observed (dashed lines). By including more data points a line with smaller slope (solid) can be drawn. It is reasonable to conclude that more hydrophobic anions are predominantly inserted into the organic phase after electrooxidation of the redox probe. On the other hand, the deviation of the slope from unity is caused by the more hydrophilic anions and indicates that the contribution of electrogenerated DMFc$^+$ cation ejection from the organic into the aqueous phase becomes important (equation 8.4). This cation transfer process clearly dominates in the presence of more hydrophilic anions like F$^-$ and SO$_4^{2-}$. A similar dependence of $E_{Red/Ox}$ on $\Delta_{aq}^{NB}\varphi_{X^-}^0$ was reported for experiments with pig electrode modified with a drop of DMFc solution in NB (Fig. 2.14) [38] and for bppg electrode modified with droplets of THPD solution in NB (Fig. 2.8) [15, 51].

For less hydrophobic redox probes, Fc and *t*BuFc solution in NB or NPOE and *t*BuFc solution in NPPhE (Figs. 8.21 and 8.22), the similar but less pronounced effects

84

are observed, indicating a preferable more hydrophilic electrogenerated cation expulsion to the aqueous phase (reaction 8.4). Interestingly, the lack of anion effect on $E_{Red/Ox}$ was also observed for undiluted tBuFc droplets deposited on bppg electrode [47]. Whereas some effect was observed for CCE impregnated with this redox probe indicating the influence of silicate matrix [21].

On the basis of the above results preliminary conclusions about mechanism of electrogenerated ion transfer studied can be drawn (Fig. 8.24).
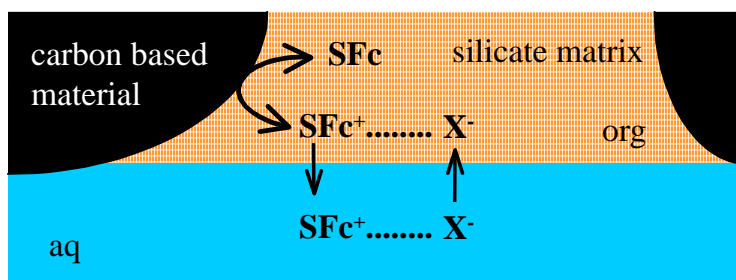

Figure 8.24. *The scheme of the three-phase junction and possible ion transfers across liquid / liquid interface supported by CCE modified with redox probe solution in organic polar solvent.*

As it was already examined by SEM small aggregates of graphite particles or CNFs (Fig. 8.24) within a mesoporous silicate matrix are present on the surface of CCE. They act as a source or sink of electrons. Redox liquid fills hydrophobic pores of the matrix close to the electrode surface. The redox probe undergoes the electrooxidation at potential close to $E_{Red/Ox}$ exchanging electrons with graphite particles being in contact with the aqueous phase. Two types of ion transfer reaction across liquid / liquid interface occur in order to maintain the electroneutrality of the organic phase. Their contribution depends on the hydrophobic / hydrophilic properties of redox probes and anions present in the aqueous phase. The insertion of anion from the aqueous to organic phase is preferred for the most hydrophobic redox probe: DMFc and less hydrophilic electrolyte anions. The ejection of electrogenerated cation to the aqueous phase dominates for less hydrophobic redox probes: Fc and tBuFc and more hydrophilic electrolyte anions: F^- and SO_4^{2-}. The last process leads to the loss of redox probe but it is compensated by the continuous supply of redox active molecules from the bulk of the electrode (see Fig. 8.12).

In order to qualitatively estimate the influence of redox probe on mechanism of ion transfer across liquid / liquid interface the slope of $E_{Red/Ox}$ vs. $\Delta_{aq}^{NB}\varphi_{X^-}^0$ dependence obtained in the presence of more hydrophobic anions can be compared (Table 8.1).

Table 8.1.   The slopes of $E_{Red/Ox}$ vs. $\Delta_{aq}^{NB}\varphi_{X^-}^0$ dependence for different types of CCE and different redox liquid systems. Data for PF_6^-, ClO_4^-, SCN^-, NO_3^-, Br^- and Cl^- anions were arbitrarily selected.

Electrode	Redox system		Slope
CCE (20 μm graphite particles)	NB	Fc	0.39 ± 0.19
		tBuFc	0.74 ± 0.29
		DMFc	1.22 ± 0.21
	NPOE	Fc	0.50 ± 0.16
		tBuFc	0.32 ± 0.18
		DMFc	0.87 ± 0.21
	NPPhE	tBuFc	0.43 ± 0.05
		DMFc	0.90 ± 0.03
CCE (20 μm graphite particles with CNFs)	NPOE	tBuFc	0.56 ± 0.16

It is clearly visible that unity slope is observed only for DMFc-based system. As it was mentioned before this redox probe is highly hydrophobic and insertion of anion to the aqueous phase is preferable. It means, that for DMFc based redox liquids the transfer counterion from the aqueous to organic phase dominates for all types of CCE. On the other hand the strong deviation of the slope of $E_{Red/Ox}$ vs. $\Delta_{aq}^{NB}\varphi_{X^-}^0$ plot from unity indicates that electrogenerated cation ejection is important for Fc and tBuFc based systems. Clearly, the less hydrophobic electrooxidized redox probe is more easily ejected to the aqueous solution. This reaction seems to dominate for all studied electrodes immersed into hydrophilic F^- or SO_4^{2-} electrolyte solutions.

Chapter 9.   Ion transfer across hydrophobic polar solvent / aqueous phase solution supported by carbon paste electrode

To comprehend whether the silicate matrix affects the voltammetric response of electrode modified with redox liquid and mechanism of ion transfer across liquid / liquid interface, it was eliminated from the electrode. For this purpose the redox probe solution in viscous organic polar solvent – NPOE was directly mixed with graphite powder. This mixture was used for preparation of electroactive CPE in analogous way to that introduced four decades ago by Kuwana and French [172]. Although the use of NPOE as a binder in CPE was once reported [154], no electrogenerated ion transfer across liquid / liquid interface was detected.

The formation of the three-phase junction on the surface of electronically conductive particles present close to the liquid / liquid interface formed by organic phase at CPE can be related to that formed at CCE modified with the organic phase (Fig. 9.1). The absence or presence of silicate matrix seems to be the only difference.
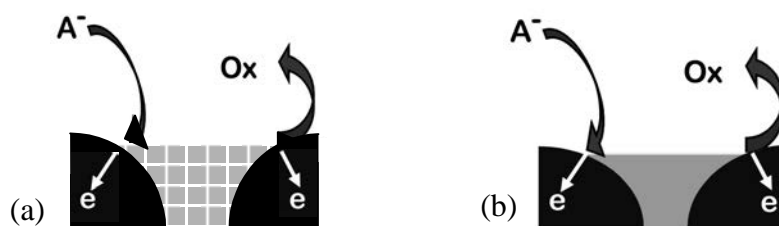

Figure 9.1.   *The schematic drawing showing electrochemistry of redox probe dissolved in an organic solvent deposited into CCE (a) and dissolved in a viscous organic solvent acting as a binder of CPE (b).*

9.1   Features of cyclic voltammograms

The importance of the presence of the three-phase junction at CPE is confirmed by experiments with different size of graphite particles. Obviously, the decrease of their size causes the increase of peak current (Fig. 9.2). This is caused by the increase of efficiency of the electrode process by the presence of smaller graphite particles or CNF's.

This effect can be explained by extension of the length of triple-phase boundary in the presence of smaller conductive particles. The significant increase of the peak

current in the presence of CNFs is qualitatively similar to results observed with CCE (Fig. 8.9) prepared with mixture CNF and graphite particles in the same ratio.
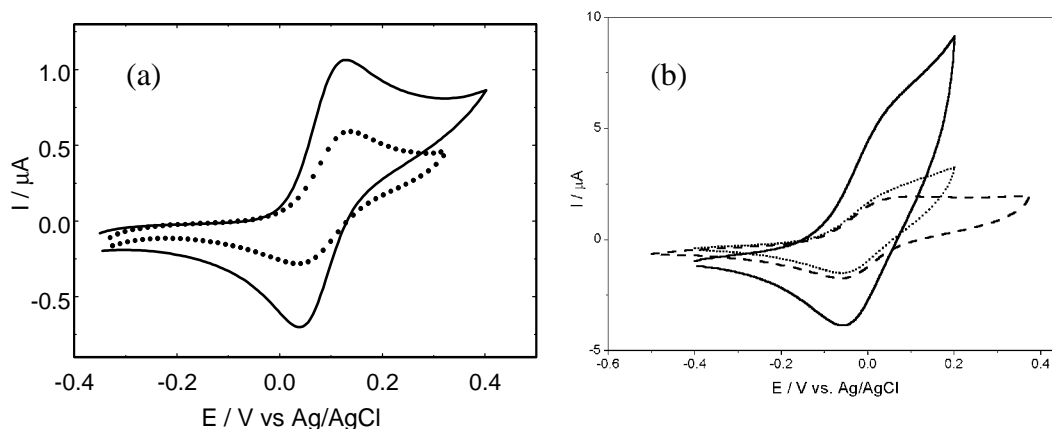

Figure 9.2.   Cyclic voltammograms obtained with 0.01 mol dm^{-3} DMFc solution in NPOE modified CPE composed of graphite particles having diameter 1 μm (solid line) and 20 μm (dotted line) immersed in 0.1 mol dm^{-3} aqueous KCl (a) and CPE composed of CNF (solid), CNF and graphite particles (1:3 ratio) (dotted) and graphite particles (dashed) (b) immersed into 0.1 mol dm^{-3} aqueous NaClO$_4$.

Obviously the effect of silicate matrix on this phenomenon seems to be not important.

Therefore one may conclude that similarly to the drop or droplets based system the electrode process occurs at the three-phase junction (Fig. 9.1, b). It is presumably formed at circumference of graphite particles or CNFs at the surface of CPE.

9.2   Stability of cyclic voltammograms

Typical cyclic voltammograms obtained during continuous potential scanning of CPEs containing Fc, *t*BuFc and DMFc solution in NPOE are presented in Fig. 9.3.

One can observe, that similarly to CCE modified with redox probe solution in NPOE (see p. 67) the stability of CV curves depends on hydrophobic / hydrophilic properties of the redox probe dissolved in the binder and anion present in the aqueous phase. For the most hydrophobic redox probe, such as DMFc, and the less hydrophilic studied anion, such as ClO$_4^-$ (Fig 9.3, c), the magnitude of the current is changed only slightly on repeated oxidation and reduction scans. This is not the case for less hydrophobic redox probes: *t*BuFc and Fc where decrease of the current during first few scans is observed (Fig. 9.3, a, b). Also for a given cycle the largest ratio of anodic and cathodic peak current being larger than unity, is observed for less hydrophobic redox probe Fc present in the binder. In the case of SO$_4^{2-}$ (Fig. 9.4) - the most hydrophilic

among studied anions, even after the 20th polarisation cycle with the least hydrophobic redox probe, Fc, present in the binder a further current decrease is observed (Fig. 9.4).
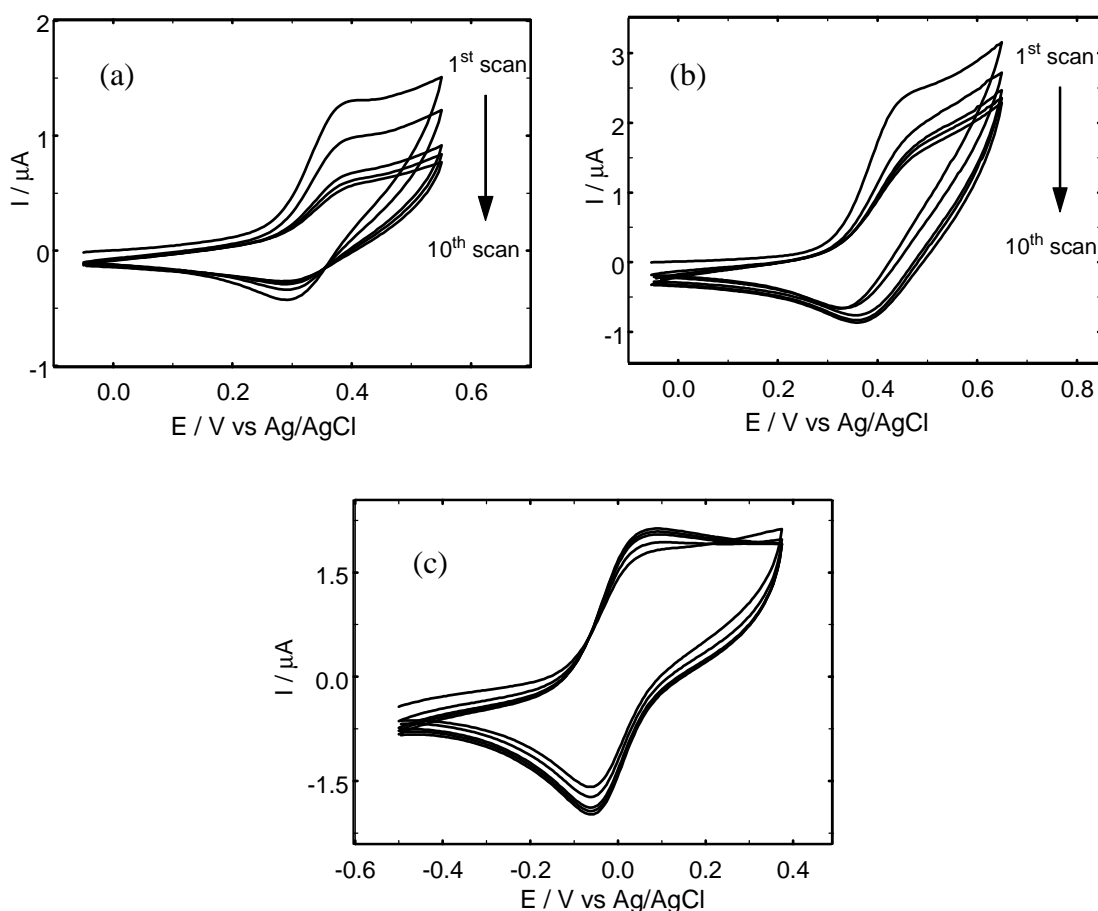

Figure 9.3. *Cyclic voltammograms obtained with CPE prepared with 0.01 mol dm^{-3} Fc (a), tBuFc (b) and DMFc (c) solution immersed into 0.1 mol dm^{-3} aqueous NaClO$_4$. The 1st, 2nd, 5th, 7th and 10th cycles are shown and arrows indicate the increasing number of scan.*

The decrease of the voltammetric response during consecutive potential cycles and the difference between anodic and cathodic charges can be attributed to the partial loss of electrooxidized redox probe from NPOE into the aqueous phase according to (8.4). Similarly to CCE the redox process observed in studied system is connected with the electrochemical oxidation of SFc (8.2). In order to maintain the electroneutrality two following processes (8.3) and (8.4)are possible. The last one is typical for electroactive CPE based on the redox probe solution in non-polar viscous oil [137]. This is because of low polarity of liquid binder, the expulsion of electrogenerated charged product of the electrochemical reaction (8.2) is the only way to maintain local neutrality.
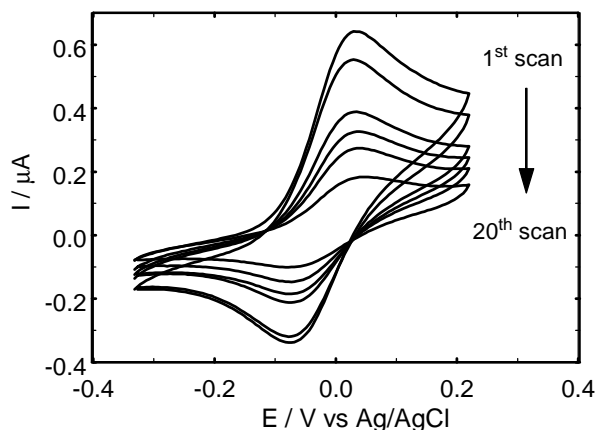
Figure 9.4.   Cyclic voltammograms obtained with CPE prepared with 0.01 mol dm^{-3} DMFc solution immersed into 0.1 mol dm^{-3} Na$_2$SO$_4$. The 1st, 2nd, 5th, 7th 10th and 20th cycles are shown and arrow indicates the increasing number of scan.

The reaction (8.3) is possible only for the electrode modified with polar binder (see Table 2.1).

One may conclude that CPE prepared with solution used as modifier for CCE shows voltammetric responses quite similar to CCE. Other likenesses are described below.

9.3   Anion concentration effect

The concentration dependence of $E_{Red/Ox}$ was examined for CPE modified with DMFc solution and immersed in perchlorate aqueous solution. On the basis of voltammograms (Fig. 9.5) it can be seen that this parameter systematically shifts to more positive potentials as the ClO$_4^-$ concentration is decreased. As it was already discussed in Chapter 8, for electrochemical electron transfer reaction followed by reaction (8.3) the anion dependence of $E_{Red/Ox}$ can be described by Nernstian type equation (8.5). Therefore, if there is no contribution of reaction (8.4) one should expect linear $E_{Red/Ox}$ vs. *log c$_{X^-}$* dependence with -0.059 V / decade slope. However, the approximately linear dependence with less negative slope (-0.036 V / decade) is observed in Fig. 9.6.

Such deviation was also observed for CCE (see p. 80). It is now clear, that the deviation from Nersntian slope is not connected with the presence of the silicate matrix in CCE.
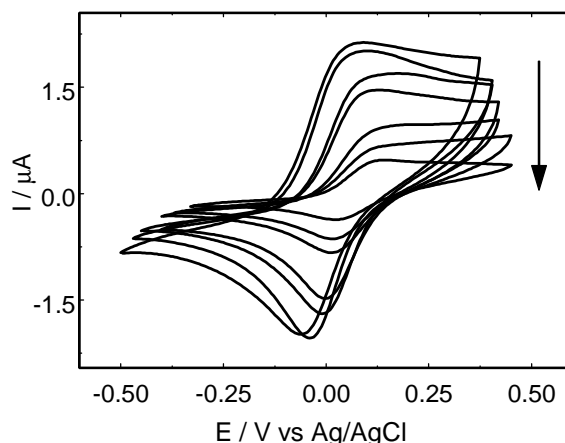
Figure 9.5. *Cyclic voltammorgams obtained with CPE prepared with 0.01 mol dm^{-3} DMFc immersed in 0.0001, 0.0005, 0.001, 0.005, 0.01, 0.05 and 0.1 mol dm^{-3} aqueous NaClO$_4$. The arrow shows decreasing NaClO$_4$ concentration.*
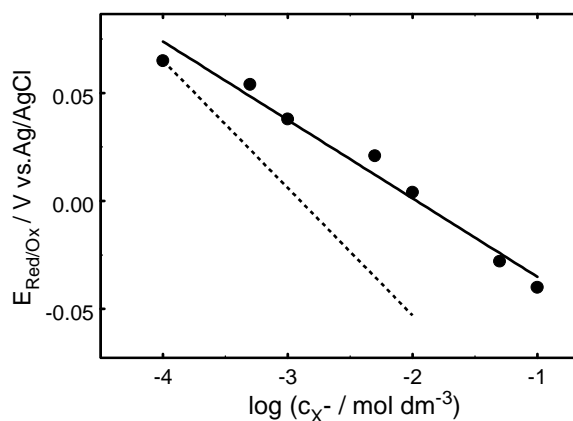

Figure 9.6. *Plot of $E_{Red/Ox}$ vs. log (c_{X^-}). $E_{Red/Ox}$ values were determined from cyclic voltammograms (Fig. 9.5) obtained with 0.01 mol dm^{-3} DMFc solution in 0.1 mol dm^{-3} aqueous NaClO$_4$. The straight line was obtained by linear regression. The dotted line is indicating Nernstian slope.*

It has to be emphasized that close to Nernstian behavior was reported for single drop of DMFc solution in NPOE deposited onto bppg, where the slope of the linear relationship between $E_{Red/Ox}$ and *log* c_{X^-} close to –0.060 V / decade was observed [69]. The reason of this difference is not clear. Obviously, the deviation from Nerstian slope is possible due to competing cation expulsion (8.4). For example, this process may be promoted, for example by adsorption of anions close to the three-phase junction [47] being more extended for graphite particles based system.

9.4   Anion effect

The analysis of anion effect is similar as in the case of CCE. In order to discriminate between anion transfer and electrogenerated cation expulsion the values $E_{Red/Ox}$ obtained in the presence of different anions in the aqueous solution were compared. For some systems where cyclic voltammetric peaks were not well developed reliable $E_{Red/Ox}$ values were obtained by DPV. Figs. 9.7 and 9.8 show the dependence of $E_{Red/Ox}$ on $\Delta_{aq}^{NB}\varphi_{X^-}^0$ for two types of CPE. For anions where $\Delta_{aq}^{NPOE}\varphi_{X^-}^0$ data were available the second plot $E_{Red/Ox}$ vs. $\Delta_{aq}^{NPOE}\varphi_{X^-}^0$ was also prepared.
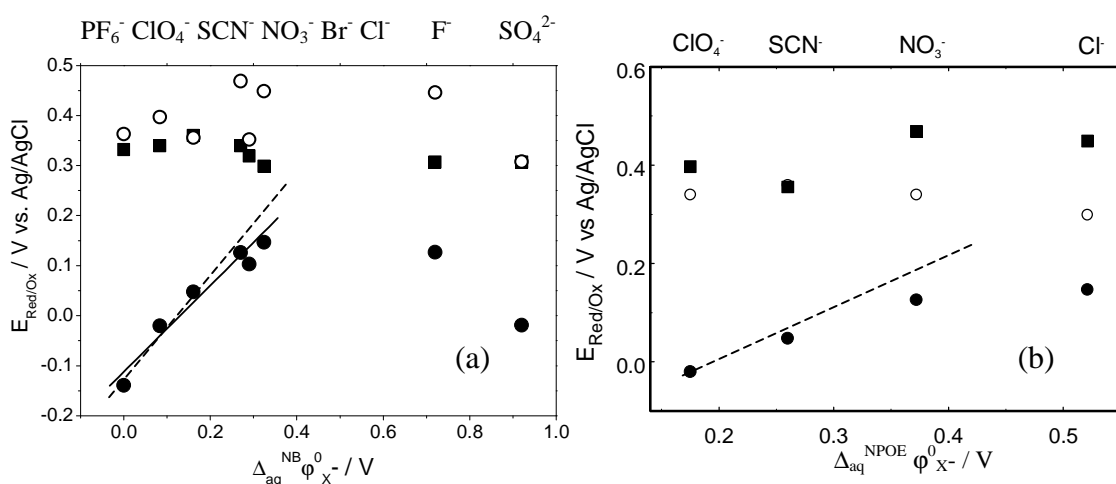

Figure 9.7.   *Plots of $E_{Red/Ox}$ vs. $\Delta_{aq}^{NB}\varphi_{X^-}^0$ (a) and $E_{Red/Ox}$ vs. $\Delta_{aq}^{NPOE}\varphi_{X^-}^0$ (b) dependences obtained with CPE modified with 0.01 mol dm^{-3} Fc ($\circ$), tBuFc ($\blacksquare$) and DMFc ($\bullet$) solution in NPOE. $E_{Red/Ox}$ values were determined from DPV. The solid line was obtained by linear regression. The dashed line indicates unity slope. The sequence of anions is indicated on top of the plot.*

Although the points in $E_{Red/Ox}$ vs. $\Delta_{aq}^{NB}\varphi_{X^-}^0$ and $E_{Red/Ox}$ vs. $\Delta_{aq}^{NPOE}\varphi_{X^-}^0$ plots are somewhat scattered, it is clear that anion transfer (8.3) across the liquid / liquid interface generated by electrochemical redox reaction dominates for DMFc and the less hydrophilic anions. On the other hand electrogenerated Fc$^+$ and *t*BuFc$^+$ cations (Fig. 9.7) rather escape from the organic phase for all studied electrolytes.

Summarizing all results presented in this Chapter one can conclude that the mechanism of electrode reaction strongly depends on the anions present in the aqueous phase. For more hydrophobic anions the dependence $E_{Red/Ox}$ vs. $\Delta_{aq}^{NB}\varphi_{X^-}^0$ is approximately linear (Figs. 9.7 (a) and 9.8 (a), solid line) with some deviation from unity slope (dashed line) as expected from Nernstian equation (8.5).
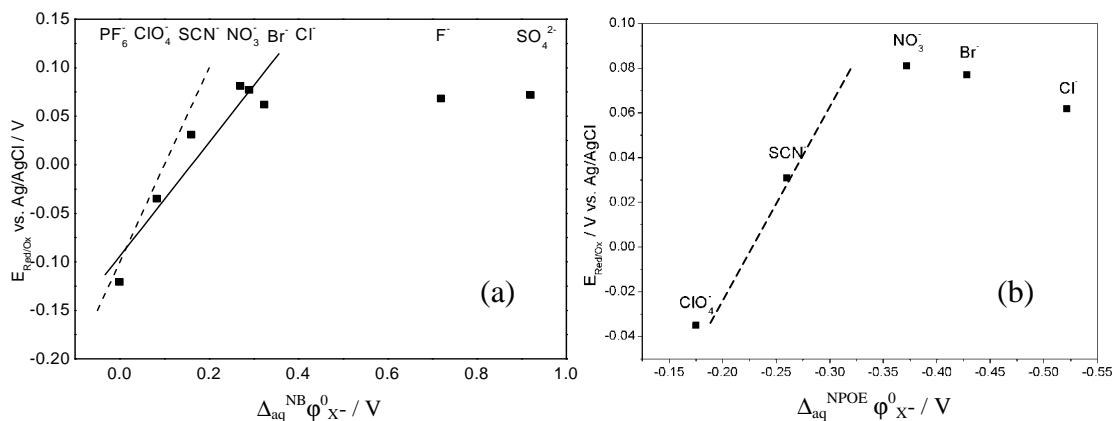
Figure 9.8. *Plots of $E_{Red/Ox}$ vs. $\Delta_{aq}^{NB}\varphi_{X^-}^0$ (a) and $E_{Red/Ox}$ vs. $\Delta_{aq}^{NPOE}\varphi_{X^-}^0$ (b) obtained with CPE prepared with CNF and 0.01 mol dm^{-3} DMFc solution in NPOE. The $E_{Red/Ox}$ values were determined from DPV. The solid line was obtained by linear regression. The dashed line is indicating unit slope. The sequence of anions is indicated on top of the plot.*

The transfer of these anion to the organic phase is more preferred than transfer of cation to the aqueous phase. However, in the case of more hydrophilic anions, such as F$^-$ and SO$_4^{2-}$, the transfer of electrogenerated DMFc$^+$ cation to the aqueous phase (8.4) dominates. Similar situation is observed for the dependence $E_{Red/Ox}$ vs. $\Delta_{aq}^{NPOE}\varphi_{X^-}^0$. The slopes of this dependence obtained with CPE are grouped in Table 9.1.

Table 9.1.   *The slopes of $E_{Red/Ox}$ vs. $\Delta_{aq}^{NB}\varphi_{X^-}^0$ dependence for different types of CPE and different redox liquid systems. Only data PF$_6^-$, ClO$_4^-$, SCN$^-$, NO$_3^-$, Br$^-$ and Cl$^-$ anions were arbitrary selected.*

Electrode	Redox system		Slope
CPE (20 µm graphite particles)	NPOE	Fc	-0.07 ± 0.09
		*t*BuFc	0.31 ± 0.13
		DMFc	0.86 ± 0.10
CPE (CNFs)	NPOE	*t*BuFc	0.59 ± 0.10

The slope of $E_{Red/Ox}$ vs. $\Delta_{aq}^{NPOE}\varphi_{X^-}^0$ decreases from close to unity for DMFc to close to zero for Fc organic solution. The tendency is very similar as for CCE. It indicates

gradual transition from anion to electrogenerated cation transfer from more hydrophobic to more hydrophilic redox probe, respectively.

On the basis of obtained results the scheme of possible reactions closed to three-phase junction seems to be identical to that presented in Fig. 8.24. Therefore the mechanism of electrode process for CPE and CCE modified with polar solvent is quite similar. It seems to be not affected by the presence of silicate matrix.

It is also important to say that although easy and quick preparation procedure is an advantage of CPE and the electrochemical behavior of NPOE solution based CPE and CCE is similar, the mechanical stability of the latter is better. This may be a advantage when less viscous organic solvent is used.

Chapter 10. Proton transfer across liquid acid-base complex / liquid interface supported by basal plane pyrolytic graphite, carbon ceramic and carbon paste electrodes

The electrodes described in Chapters 8 and 9 were modified with redox probe solution in polar solvent. The results presented in this chapter were mainly obtained with CCE and CPE modified with mixture of liquid redox probe and liquid complexing agent. Highly water insoluble acid-base complex formed by HDOP and DDPD was chosen for this experiments. It was expected that N-atom of DDPD with free electron pair creates hydrogen bond with H-atom of HDOP [173]. The electrochemical properties of HDOP-DDPD complex modified electrode and sensitivity of this electrode to pH are presented in this Chapter. As before special attention was paid to electrogenerated ion transfer across liquid / liquid interface.

The electrochemical behavior of this type of liquid deposit was not studied before. Therefore at first this system was studied at bppg electrode. This electrode material is suitable for the voltammetric studies of droplets deposited onto surface of the electrode [17]. The surface of this electrode is rough, owing to this fact the oil droplet keep stick to the surface.

10.1   Microdroplets of acid-base complex deposited on basal plane pyrolytic graphite electrode

Mixture of HDOP and DDPD were deposited in the form of microdroplets onto the surface of bppg by evaporation of its acetonitrile (ACN) solution. The resulting electrode was immersed in the aqueous electrolyte solution. The experiments with pure DDPD deposit were performed to compare its electrochemical behavior with that HDOP-DDPD complex.

The voltammogram of DDPD is characterized by sharp and well-defined anodic and cathodic peaks, with a midpoint potential, $E_{Red/Ox} = 0.12$ V vs. SCE (Fig. 10.1, curve A), which is consistent with previous study [57]. The process is highly reversible and the value $E_{Red/Ox}$ is affected by the concentration of perchlorate in the aqueous solution as expected for Nernstian behavior [51]. Approximately linear dependence of peak current on scan rate indicates the absence of diffusion control [153].
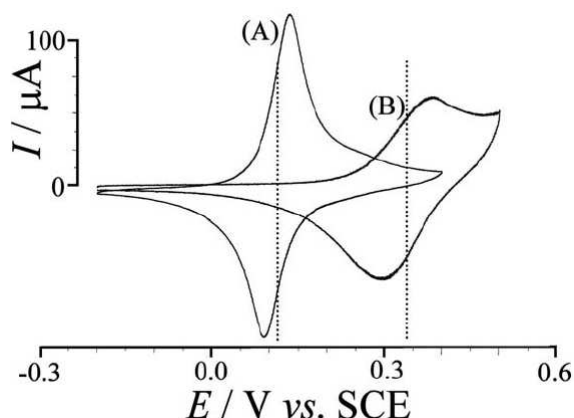
95

*Figure 10.1.   Cyclic voltammograms obtained for bppg electrode modified with microdroplets of
1.3 μg of DDPD (2.6 nmol) (A) and 1.3 μg of DDPD together with 43 μg of HDOP (133.5 nmol) (B) and
immersed into aqueous 0.1 mol dm^{-3} NaClO$_4$.*

The electrooxidation process is connected with the following reaction [17]:

$$DDPD_{(org)} + ClO_4^-{}_{(aq)} - e^-{}_{(electrode)} \leftrightarrow [DDPD^+ClO_4^-]_{(org)} \qquad (10.1)$$

Addition a little amount of HDOP to DDPD deposit dramatically changes the
voltammetric curve (Fig. 10.1, curve B). HDOP may be regarded as a highly
hydrophobic acid and the interaction of this acid with DDPD leads to liquid acid-base
complex (Fig. 10.2).
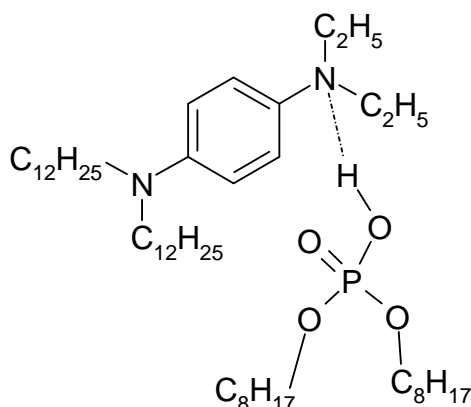

Figure 10.2.   The proposed structure of HDOP-DDPD complex.

The formation of this complex at the flat surface was proven by FTIRRAS
experiments [173]. It is also possible that HDOP molecules in contact with aqueous
phase dissociate and the ion pair DDPDH$^+$-DPO$^-$ is formed. This may occur because of
surface dissociation of HDOP molecules (surface pK_a of HDOP is equal 2.9 [174]).

The electrode process can be identified as a one-electron oxidation of the HDOP-DDPD complex accompanied by proton expulsion into the unbuffered aqueous solution:

$$[HDOP\text{-}DDPD]_{(org)} - e_{(electrode)} \leftrightarrow [DPO^-\text{-}DDPD^+]_{(org)} + H^+ \qquad (10.2)$$
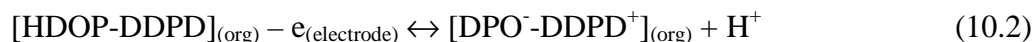
For a 1:1 acid-to-base ratio in the deposit, the voltammetric response associated with process (10.1) is diminished and process (10.2) dominates. The shift of $E_{Red/Ox}$ to more positive potentials (Fig. 10.1, B) is connected with the replacement of the anion transfer (10.1) with proton transfer (10.2) in a wide pH range. It indicates, that mechanism of the electrode reaction is changed, because the new acid-base complex is formed. However, during repeated potential cycling, depletion of HDOP and a reappearance of signal connected with process (10.1) are observed, probably due to loss or slow hydrolysis of the organic phosphate at the liquid / liquid interface. Increasing the amount of HDOP (not shown) does not significantly change the electrochemical process.

To find optimal mass ratio HDOP : DDPD with maximum of conversion in the electrode process the experiments with different mass ratio HDOP : DDPD in buffered solution systems were performed (Fig. 10.3).
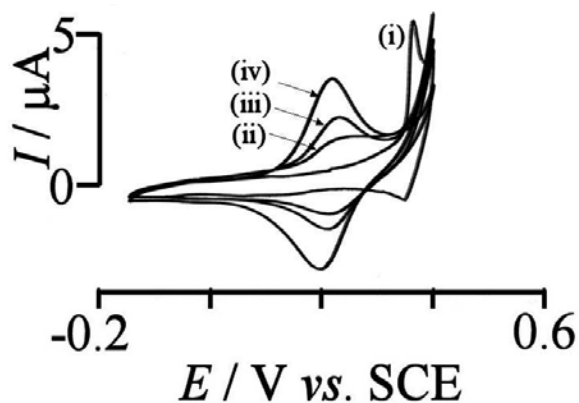
Figure 10.3.   Cyclic voltammograms obtained with bppg modified with 0.5 µg of DDPD (1 nmol) and 0 µg (0 nmol) (i), 1 µg (3.1 nmol) (ii), 2 µg (6.2 nmol) (iii) and 8 µg (24.8 nmol) (iv) µg of HDOP immersed into aqueous 0.1 mol dm^{-3} phosphate buffer (pH 7).

In voltammograms obtained in absence of HDOP (Fig. 10.3, i) the phosphate electroinsertion reaction (10.3) is detected at $E_{Red/Ox}$ = 0.35 V vs. SCE.

$$DDPD_{(org)} + KHPO_4^-{}_{(aq)} - e^-{}_{(electrode)} \leftrightarrow [DDPD^+KHPO_4^-]_{(org)} \qquad (10.3)$$

This process is more complex and here tentatively assigned to a process associated with simultaneous potassium coinsertion [56]. In the presence of HDOP in liquid deposit the voltammetric response changes dramatically (Fig. 10.3). A total charge obtained from curve 3 (iv) is equal ca. 30 μC that is consistent with a one-electron electrolysis of 30% of the 1 nmol of DDPD present on the electrode surface. The charge under the voltammetric response increases with addition of more HDOP up to 8 μg but decreases with its further addition (not shown). It can be concluded, that the addition of HDOP improves mass transport via diffusion in the organic phase. Further addition of HDOP increases the droplet size and decreases the concentration of DDPD and leading to reduced currents and conversion.

In order to prove the participation of proton in the electrode reaction (10.2) the effect of pH on the voltammetric response was investigated (Fig. 10.4).
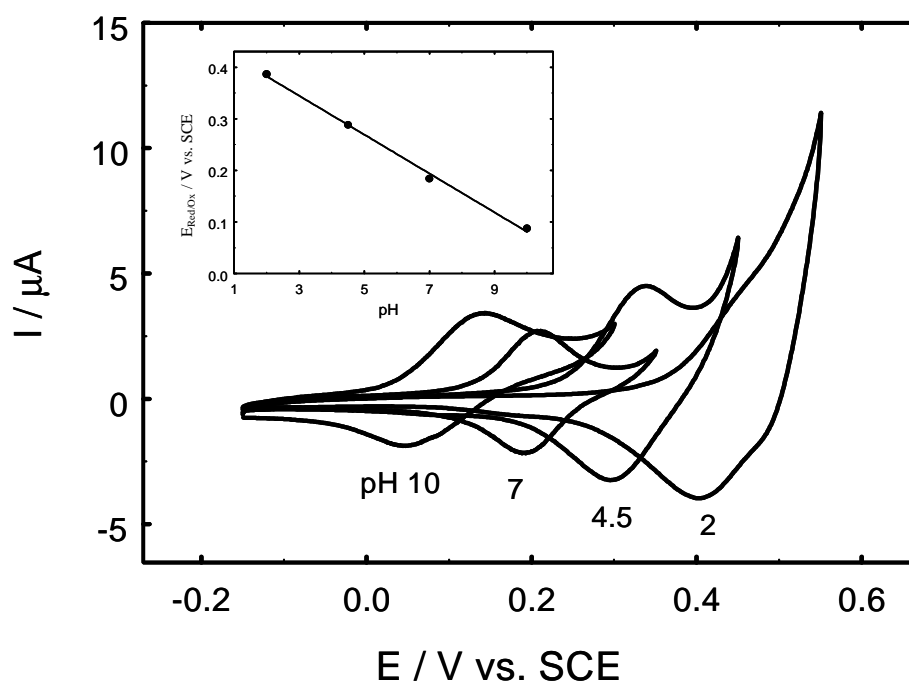
Figure 10.4.   Cyclic voltammograms obtained with bppg modified with 0.5 μg of DDPD (1 nmol) with 8 μg (24.8 nmol) of HDOP immersed in aqueous phosphate buffer at different pH. The inset shows $E_{Red/Ox}$ vs. pH plot.

The $E_{Red/Ox}$ values for the voltammograms systematically shift to more positive potential side with increasing proton activity (Fig. 10.4, inset). This behavior can be described by the appropriate Nernstian equation derived for process (10.2):

98

$$E = E^{0\,'} + \frac{RT}{F}\ln\frac{[DPO^- - DDPD^+](org)}{[HDOP - DDPD](org)} - 2.303\frac{RT}{F}pH \qquad (10.4)$$

However, the observed linear $E_{Red/Ox}$ vs. *pH* dependence exhibits sub-Nerstian slope equal –0.041 V / pH unit. This deviation from the value predicted by the Nernstian equation, -0.059 V / pH unit (10.4), can be tentatively attributed to a weak coupling of the proton activities in the aqueous and organic phase, e.g., by a pH-dependent surface potential of the reduced form of the microdroplets. The similar dependence of $E_{Red/Ox}$ on *pH* was also observed for THPD deposited onto bppg [52]. This amine can be protonated, but in that case H^+ comes from water [45] (see Fig. 2.10).

10.2.   Liquid acid-base complex supported by carbon ceramic and carbon paste electrodes

Next, electrogenerated ion transfer reaction across liquid acid base complex / liquid interface was studied using CCE and CPE. Liquid DDPD and its solution in HDOP were immobilized into CCE by two ways: through impregnation and deposition from solution of the redox liquid in volatile solvent. In the case of CPE solution of DDPD in HDOP acts as a binder. These experiments were performed to understand whether the form of three-phase junction and presence of silicate matrix affects the voltammetric response obtained with the acid-base complex and the mechanism of electrode process.

Similar to bppg electrode modified with microdroplets of redox liquid, modified CCE or CPE provides the formation of the three-phase junctions on the electrode surface, however their geometries are different (Fig. 10.5).

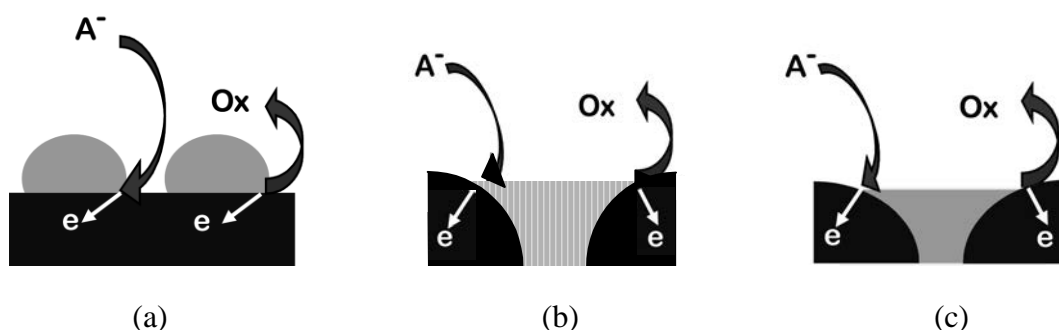(a)   (b)   (c)

Figure 10.5.   The schematic drawing showing electrochemistry of redox liquid deposited on a bppg electrode (a), in CCE (b) or acting as a binder of CPE (c).

99

Moreover CCE and CPE are bulk-modified electrodes. They consist excess of liquid modifier present in the electrode body.

For CCE modified with DDPD droplets immersed into an aqueous perchlorate solution sharp voltammetric oxidation responses are observed (Fig. 10.6).
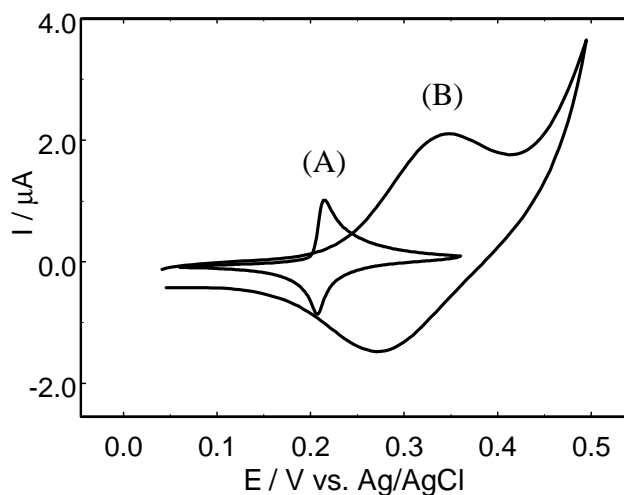

Figure 10.6.   *Cyclic voltammograms obtained with CCE modified with 1.9 nmol of DDPD undiluted (A) and diluted (1:8) with HDOP (B) and immersed into 0.1 mol dm^{-3} aqueous KClO$_4$.*

The efficiency of the electrode process is 12 times below than that observed for bppg. However, the modification of the CCE with DDPD solution in HDOP leads to an increase in the current – opposite to the effect observed at bppg (Figs. 10.1 and 10.6). The substantial shift of $E_{Red/Ox}$ in positive direction indicates a change of the mechanism of the process from (10.1) to (10.2). Interestingly, the anodic charge is about 10 times larger than that obtained on Au and Au covered with silicate thin film electrodes [173] indicating more effective "microphasing" – extension of the length of three-phase junction in the presence of the composite silicate carbon material structure. The efficiency of the electrode process is in the range of few percent and therefore larger than that for thin film silicate electrodes. It is because of the higher surface area of embedded graphite particles that is responsible for this effect (Fig. 10.5, a).

For experiments at different pH, CCE was modified with DDPD solution in volatile solvent (1.9 nmol of DDPD diluted with hexane) or impregnated with a mixture of DDPD and HDOP in the same volatile solvent (the amount of DDPD is unknown, but it is larger than 1.9 nmol). ACN was replaced by hexane because it was noticed that

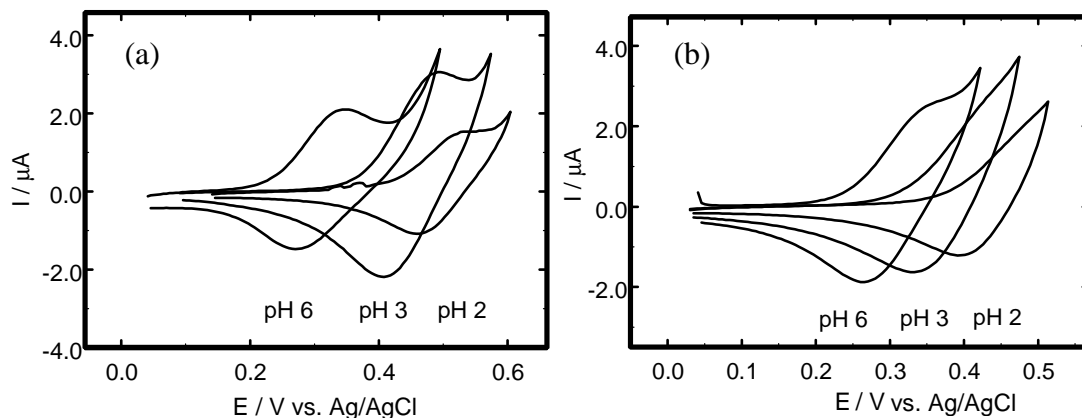the former destroy CCE. Some differences in behaviors of these electrodes are observed (Figs. 10.7 and 10.8).

Figure 10.7.   *Cyclic voltammograms obtained with CCE modified with 1.9 nmol (a) and continuous phase (b) of DDPD diluted (1:8) with HDOP and immersed into 0.1 mol dm^{-3} phosphate buffer at pH 2, 3 and 6.*
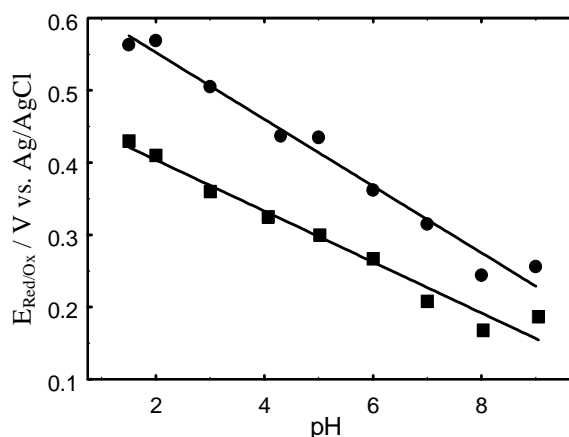

Figure 10.8.   *Plot of E$_{Red/Ox}$ vs. pH obtained with CCE modified with microphases (●) and continuous phase (■) of DDPD diluted (1.8) with HDOP and immersed into 0.1 mol dm^{-3} phosphate buffer.*

Obviously, the voltammograms obtained with microdroplets modified CCE are better defined. For both electrodes approximately linear dependence between $E_{Red/Ox}$ and pH with sub-Nernstian slopes (-0.046 and -0.035 V / pH unit for microphases and bulk modified electrodes, respectively) are observed. Microphase modified CCE is more sensitive to pH. However, a possible application of the studied electrode as a pH sensor is limited to the acidic and neutral pH range due to the known silicate decomposition in alkaline media. It has to be emphasized that the modified CCE has been already

101

proposed as pH sensors [114] (see Fig. 3.7). In that case sol was doped with modifier during preparation of CCE.

Similarly to polar solvent modified electrodes (Chapter 9) the effect of matrix was studied preparing CPE from graphite powder directly mixed with DDPD solution in HDOP. This acid is fortunately a viscous liquid at room temperature and preparation of CPE with HDOP as a binder was possible. The obtained cyclic voltammograms with CPE prepared with DDPD solution HDOP as a binder are presented in Fig. 10.9 (a).
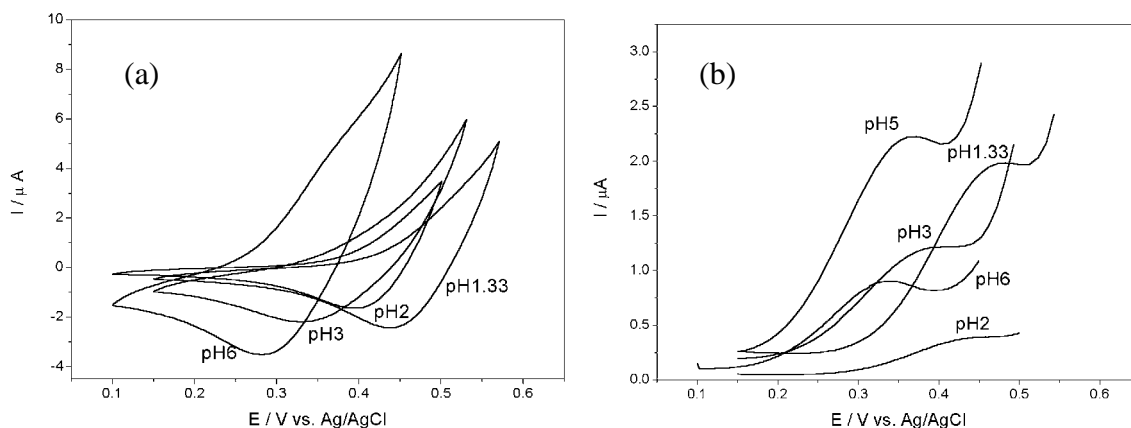

Figure 10.9.   Cyclic voltammograms (a) and differential pulse voltammograms (b) obtained with CPE prepared with DDPD solution in HDOP in 1:9 volume ratio and immersed into 0.1 mol dm^{-3} phosphate buffer.

The anodic peaks on CV curves (Fig. 10.9, a) are poorly defined. This makes difficult to determine $E_{Red/Ox}$ similarly as for other electrodes. In order to more clearly estimate the values of $E_{Red/Ox}$ the DPV technique was used (Fig. 10.9, b). Relatively well-defined peaks are observed followed by current increase at more positive potentials are observed on DPV curves. The further oxidation of the acid-base complex probably results in decomposition of DDPD similarly to THPD [52].

The dependence of E_p on pH has can be divided into two parts (Fig. 10.10). In pH 1-7 range one can observe approximately linear dependence with sub-Nernstian slope (-0.029 V / pH unit). The deviation from Nernstian behavior is larger than observed for CCE modified with microphases and continuous phase of acid-base complex (see Fig. 10.8). At pH above 7 the value of E_p is almost insensitive to variable pH. Due to possible destruction of silicate matrix at higher pH, it is impossible to compare the behavior both electrodes at pH above 7.
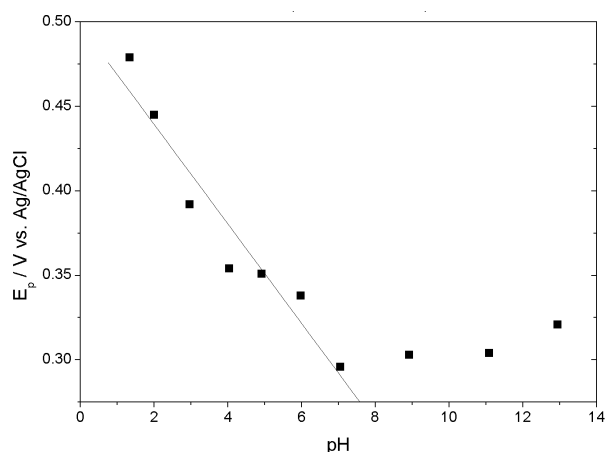
Figure 10.10.   Plot of E_p vs. pH obtained with CPE prepared with DDPD solution in HDOP in 1:9 volume ratio and immersed into 0.1 mol dm^{-3} phosphate buffer at different pH. The values E_p were obtained from DPV curves. Solid line was obtained by linear regression.

In order to understand the mechanism of reaction at electrodes modified with DDPD-HDOP complex all above results were taken into account. This is summarized in schematic drawing in Fig. 10.11.
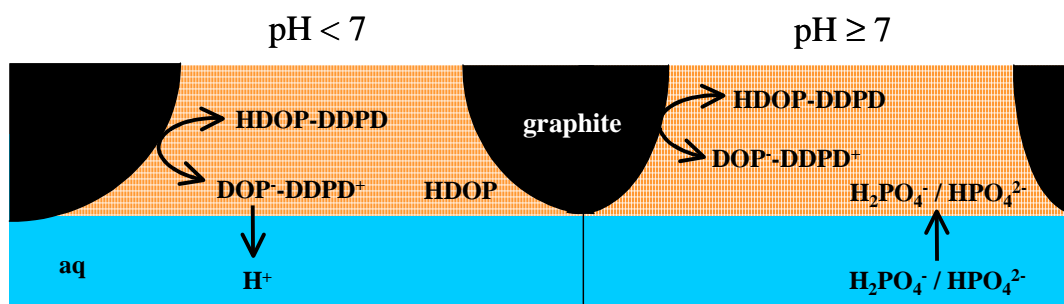
Figure 10.11.   The scheme of the mechanism of the electrode reactions connected with electrooxidation HDOP-DDPD complex supported by CCE or CPE immersed into buffer solution.

When pH of the aqueous buffer is lower than 7 the electrode is sensitive to proton concentration. In these conditions proton are transferred into the aqueous phase after electrogenerated electron transfer. For more basic aqueous solution in order to maintain electroneutrality of the organic phase, the anions have to be transferred to the HDOP from the aqueous phase. Taking into account dissociation equilibriums and the values of pK_a of dissociation of phosphoric acid [175]:

$$H_3PO_4 \leftrightarrow H_2PO_4^- + H^+ \qquad pK_a = 2.12 \qquad (10.5)$$

$$H_2PO_4^- \leftrightarrow HPO_4^{2-} + H^+ \qquad pK_a = 7.20 \qquad (10.6)$$

103

$$HPO_4^{2-} \leftrightarrow PO_4^{3-} + H^+ \qquad pK_a = 11.9 \qquad (10.7)$$
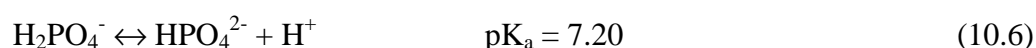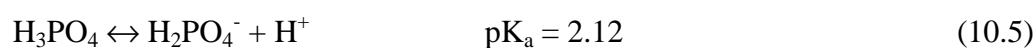
one may conclude that at pH above 7 two dissociated forms, $H_2PO_4^-$ and HPO_4^{2-}, are inserted after electrogenerated cation formation.

All above experiments concerned to the electrochemical studies of the electrodes modified with acid-base complex, HDOP-DDPD. Also an attempt was made to check whether HDOP based CPE is sensitive on the concentration of proton in the aqueous phase in the absence of acid-base complex. For this investigation DDPD was replaced by tBuFc, which does not form a complex with HDOP.

Interestingly, the pH dependent shift of $E_{Red/Ox}$ on potential scale is also observed for CPE prepared from tBuFc solution in HDOP (Fig. 10.12).
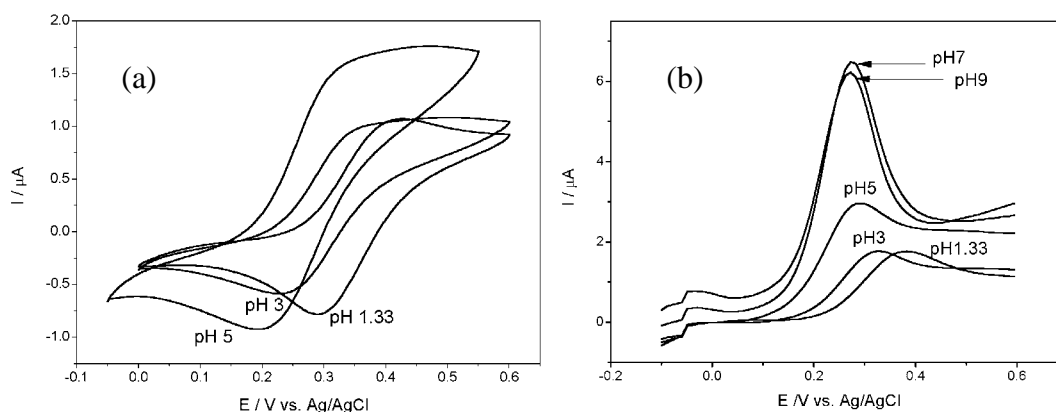
Figure 10.12. *Cyclic (a) and differential pulse (b) voltammograms obtained with CPE prepared from 0.01 mol dm^{-3} tBuFc solution in HDOP and immersed into buffer solution at different pH marked on the figure.*

It is clearly visible, that for larger pH the more negative value of $E_{Red/Ox}$ is observed. As before, DPV technique was used for more accurate determination of $E_{Red/Ox}$ (Fig. 10.12 (b)). Fig. 10.13 presents the dependence of E_p on pH.

The shape of E_p vs. pH dependence is similar to that observed in the case of acid-base complex. However the change in the mechanism of the electrode process from proton expulsion to anion insertion occurs at lower pH, equal about 5. Therefore it can be concluded, the formation of acid-base complex with redox probe and solvent is not necessary to promote the voltammetric sensitivity of CPE on pH aqueous solution. The possible mechanism of electrode reaction is presented in Fig. 10.14. This scheme is similar to that presented on Fig. 10.11, with important difference.

Figure 10.13.   The plot of E_p vs. pH obtained with CPE prepared with 0.01 mol dm^{-3} tBuFc solution in HDOP and immersed into 0.1 mol dm^{-3} phosphate buffer at different pH. The values E_p were obtained from DPV curves (Fig. 10.12).
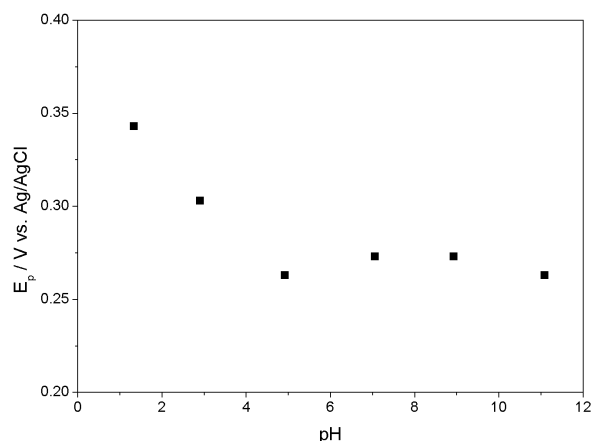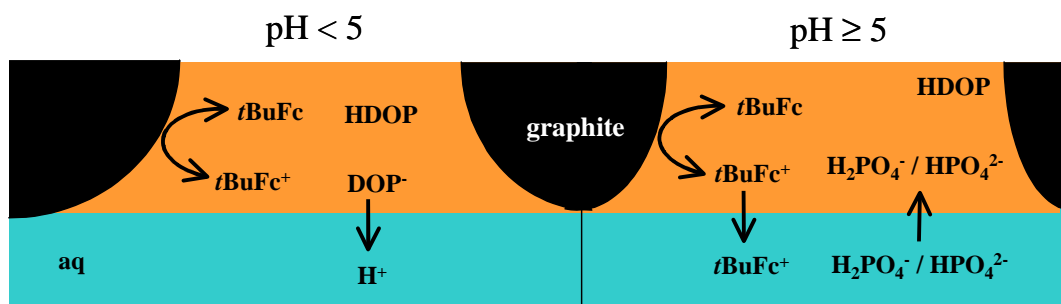

Figure 10.14.   The schematic drawing of possible electrode reactions connected with electrooxidation tBuFc solution in HDOP supported by CPE immersed into buffer solution.

First the value of pH, where proton transfer across liquid / liquid interface is replaced by ion transfer, is smaller. The second, the ejection of electrogenerated cation from the organic to the aqueous phase is also possible at pH above 5. This is possible in the presence hydrophilic anions like $H_2PO_4^-$, HPO_4^{2-}, PO_4^{3-} in the aqueous phase. At the moment it is impossible to say whether cation ejection to the aqueous phase or anion injection to the organic phase is preferred. The understanding of contribution these transfers to mechanism of the electrode reaction requires more experiments.

The above results lead us to the following conclusions about electrochemical behavior of studied system:

1.   Water-insoluble redox liquid DDPD deposit undergoes electrochemical oxidation accompanied by anion insertion. An acid-base HDOP-DDPD complex

deposited onto bppg or present in CCE or CPE undergo oxidation accompanied by proton expulsion. However, the range of pH, where the latter reaction occurs depends on the electrode material. It is equal 1 – 10 for bppg, 1 – 9 for CCE and 1 – 7 for CPE. In this respect some effect of silicate matrix is observed for bulk modified electrodes.

2.   Bppg and CCE modified with microdoplets of HDOP-DDPD complex are more sensitive to pH of the aqueous phase than CCE modified and CPE prepared with the same acid-base complex.

3.   The acid-base complexation of the redox probe in CPE binder is not essential to induce proton transfer reaction across liquid / liquid interface.

Chapter 11. Ion transfer across ionically conductive organic phase / aqueous solution interface supported by carbon ceramic and carbon paste electrodes

In experiments described in previous chapters the organic phase filling CCE body was ionically non-conductive. As a consequence the electrochemical reaction of the dissolved redox probe starts at three-phase junction: electrode / organic phase / aqueous phase. When organic phase contains dissolved salt or is exclusively composed of ions, such as room temperature molten salt, the electrochemical reaction is expected to be not restricted to the three-phase junction [79, 82-84]. Still the ion transfer across liquid / liquid interface has to occur. The results of electrochemical studies of CCE modified with redox probe solution in salt containing organic liquid or room temperature ionic liquid, RTIL are presented below. All voltammograms presented in this chapter were obtained in conditions when they were not affected by subsequent scanning.

11.1   Carbon ceramic electrode modified with salt containing nitrobenzene

For this study tBuFc solution in NB containing dissolved tetrabutylammonium perchlorate (TBAP) was used as the modifier. Cyclic voltammograms obtained with modified electrode change during first subsequent scans, namely both anodic and cathodic current decrease (not shown). However, after 5-7 cycles they become stable, similarly as it was observed for CCE modified with tBuFc solution in pure NB. Also their shape is similar to voltammetric response of CCE modified with this organic phase (see p. 66). However, the peak current magnitude obtained with CCE modified with salt containing redox liquid is approximately 3-4 times larger (Fig. 11.1).

Typically, in CV experiments with these systems during polarization towards anodic direction the not well-developed peak is formed, whereas during backward direction the peak-shaped curve appears. The redox process is attributed to the oxidation of tBuFc within NB phase according to (8.2). It is expected the presence of ionically conducting organic phase enlarges the reaction zone from the three-phase junction to two-phase junction: graphite particle / salt containing organic phase. Therefore one may expect that the active electrode surface correspond to the surface of all graphite particles forming percolation paths within the electrode body.
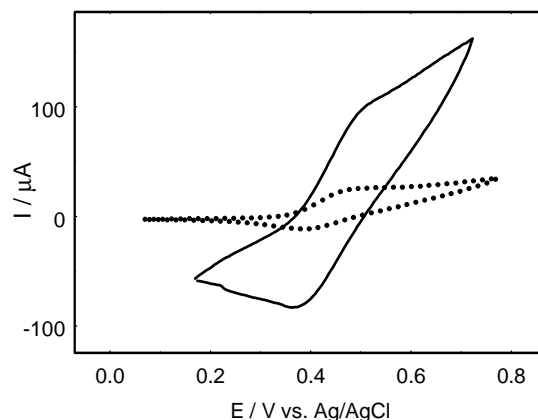
*Figure 11.1.   Cyclic voltammograms obtained with CCE modified with 0.45 mol dm⁻³ tBuFc (dotted)
and 0.45 mol dm⁻³ tBuFc and 0.1 mol dm⁻³ TBAP (solid) solution in NB immersed into 0.1 mol dm⁻³
aqueous KNO₃.*

The estimated geometric surface of all graphite particles filling CCE, assuming their spherical shape and hexagonal close-packed structure arrangement, is equal 13.9 cm^2.Then, the theoretical peak current for the diffusion controlled oxidation of tBuFc in salt containing system under these conditions (geometric area = 13.9 cm^2, D = 4.78 × 10^{-7} cm^2 s^{-1} (see p. 77), v = 0.01 V s^{-1}) can be calculated from Randles-Sevcik equation (1.18) as 116 mA. It is almost three orders of magnitude larger than observed (Fig. 11.1). There are three reasons expected to cause these effect: (i) the almost complete covering of graphite particles by silicate matrix making them inaccessible for redox liquid; (ii) only graphite particles being close to the liquid / liquid interface participate in the electrode reaction, due to slow ion transfer kinetics or to the ohmic drop; (iii) sharing of diffusion layers near neighboring graphite particles. Interestingly, (see Fig. 2.11) in studies of conductive redox liquid containing of *tetra*-alkylphenylenediamine deposited on the flat electrode surface [30] it has been proven that the electrode reaction takes place at the whole organic / aqueous interface. This may indicate that for CCE the reason (i) seems to be most probable.

As for CCE modified with organic phase (see p. 76 and 78) the shape of the voltammograms and the current magnitude system depend on both $c_{tBuFc(org)}$ and c_{X^-} (Figs. 11.2, 11.3). The voltammograms are wave-shaped with noticeable exception for the smallest $c_{tBuFc(org)}$. For a given c_{X^-} the current magnitude is proportional to $c_{tBuFc(org)}$, that is analogous with behavior of CCE modified with NB phase (Fig. 8.19), however

this dependence is not linear. It probably results from the availability of anions at liquid / liquid interface and their transfer to the organic phase according to (8.3).
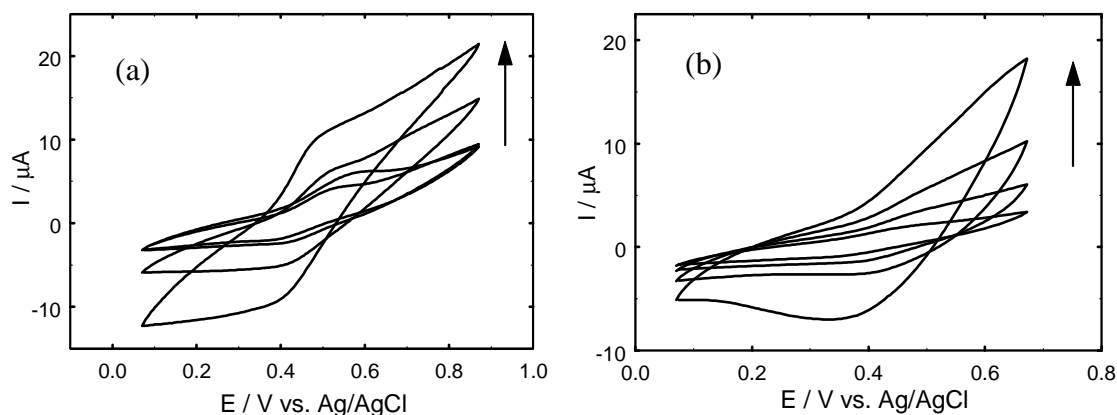
Figure 11.2.   Cyclic voltammograms obtained with CCE modified with 0.045 (a) and 0.0045 (b) mol dm^{-3} tBuFc and 0.1 mol dm^{-3} TBAP solution in NB immersed into 0.001, 0.01, 0.1 and 1 mol dm^{-3} aqueous KNO$_3$. The arrows show increasing KNO$_3$ concentration.
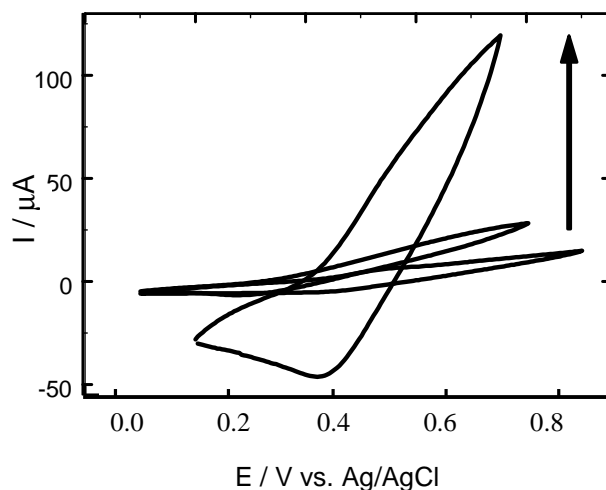
Figure 11.3.   Cyclic voltammograms obtained with CCE modified with 0.45, 0.045 and 0.0045 mol dm^{-3} tBuFc and 0.1 mol dm^{-3} TBAP solution in NB immersed into 0.01 mol dm^{-3} aqueous KNO$_3$. The arrow shows increasing tBuFc concentration.

The shape of CV curves, especially anodic scan, may indicate significant contribution of radial diffusion. To answer the question whether this is the case the potential step experiments were performed. The dependence of current, I vs. time, t obtained from anodic step for longer times has positive intercept, whereas that obtained from cathodic one seems to approach zero (Fig. 11.4).
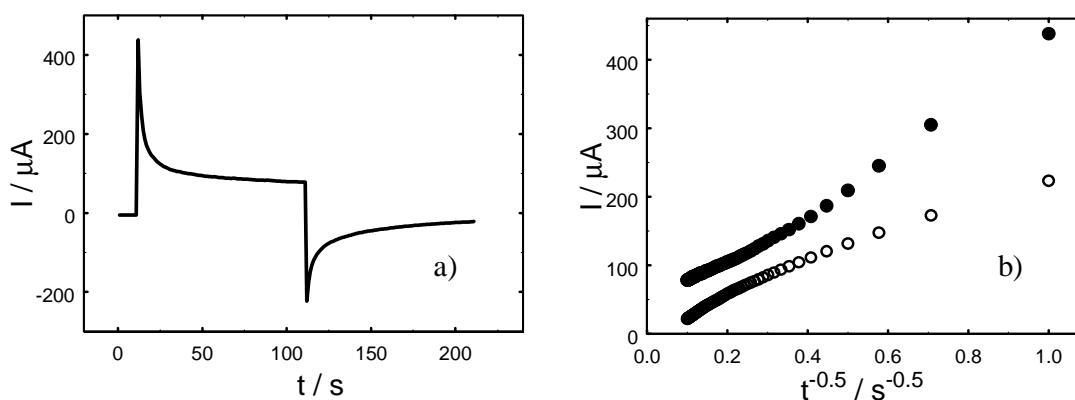
109

Figure 11.4.   Plot of I vs. t (a) obtained from CA experiment with CCE modified with 0.45 mol dm^{-3} tBuFc and 0.1 mol dm^{-3} TBAP solution in NB immersed into 0.1 mol dm^{-3} aqueous KNO$_3$. The Cottrell plot (I vs. t$^{-0.5}$) (b) of anodic (●) and cathodic (○) current obtained from the CA experiment.

This indicates ultramicroelectrode like behavior for anodic process [176, 177]. The positive deviation from this dependence at shorter times may be connected with transition from linear to semiinfinite diffusion regime.On the other hand the deviation from linearity observed for cathodic step at longer times is typical for diffuse layer depletion in ultramicroelectrode assembly [176, 177] and it was already observed for CCE modified with pure redox liquid [61]. The ultramicroelectrode like behavior is connected with the small size of graphite particles and their aggregates (see Fig. 7.3). They probably act as an assembly of microelectrodes having not well-defined geometry and size distribution. This result also indicates that only graphite particles placed close to liquid / liquid interface are electrochemically active, even for ionically conductive organic phase (Fig. 11.5).
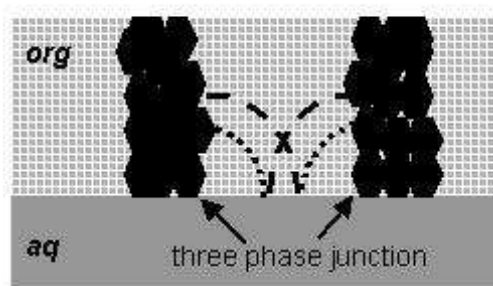

Figure 11.5.   The scheme of cross section view of CCE modified with redox liquid and immersed in aqueous solution. Dotted and dashed lines represent the size of diffusion layer at shorter and longer times respectively [61].

Summarizing, in the case of CCE impregnated with redox probe and salt solution in hydrophobic polar solvent only small fraction of carbon particles acts as electronic conductor for the electrode reaction. It seems to that similarly as CCE modified with ionically non-conductive redox liquid, the oxidation of salt containing redox liquid is followed by anion insertion into the organic phase and/or cation ejection to the aqueous phase. It is not inconceivable that TBA^+ cation is also ejected to the aqueous solution instead of or together with $t\text{BuFc}^+$ [37]. This point was further studied with RTIL modified electrodes (see below).

11.2   Room-temperature ionic liquid modified electrodes

The room-temperature ionic liquids are molten salts. Due to their ionic conductivity it is expected that the electrode process at the electrode modified with redox probe solution in RTILs not necessary starts at the three-phase junction, similarly to the electrode modified with salt containing redox liquid (see p. 107). RTIL is in fact room-temperature molten salt without any solvent.

Below, the electrochemical properties of CCE modified and CPE prepared with redox probe – $t\text{BuFc}$ solution in hydrophobic $C_4\text{mimPF}_6$ or more hydrophobic $C_{10}\text{mimN(Tf)}_2$ will be described.

11.2.1 Carbon ceramic electrode modified with room-temperature ionic liquid

We observed that CCE prepared from MTMOS-based sol is not well wetted by RTILs mentioned above. This occurs despite the hydrophobic properties of both silicate matrix and RTIL. Probably the difference between their polarity plays important role. Silicate matrix prepared from MTMOS is non-polar, whereas TMOS based one is polar. Indeed, the penetration of silicate matrix by RTIL was improved, when this hydrophilic precursors (TMOS) was main component of the sol. Therefore CCE further modified with RTIL were prepared from the mixture of hydrophilic and hydrophobic precursor (TMOS:MTMOS = 99:1).

The CV curves obtained with this CCE modified with $C_4\text{mimPF}_6$ based redox solution and immersed in the aqueous solution saturated with KPF_6 and $C_4\text{mimPF}_6$ are presented in Fig. 11.6. The aqueous solution was saturated with RTIL in order to diminish the solubility of the latter in the aqueous phase. The voltammograms are symmetric and its shape resembles that of quasi-reversible heterogeneous electron transfer reaction with both anodic and cathodic peaks not well-defined.
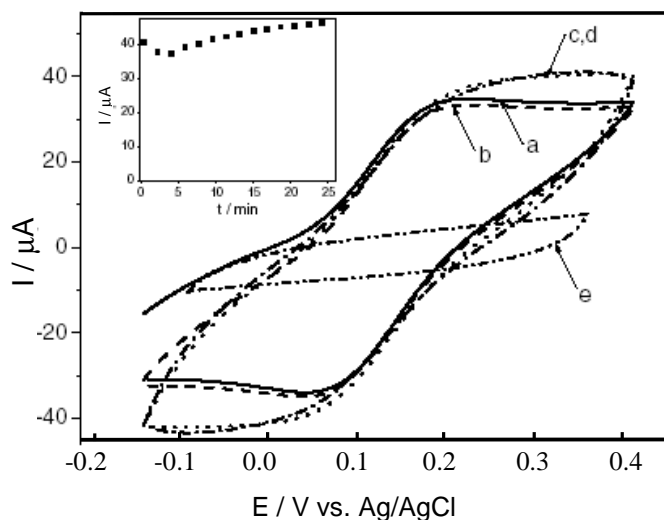
111

Figure 11.6.   Cyclic voltammograms obtained with CCE prepared from TMOS:MTMOS (99:1) mixture modified with 2 μl 0.01 mol dm^{-3} tBuFc solution in C$_4$mimPF$_6$. CCE was immersed in saturated aqueous KPF$_6$. The 1st (a), 2nd (b) 30th (c) and 100th (d) cycles are shown. Voltammograms obtained for CCE modified with pure C$_4$mimPF$_6$ (e). Inset shows current, at E = 0.206 V vs. Ag/AgCl vs. time, t, dependence.

The comparison CV obtained with CCE modified with pure RTIL and *t*BuFc solution in RTILs indicates that the peak-shaped voltammogram results from electrooxidation of *t*BuFc dissolved in RTIL:

$$tBuFc_{(RTIL)} - e_{(electrode)} \leftrightarrow tBuFc^+{}_{(RTIL)} \tag{11.1}$$

During continuous scanning after initial decrease some increase of the cathodic and anodic current is observed (Fig. 11.6, inset). This can be explained by viscosity decrease caused by dissolution of some amount of H$_2$O in RTILs phase. The solubility of water in C$_4$mimPF$_6$ and solubility C$_4$mimPF$_6$ in water constitute few percent (see Table 6.1). In these experiments the dissolution of RTIL in the aqueous phase is avoided by saturation of aqueous phase with RTIL. The effect of hygroscopic properties of C$_4$mimPF$_6$ was also observed during electrochemical experiments performed in the presence of water vapors [88]. In fact the dissolution of some amount of water in RTIL phase may lead to two effects: the decrease of RTILs viscosity enhancing diffusion of *t*BuFc in RTIL phase and decrease of *t*BuFc concentration. The observed change of current magnitude indicates that first effect is more significant.

The value of $E_{Red/Ox}$ is equal to 0.13 V vs. Ag/AgCl and similar to that obtained on Au electrode modified with the same amount of tBuFc solution in C$_4$mimPF$_6$ (0.14 V vs. Ag/AgCl) (Fig. 11.7).
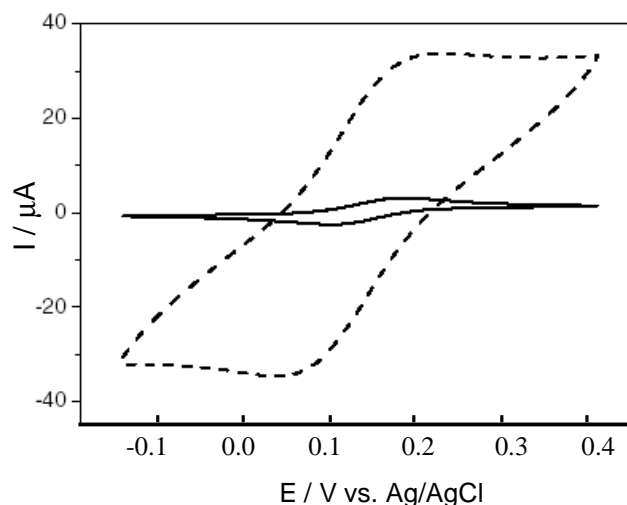

Figure 11.7.   Cyclic voltammograms obtained with CCE prepared from precursors mixture: TMOS:MTMOS (99:1) modified with 2 μl of 0.01 mol dm^{-3} tBuFc solution in C$_4$mimPF$_6$ (dashed) and Au disc electrode modified with 2 μl drop of the same solution. Both electrodes were immersed in saturated aqueous KPF$_6$ (solid).

The current magnitude obtained with CCE is about 10 times larger than that obtained at Au electrode having the same apparent surface (Fig. 11.7). The hydrophobic-hydrophilic porous structure of CCE and its more developed surface seems to be responsible for this effect. Possibly, the silicate matrix promotes formation of RTIL microphases similarly to CCE modified with polar organic solvent (Chapter 8.2) and even more to salt containing polar organic solvent (Chapter 11.1). Thus the extension of the length of three-phase boundary is provided by dispersion of conductive particles within silicate matrix.

Despite of poor wetting of MTMOS based silicate matrix by C$_4$mimPF$_6$ next experiments were performed at CCE prepared from pure MTMOS to compare with that obtained with polar organic solvent modified CCE.

The peak current obtained with CCE modified with tBuFc solution in RTIL is one order of magnitude larger than that for CCE modified with the same redox probe solution in NPOE (Fig. 11.8). The viscosity of C$_4$mimPF$_6$ is more than one order of magnitude larger than the viscosity of NPOE (see Table 6.1). This implies slower mass

113

transport in RTIL and smaller current. However, the opposite effect is observed (Fig. 11.8).
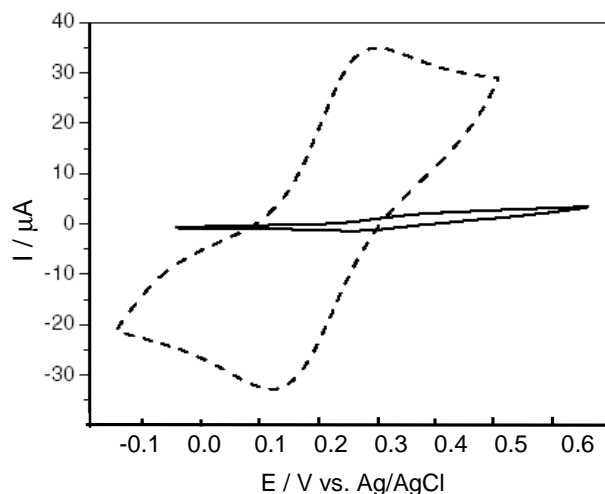

Figure 11.8.   Cyclic voltammograms obtained with CCE prepared from MTMOS and modified with 2μl 0.01 mol dm^{-3} tBuFc solution in C$_4$mimPF$_6$ and immersed into saturated aqueous KPF$_6$ (dashed) and CCE modified with 2μl 0.01 mol dm^{-3} tBuFc solution in NPOE and immersed into 0.1 mol dm^{-3} KPF$_6$ (solid).

Assuming that only viscosity plays important role, replacement of NPOE with RTIL induces more than two orders of magnitude enhancement of the efficiency of the electrode process. There are many possible reasons of this effect. They include much faster formation of tBuFc$^+$ in RTIL than in NPOE and/or much faster anion transfer across RTIL / aqueous solution interface than across NPOE / aqueous solution interface. The latter may be affected by potential drop at RTIL / aqueous solution interface. Due to ionic conduction of RTIL the larger effective electrode surface represents another possibility. As it was in the case of CCE modified with polar organic solvent with added salt, the electrode reaction may occur not only close to the three-phase junction. The estimated I_p for this redox system is equal 460 μA. It was calculated in the same manner as in Chapter 11.1, assuming that D of tBuFc in C$_4$mimPF$_6$ is equal 1.5×10^{-8} cm^2 s^{-1} The calculated peak current is one order of magnitude larger than observed (Fig. 11.8). Therefore reaction does not take place at whole electrode surface, namely geometric area of all graphite particles filling CCE.

Thus, it is reasonable to say that electrode process occurs mainly close to the three-phase junction formed at graphite particle / organic phase / aqueous solution. The observed current difference between organic polar solvent system and ionically

114

conductive polar solvent system (Fig. 11.8) may indicate that only fraction of the electronic conductor surface (graphite particles or gold) covered by RTIL are electrochemically active due to ionic conductivity of the organic phase.

The replacement of C_4mimPF_6 with more viscous $C_{10}mimN(Tf)_2$ results in similar voltammetric response (Fig. 11.9).
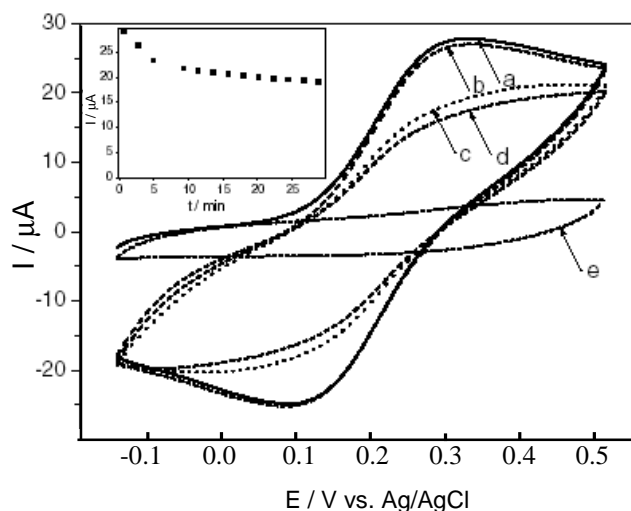

Figure 11.9.   Cyclic voltammograms obtained with CCE prepared from TMOS:MTMOS (99:1) mixture and modified with 2 μl 0.01mol dm^{-3} tBuFc solution in $C_{10}mimN(Tf)_2$ and immersed into saturated aqueous KPF_6. The 1st (a), 2nd (b), 30th (c) and 100th (d) cycles are shown. Voltammogram obtained for CCE modified with pure $C_{10}mimN(Tf)_2$ (e). Inset shows current (at E = 0.326 V vs. Ag/AgCl) vs. t dependence.

The shift of $E_{Red/Ox}$ of $C_{10}mimN(Tf)_2$ based system into positive direction by 0.06 V in comparison to C_4mimPF_6 based system indicates that tBuFc dissolved in this more hydrophobic RTIL is more difficult to electrooxidize. This is understandable because $C_{10}mimN(Tf)_2$ is expected to be less polar than C_4mimPF_6. Moreover, contrary to CCE modified with C_4mimPF_6 based solution the current magnitude obtained with CCE modified with $C_{10}mimN(Tf)_2$ based solution gradually decreases during subsequent scans. After 30 scans, it reaches a constant value. This change seems to be connected with some rearrangement of the liquid / liquid interface during continuous scanning or expulsion of part of electrogenerated tBuFc$^+$ cation to the aqueous phase:

$$tBuFc^+_{(RTIL)} \rightarrow tBuFc^+_{(aq)} \tag{11.2}$$

This reaction also occurs in the case of C_4mimPF_6 modified electrode. Since the concentration of non-electroactive C_nmim^+ (n = 4, 10) cations is almost three orders of

115

magnitude larger than that of the redox probe, their ejection to the aqueous phase is more probable:

$$C_n mim^+_{(RTIL)} \rightarrow C_n mim^+_{(aq)} \tag{11.3}$$

Similarly to organic polar solvent system the ion transfer across RTIL / aqueous solution interface is caused by electrooxidation of tBuFc in RTIL phase. After electrogeneration of tBuFc$^+$ local deficiency of charge within RTIL occurs. Therefore, reaction (11.1) has to be followed by ion transfer across RTIL / aqueous solution interface. Except of two types of cation transfer across liquid / liquid interface (11.2 and 11.3), the anion insertion from the aqueous phase may also take place:

$$t BuFc^+_{(RTIL)} + X^-_{(aq)} \rightarrow t BuFc^+_{(RTIL)} + X^-_{(RTIL)} \tag{11.4}$$
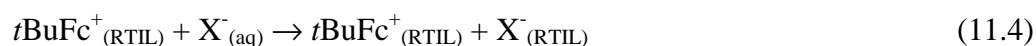
In order to determine whether tBuFc$^+$ cation is ejected to aqueous phase or counterion is injected into RTIL phase, the experiments in presence of different anions were performed. Fig. 11.10 presents DPV curves obtained for CCE modified with tBuFc solution in $C_{10}mimN(Tf)_2$.
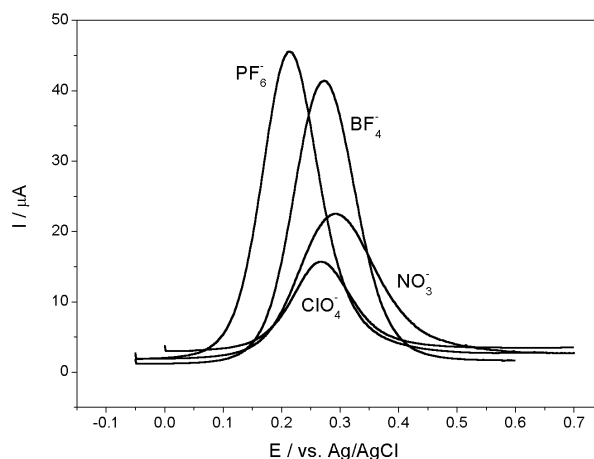
Figure 11.10.   Differential pulse voltammograms (step potential 0.01 V, modulation amplitude 0.01 V, modulation time 0.05 s, interval time 1s) obtained with CCE modified with 2 μl 0.01 mol dm^{-3} tBuFc solution in C_{10}mimN(Tf)$_2$ and immersed into 0.1 mol dm^{-3} aqueous solution separately containing: KPF$_6$, NaBF$_4$, NaClO$_4$, NaNO$_3$.

Similarly to organic polar solvent system the shift of $E_{Red/Ox}$ is consistent with the order of hydrophobicity of anions, namely it is easier to electrooxidize tBuFc in RTIL in the presence of more hydrophobic anion in the aqueous phase. This behavior is observed only for hydrophobic anions, like PF$_6^-$, BF$_4^-$, ClO$_4^-$. For very hydrophilic ones like F$^-$ or

SO_4^{2-}, such dependence is not detected (Fig. 11.11). Although the points in Fig. 11.11 are somewhat scattered, the approximately linear dependence for all points, except points corresponding to F^- and SO_4^{2-}, with slope much below unity (0.28) is observed.

Figure 11.11.   Plot of $E_{Red/Ox}$ vs. $\Delta_{aq}^{NB}\varphi_{X^-}^0$ obtained with CCE modified with 2μl 0.01 mol dm^{-3} tBuFc

solution in $C_{10}mimN(Tf)_2$. The dashed line is indicating unit slope. The solid line was obtained by linear

regression. The sequence of anions is indicated on the top of the graph.

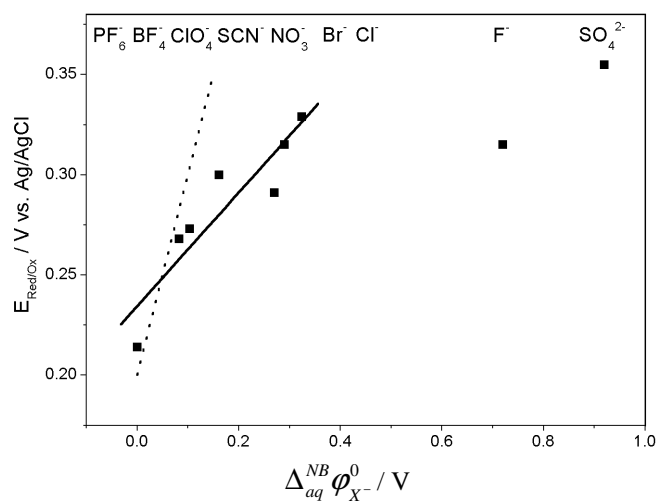The unity slope of dependence $E_{Red/Ox}$ vs. $\Delta_{aq}^{RTIL}\varphi_{X^-}^0$ is expected from a Nernstian type equation [13] (see p. 21):

$$E_{Red/Ox} = E^0_{tBuFc^+_{RTIL}/tBuFc_{RTIL}} + \Delta_{aq}^{RTIL}\varphi_{X^-}^0 - \frac{RT}{F}\ln c_{X^-} + \frac{RT}{F}\ln\frac{c^*_{tBuFc_{RTIL}}}{2} \qquad (11.5)$$

where $E^0_{tBuFc^+_{RTIL}/tBuFc_{RTIL}}$ is the standard redox potential of the tBuFc/tBuFc$^+$ couple in RTIL, $\Delta_{aq}^{RTIL}\varphi_{X^-}^0$ is the standard transfer potential of X$^-$ from water to RTIL. The latter parameter is unavailable and it was replaced with $\Delta_{aq}^{NB}\varphi_{X^-}^0$, as a measure of the anion hydrophobic-hydrophilic properties. Actually the strong deviation of the slope of $E_{Red/Ox}$ vs. $\Delta_{aq}^{NB}\varphi_{X^-}^0$ dependence from unity may be caused by selection of this parameter.

Therefore, one can conclude that in presence of hydrophobic anions in the aqueous phase the reaction (11.1) is followed by counterion injection into RTIL phase according to (11.4). However the competition between reactions (11.2 or 11.3) and (11.4) is possible. For hydrophilic anions, such as F^- and SO_4^{2-}, the reaction (11.1) is probably followed by reaction (11.2 or 11.3). This mechanism and its anion dependence

is similar to that observed for CCE supported organic polar solvent / aqueous solution interface.

11.2.2 Carbon paste electrode based on room-temperature ionic liquid

Analogously to CPE prepared with redox probe solution in NPOE (Chapter 9) RTIL-based CPE was prepared and studied. Such electrode was never reported in literature. It can be used to elude the effect of silicate matrix on electrogenerated ion transfer across RTIL / aqueous interface. Additionally the electrochemical behavior of redox probe modified CPE with polar non-conductive solvent (NPOE) and ionically conductive solvent could be compared. This electrode was prepared using $C_{10}mimN(Tf)_2$ as a binder. It is a good candidate, because it is even more viscous than NPOE (see Table 6.1). It can be expected that, the formation of the three-phase junction on the surface of electronically conductive particles present close to the liquid / liquid interface formed by RTIL phase at CPE is compared to that formed at CPE prepared with organic polar phase (Fig. 9.1).

Typical cyclic voltammograms obtained during continuous scanning of CPE containing tBuFc solution in $C_{10}mimN(Tf)_2$ are presented in Fig. 11.12.
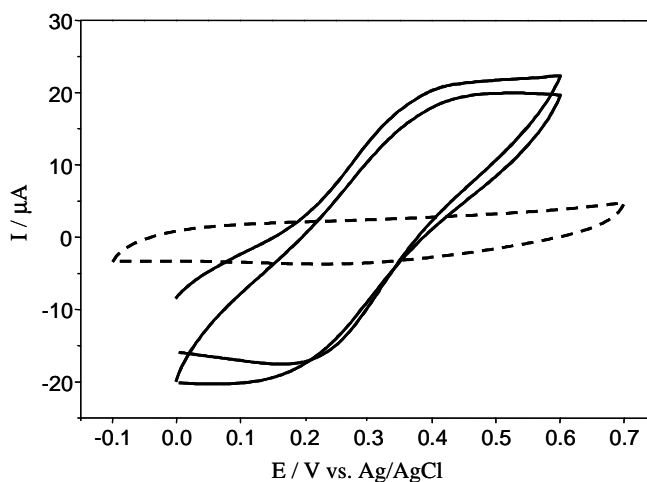
Figure 11.12.   Cyclic voltammograms obtained with CPE prepared with 0.01 mol dm^{-3} tBuFc solution in $C_{10}mimN(Tf)_2$ (1st and 10th scans (solid)) and pure $C_{10}mimN(Tf)_2$ (dashed) and immersed into 0.1 mol dm^{-3} aqueous NaClO$_4$.

There is slight difference between the shape and the current magnitude of CV curves obtained at 1st and 2nd scans, whereas 2nd and 10th scans are almost identical. Since more than 10 cycles were not measured, one can conclude that some period of stability of

cyclic voltammograms is observed. Similarly to CCE modified with the same solution, the voltammetric response obtained with CPE is characterized by similar magnitude of the current, symmetric and not-well defined both anodic and cathodic peaks. They result from reversible electrooxidation of tBuFc in RTIL phase according to reaction (11.1).

The value of peak current obtained with CPE prepared with tBuFc solution in RTIL is one order of magnitude larger than for CPE prepared from the same redox solution in NPOE (Fig. 11.13).
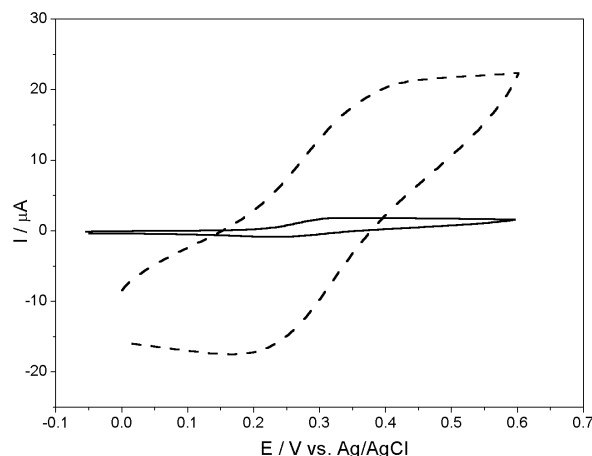
Figure 11.13.   The effect of solvent on cyclic voltammograms obtained with CPE prepared with 0.01 mol dm^{-3} tBuFc solution in C$_{10}$mimN(Tf)$_2$ (dashed) and CPE prepared with 0.01 mol dm^{-3} tBuFc solution in NPOE (solid) and immersed into 0.1 mol dm^{-3} NaClO$_4$.

Contrary to voltammetric results obtained with analogous CCE (Fig. 11.8), there is almost no difference between midpoint potential obtained with RTIL and NPOE based electrodes. However, the similar difference between their current magnitudes is visible. The reason for such voltammetric response seems to be the same as for CCE electrode modified with RTIL-based solution (see p. 113). Namely, due to ionic conductivity of RTIL the efficiency of electrode process is larger than in the case of non-conducting NPOE phase. Probably, in the case of RTIL-based CPE the larger amount of graphite particles are active in the electrode process. It has to be also emphasized, that the presence of silicate matrix has no important influence on ion transfer across liquid / liquid interface. One can conclude, that this matrix does not hinder redox probe access to graphite particles.

Next experiments were performed in order to more clearly understand the mechanism of electrode reaction involving the ion transfer across RTIL / aqueous solution interface.

According to equation (11.5) for anion transfer (11.4) $E_{Red/Ox}$ is expected to depend on concentration of anion present in the aqueous phase. Fig. 11.14 shows normalized DPV curves for electroactive CPE immersed into aqueous solutions at different concentration.

Figure 11.14.   Normalized differential pulse voltammograms (step potential 0.01 V, modulation amplitude 0.01 V, modulation time 0.05 s, interval time 1s) obtained with CPE prepared with 0.01 mol dm^{-3} tBuFc solution in C_{10}mimN(Tf)$_2$ and immersed into aqueous KPF$_6$ (a) and KNO$_3$ (b) solution. The voltammograms were normalized adjusting their background currents.

It can be seen that the midpoint potential systematically shifts to more positive potential side as concentration decreases (Fig. 11.15).
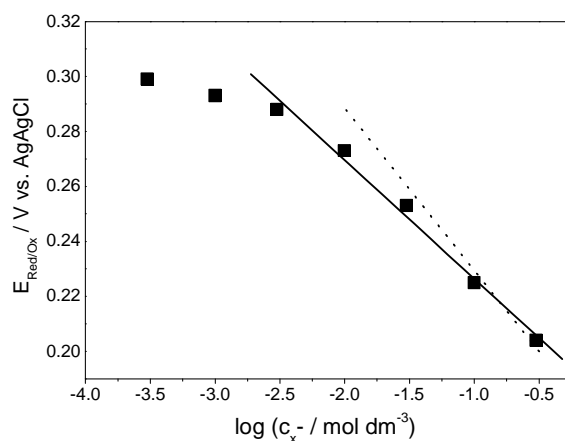
Figure 11.15.   Plot of $E_{Red/Ox}$ vs. log c_{X^-} obtained with CPE prepared with 0.01 mol dm^{-3} tBuFc solution in C_{10}mimN(Tf)$_2$ and immersed into aqueous KPF$_6$. $E_{Red/Ox}$ values were determined from DPV curves in Fig. 11.14. Solid line was obtained by linear regression for five points. The dotted line is indicating Nernstian slope.

120

A linear dependence of $E_{Red/Ox}$ vs. *log* c_{X^-} with sub-Nernstian slope (-0.043 V / decade) is observed only for points corresponding to more concentrated aqueous solutions. For lower c_{X^-} less negative slope is observed. This deviation is probably connected with the increase of contribution of cation transfer to the aqueous phase according to reactions (11.2) or (11.3). This can be explained by the large c_{tBuFc}/c_{X^-} ratio. It causes the lack of counterion to compensate electrogenerated cation and as a consequence not compensated cation is ejected to the aqueous phase.

Interestingly, as for other redox systems studied at CCE and CPE, the effect of the electrolyte concentration is visible on the reduction in peak current with decreasing concentration of the aqueous electrolyte (Fig. 11.14). The dependences log (I_p) vs. log (c_{X^-}) has barely visible S-shaped feature (Fig. 11.16).
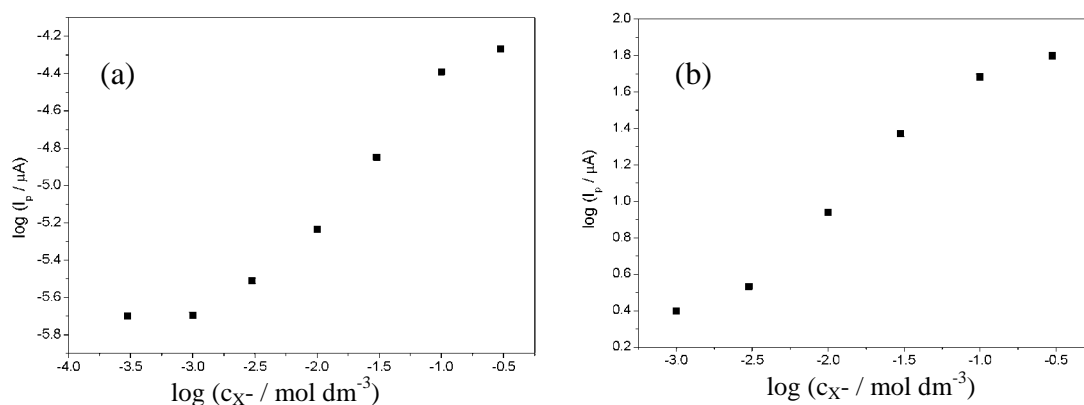
Figure 11.16.   Plots of log (I_p) vs. log (c_{X^-}) for CPE prepared from 0.01 mol dm^{-3} tBuFc solution in C$_{10}$mimN(Tf)$_2$ and immersed into aqueous KPF$_6$ (a) and KNO$_3$ (b) solutions. The values I_p were estimated from normalized DPV curves in Fig. 10.14.

Similarly as in the case of $E_{Red/Ox}$ the deviation from linearity for less concentrated KPF$_6$ solution can be connected also with the influence of cation ejection from RTIL to the aqueous phase. As for CCE modified with redox probe solution in organic polar solvent (see p. 79) for the largest value of $c_{tBuFc(RTIL)}/c_{X^-}$ the influence of reactions (11.2) or (11.3) is dominating. The deviation observed for more concentrated electrolyte solution is difficult to explain.

To study the competition between cation and anion transfer the results of experiments with different anion present in the aqueous phase were compared (Fig. 11.17).

As for previously studied systems the shift of the voltammetric signals depends on the nature of the anions present in the aqueous phase (Fig. 11.17).
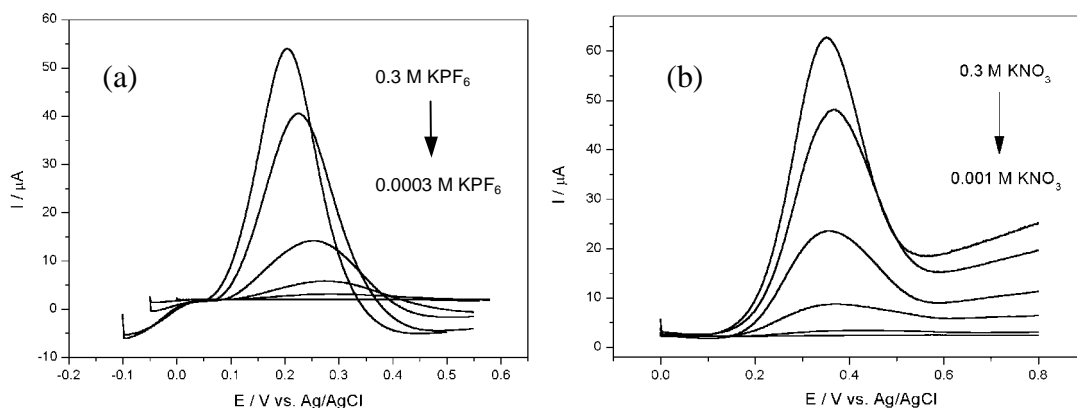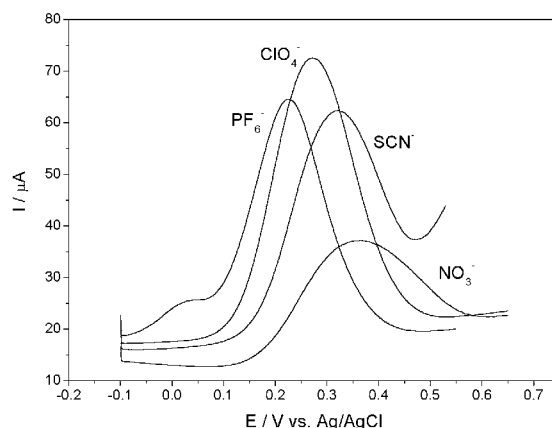

Figure 11.17.   Differential pulse voltammograms (step potential 0.01 V, modulation amplitude 0.01 V, modulation time 0.05 s, interval time 1s obtained with CPE prepared with 0.01 mol dm^{-3} tBuFc solution in $C_{10}mimN(Tf)_2$ and immersed into 0.1 mol dm^{-3} aqueous solution separately containing: KPF$_6$, NaClO$_4$, NaSCN or KNO$_3$.

The data obtained in the presence of all studied anions are summarized in Fig. 11.18, which presents the measured peak potential as a function of $\Delta_{aq}^{NB}\varphi_{X^-}^0$.
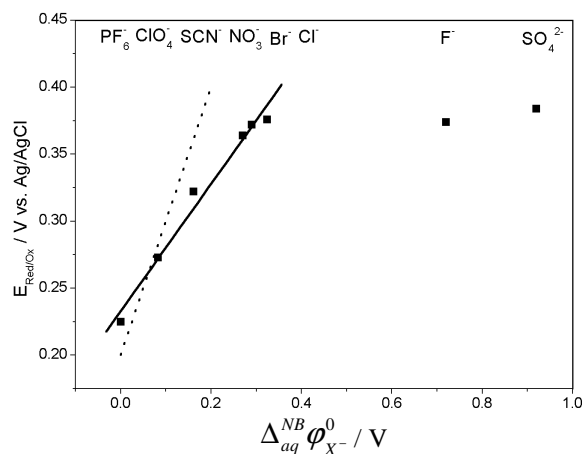
Figure 11.18.   Plot of $E_{Red/Ox}$ vs. $\Delta_{aq}^{NB}\varphi_{X^-}^0$ obtained with CPE prepared with 0.01 mol dm^{-3} tBuFc solution in $C_{10}mimN(Tf)_2$. The dotted line is indicating unit slope. The sequence of anions is indicated on the top of the plot.

The linear correlation between $E_{Red/Ox}$ and $\Delta_{aq}^{NB}\varphi_{X^-}^0$ for all studied anions, except strongly hydrophilic anions, like F$^-$ and SO$_4^{2-}$, is visible. The points are much less scattered and deviation of the slope (0.47) from unity is smaller than it was observed for

122

CCE modified with the same RTIL-based solution. Obviously, the silicate matrix has some influence on the voltammetric response. Interestingly, almost unity slope was observed for Au electrode modified with droplets of $C_{10}mimN(Tf)_2$ [79]. However, from thermodynamic point of view the type of the electrode surface should not affect the dependence $E_{Red/Ox}$ vs. $\Delta_{aq}^{NB}\varphi_{X^-}^0$.

Summarizing all results obtained at CCE and CPE electrode based on salt containing NB and RTILs solutions several the most important points should be distinguished.

At first, these electrodes exhibit electrochemical signal connected with electrode reaction of the salt containing redox liquids. In addition, for all types of electrodes and both RTIL-based solutions some period of stability of cyclic voltammograms is observed.

Second, both electrodes modified with RTILs-based solution show sensitivity towards the hydrophobicity of the anion present in the aqueous phase and their concentration. The possible mechanism of electrode reaction involving ion transfer across RTIL / aqueous phase interface is presented in Fig. 11.19.
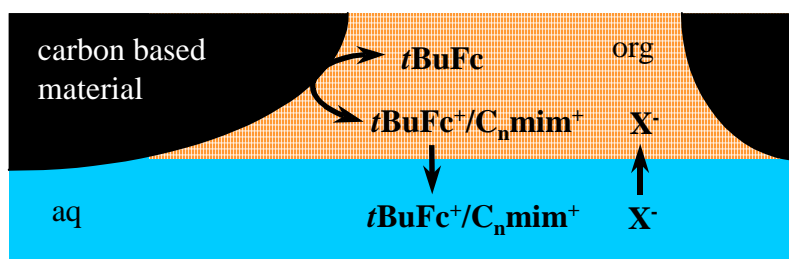
Figure 11.19.   *The schematic drawing of possible reaction pathways connected with electrooxidation of tBuFc solution in the RTIL supported by CCE or CPE immersed into aqueous solution.*

Third and last, the efficiency of the electrode process is much larger than that observed for CCE and CPE modified with the redox probe solution in less viscous organic polar solvent. Moreover, it has been shown that heterogeneous material enhances substantially efficiency of the electrode process in comparison to smooth electrode support. However only small fraction of conductive particles being close to liquid / liquid interface is effective for electrode process.

123

Conclusions

This thesis presents and discusses results of experimental study of electrogenerated ion transfer across liquid / liquid interface supported by carbon ceramic electrode (CCE). This liquid bulk-modified electrode belongs to the class of so called three-phase electrodes. Graphite particles, which are the source and sink of electrons, represent one phase of this system. Two other phases are immiscible liquids. Such system was created using hydrophobic silicate based composite carbon material impregnated with the organic phase immersed into the aqueous phase. When the organic phase is not ionically conductive the electrode process has to start at the three-phase interface. This is not necessary true, when organic phase is ionically conductive.

The main aim of this thesis was to study and understand the mechanism of electrogenerated ion transfer across redox liquid / aqueous solution interface supported by CCE. For this purpose the influence of different factors on this reaction was studied. Among them there are stability of voltammograms, organic solvent, type of redox probe and its concentration, type of anion present in the aqueous phase and its concentration. To study electrochemical properties of unmodified and modified CCE the voltammetric and chronoamperometric techniques were used. Additionally, to observe the morphology of CCE surface Field Emission Gun Scanning Electron Microscopy was applied.

The most important conclusions are as follows:

1. The electrooxidation of redox probe in the organic phase generates ion transfer across liquid / liquid interface. Two different ion transfer reactions are possible: ejection of electrogenerated cation to the aqueous phase and/or uptake of anion from the aqueous phase. In the case of salt containing organic phase or RTIL-based solution the ejection of corresponding non-electroactive cation can also take place. All transfers occur to maintain electroneutrality of the organic phase. Their contribution depends on the hydrophobicity of redox probe and anion present in aqueous phase. For less hydrophobic redox probe and/or more hydrophilic anion the transfer of electrogenerated cation to the aqueous phase is preferred. This process dominates for CCE modified with Fc or tBuFc solution in polar solvent or for all electrodes studied immersed to F^- or SO_4^{2-} aqueous solutions. On the other hand for more hydrophobic redox probe and less hydrophilic anion the transfer of latter to the organic phase dominates. This is especially visible for CCE modified with the most hydrophobic redox probe - DMFc solution. As

one can judge from the shift of the redox potential this electrode exhibits selectivity towards less hydrophilic anions present in the aqueous phase.

2.   The solution of the redox probe in organic polar solvent fills pores of CCE because of hydrophobicity of silicate matrix. This material immersed into the aqueous solution is able to support the liquid / liquid interface. The specific morphology of CCE permits to create numerous three-phase interfaces: organic phase / aqueous phase / graphite particle. The use of different size graphite particle gives possibility to change the length the three-phase boundary and in consequence to change the current magnitude obtained with CCE.

3.   The ejection of electroactive species from CCE to the aqueous phase does not cause the substantial consumption of redox probe. This is because of its continuous supply from electrode bulk to the surface. The continuous development of redox probe concentration gradient perpendicular to liquid / liquid interface exists. The hydrophobic porous structure of CCE serves as container of redox liquid.

4.   The stability and features of voltammograms obtained with modified CCE are affected by the type of redox probe and its concentration, as well as by the type of the anion present in the aqueous phase and its concentration.

5.   The concentration of anion present in the aqueous phase not only affects formal potential of the redox probe but also the magnitude of the current. The more concentrated aqueous solution the higher peak current is observed. This proves that anion is present in the reaction zone and participates in the electrode reaction. It means that CCE modified with redox liquid is sensitive to non-electroactive ionic species, especially to hydrophobic anions present in the aqueous solution.

6.   In the case of CCE modified with ionically conducting redox liquid the electrode process is not restricted to the three-phase junction. However, the electrode reaction does not take place at whole ionically conducting redox liquid / graphite particle interface and the ion transfer across liquid / liquid interface still occurs. The CCE modified with redox probe solution in room-temeprature ionic liquid also exhibits some selectivity and sensitivity towards anion present in the aqueous phase.

The advantage of CCE modified with redox probe solution in organic solvent in comparison to flat electrode modified with the same solution, used for the study of the transfer of ions between water and organic solvent, is continuous supply of redox probe to electrode surface and as a consequence the perceptible consumption of redox probe is avoided.

Obviously the possibilities of preparation of liquid modified CCE exhibiting electrogenerated ion transfer across liquid / liquid interface are not limited to these presented in this thesis. In the case of CCE modified with redox probe anchored to the silicate matrix the ejection of electrogenerated cation to the aqueous phase can be eliminated. Thus it seems that electrogenerated hydrophilic anion transfer to the organic phase can be realized. Also the selectivity of such modified CCE may be enhanced by addition of hydrophobic ligand capable to form complex with selected anion to the organic phase. It seems to that future research of these systems should follow these directions.

References

1. *The Dynamics and Structure of the Liquid / Liquid Interface, Faraday Discuss*. 129 (2005).

2. F. Reymond, D.J. Fermin, H.J. Lee, H.H. Girault, *Electrochim. Acta* 45 (2000) 2647.

3. A.G. Volkov, D.W. Deamer, *Liquid-Liquid Interfaces: Theory and Methods*, CRC Press, Boca Raton, Fla. 1996.

4. H.H. Girault, D.J. Schiffrin, *Electrochemistry of Liquid / Liquid Interfaces, in Electroanalytical Chemistry* V.15, A.J. Bard, Eds., Dekker, New York, 1989.

5. P. Vanysek, *Electrochim. Acta* 40 (1995) 2841.

6. H.H. Girault, *Analytical and Physical Electrochemistry*, EPFL Press, 2004.

7. J. Koryta, P. Vanysek, M. Brezina, *J. Electroanal. Chem.* 67 (1976) 263.

8. A.G. Volkov, D.W. Deamer, D.I. Tanelian, V.S. Markin, *Liquid / Liquid Interfaces in Chemistry and Biology*, John Wiley, New York, 1998.

9. Koryta, P. Vanysek, *Electrochemical Phenomena at the Interface of Two Immiscible Electrolyte Solutions,* in *Advances in Electrochemistry and Electrochemical Engineering*, H. Gerischer, C.W. Tobias, Eds., Vol.12, John Wiley & Sons, New York 1981, p.131.

10. J. Koryta, P. Vanysek, M. Brezina, *J. Electroanal. Chem.* 71 (1977) 211.

11. V. Marecek, M.P. Colombini, *J. Electroanal. Chem.* 241 (1988) 133.

12 F. Marken, *Phil. Trans. R. Soc. Lond. A* 362 (2004) 2611.

13. F. Scholz, U. Schroder, R. Gulaboski, *Electrochemistry of Immobilized Particles and Droplets.* Springer 2005.

14. J.S. Rowlinson, B. Widom, *Molecular Theory of Capillarity*, Clarendon Press, Oxford 1982.

15. C.E. Banks, T.J. Davies, R.G. Evans, G. Hignett, A.J. Wain, N.S. Lawrence, J.D. Wadhawan, F. Marken, R.G. Compton, *Phys. Chem. Chem. Phys.* 5 (2003) 4053.

16. F. Scholz, R. Gulaboski, *Chem. Phys. Chem.* 6 (2005) 16.

17. F. Marken, R.D. Webster, S.D. Bull, S.D. Davies, *J. Electroanal. Chem.* 437 (1997) 209.

18. F. Scholz, S. Komorsky-Lovric, M. Lovric, *Electrochem. Commun.* 2 (2000) 112.

19. K. Aoki, P. Tasakorn, J. Chen, *J. Electroanal. Chem.* 542 (2003) 51.

20. M. Opallo, M. Saczek-Maj, *Electrochem. Commun.* 3 (2001) 306.

21. M. Opallo, M. Saczek-Maj, *Chem. Commun.* (2002) 448.

22. J. Niedziolka, M. Opallo, *Electrochem. Commun.* 6 (2004) 475.

23. J. Niedziolka, B. Palys, R. Nowakowski, M. Opallo, *J. Electroanal. Chem.* 578 (2005) 239.

24. K. Nakatani, T. Uchida, H. Misawa, N. Kitamura, H. Masuhara, *J. Phys. Chem.* 97 (1993) 5197.

25. K. Nakatani, T. Uchida, H. Misawa, N. Kitamura, *J. Electroanal. Chem.* 367 (1994) 109.

26. K. Nakatani, T. Uchida, N. Kitamura, H. Masuhara, *J. Electroanal. Chem.* 375 (1994) 383.

27. K. Nakatani, M. Wakabayashi, K. Chikama, N. Kitamura, *J. Phys. Chem.* 100 (1996) 6749.

28. N. Terui, K. Nakatani, N. Kitamura, *J. Electroanal. Chem.* 494 (2000) 41.

29. E. Bak, M. Donten, Z. Stojek, *Electrochem. Commun.* 7 (2005) 483.

30. U. Schroder, R.G. Compton, F. Marken, S.D. Bull, S.G. Davies, S. Gilmor, *J. Phys. Chem. B* 105 (2001) 1344.

31. J. Chen, M. Sato, *J. Electroanal. Chem.* 572 (2004) 153.

32. M. Donten, Z. Stojek, F. Scholz, *Electrochem. Commun.* 4 (2002) 324.

33. J.D. Wadhawan, A.J. Wain, A.N. Kirkham, D.J. Walton, B. Wood, R.R. France, S.D. Bull, R.G. Compton*, J. Am. Chem. Soc.* 125 (2003) 11418.

34. J.D. Wadhawan, A.J. Wain, R.G. Compton, *Chem. Phys. Chem.* 4 (2003) 1211.

35. J.D. Wadhawan, R.G. Compton, F. Marken, S.D. Bull, S.G. Davies, *J. Solid State Electrochem.* 5 (2001) 301.

36. P. Tasakorn, J. Chen, K. Aoki, *J. Electroanal. Chem.* 533 (2002) 119.

37. S. Komorsky-Lovric, M. Lovric, F. Scholz, *J. Electroanal. Chem.* 508 (2001) 129.

38. S. Komorsky-Lovric, K. Riedl, R. Gulaboski, V. Mirceski, F. Scholz, *Langmuir* 18 (2002) 8000.

39. R. Gulaboski, F. Scholz, *J. Phys. Chem. B* 107 (2003) 5650.

40. M. Saczek-Maj, M. Opallo, *Electroanalysis* 14 (2002) 1060.

41. R. Gulaboski, V. Mirceski, F. Scholz, *Electrochem. Commun.* 4 (2002) 277.

42. V. Mirceski, R. Gulaboski, F. Scholz, *Electrochem. Commun.* 4 (2002) 814.

43. F. Scholz, R. Gulaboski, K. Caban, *Electrochem. Commun.* 5 (2003) 929.

44. R. Gulaboski, V. Mirceski, F. Scholz, *Amino Acids* 24 (2003) 149.

45. J.C. Ball, F. Marken, Q. Fulian, J.D. Wadhawan, A.N. Blythe, U. Schroder, R.G. Compton, S.D. Bull, S.G. Davies, *Electroanalysis* 12 (2000) 1017.

46. F. Marken, A.N. Blythe, J.D. Wadhawan, R.G. Compton, S.D. Bull, R.T. Aplin, S.G. Davies, *J. Solid State Electrochem.* 5 (2001) 17.

47. J.D. Wadhawan, R.G. Evans, R.G. Compton, *J. Electroanal. Chem.* 533 (2002) 71.

48. A.J. Wain, N.S. Lawrence, P.R. Greene, J.D. Wadhawan, R.G. Compton, *Phys. Chem. Chem. Phys.* 5 (2003) 1867.

49. A.J. Wain, J.D. Wadhawan, R.G. Compton, *Chem. Phys. Chem.* 4 (2003) 974.

50. J.D. Wadhawan, R.G. Evans, C.E. Banks, S.J. Wilkins, R.R. France, N.J. Oldham, A.J. Fairbanks, B. Wood, D.J. Walton, U. Schroder, R.G. Compton, *J. Phys. Chem. B* 106 (2002) 9619.

51. U. Schroder, J.D. Wadhawan, R.G. Evans, R.G. Compton, B. Wood, D.J. Walton, R.R. France, F. Marken, C.B. Page, C.M. Hayman, *J. Phys. Chem. B* 106 (2002) 8697.

52. F. Marken, R.G. Compton, C.H. Goeting, J.S. Foord, S.D. Bull, S.G. Davies, *Electroanalysis* 10 (1998) 821.

53. Q. Fulian, J.C. Ball, F. Marken, R.G. Compton, A.C. Fisher, *Electroanalysis* 12 (2000) 1012.

54. F. Marken, R.G. Compton, C.H. Goeting, J.S. Foord, S.D. Bull, S.G. Davies, *J. Solid State Electrochem*. 5 (2001) 88.

55. T.J. Davies, B.A. Brookes, A.C. Fisher, K. Yunus, S.J. Wilkins, P.R. Greene, J.D. Wadhawan, R.G. Compton, *J. Phys. Chem. B* 107 (2003) 6431.

56. F. Marken, C.M. Hayman, P.C.B. Page, *Electrochem. Commun*. 4 (2002) 462.

57. F. Marken, C.M. Hayman, P.C.B. Page, *Electroanalysis* 14 (2002) 172.

58. F. Marken, A.N. Blythe, R.G. Compton, S.D. Bull, S.G. Davies, *Chem. Commun.* (1999) 1823.

59. A. Gergely, G. Inzelt, *Electrochem. Commun.* 3 (2001) 753.

60. M. Opallo, J. Kukulka-Walkiewicz, M. Saczek-Maj, *J. Sol-Gel Sci. Technol*. 26 (2003) 1045.

61. M. Saczek-Maj, M. Opallo, *Electroanalysis* 15 (2003) 566.

62. G. Wittstock, H. Emons, W.R. Heineman, *Electroanalysis* 8 (1996) 143.

63. A.J. Wain, J.D. Wadhawan, R.R. France, R.G. Compton, *Phys. Chem. Chem. Phys.* 6 (2004) 836.

64. T. Osakai, A. Ogata, K. Ebina, *J. Phys. Chem. B* 101 (1997) 8341.

65. F. Scholz, R. Gulaboski, V. Mirceski, P. Langer, *Electrochem. Commun.* 4 (2002) 659.

66. R. Gulaboski, K. Caban, Z. Stojek, F. Scholz, *Electrochem. Commun*. 6 (2004) 215.

67. S. Komorsky-Lovric, M. Lovric, F. Scholz, *Collect. Czech. Chem. Commun*. 66 (2001) 434.

68. F. Quentel, V. Mirceski, M. L'Her, *Anal. Chem.* 77 (2005) 1940.

69. R. Gulaboski, A. Galland, G. Bouchard, K. Caban, A. Kretschmer, P-A. Carrupt, Z. Stojek, H.H. Girault, F. Scholz, *J. Phys. Chem. B* 108 (2004) 4565.

70. R. Gulaboski, K. Riedl, F. Scholz, *Phys. Chem. Chem. Phys*. 5 (2003) 1284.

71. G. Bouchard, A. Galland, P-A. Carrupt, R. Gulaboski, V. Mirceski, F. Scholz, H.H. Girault, *Phys. Chem. Chem. Phys*. 5 (2003) 3748.

72. S. Komorsky-Lovric, V. Mirceski, C. Kabbe, F. Scholz, *J. Electroanal. Chem.* 566 (2004) 371.

73. D. Giovanelli, T.J. Davies, L. Jiang, T.G.J. Jones, R.G. Compton, *Phys. Chem. Chem. Phys.* 6 (2004) 3889.

74. F. Scholz, R. Gulaboski, K. Caban, *Electrochem. Commun.* 5 (2003) 929.

75. V. Mirceski, F. Scholz, *J. Electroanal. Chem.* 522 (2002) 189.

76. F. Marken, K.J. McKenzie, G. Shul, M. Opallo, *Faraday Discuss.* 129 (2005) 219.

77. F. Scholz, R. Gulaboski, *Faraday Discuss.* 129 (2005) 169.

78. F. Scholz, R. Gulaboski, V. Mirceski, P. Langer, *Electrochem. Commun.* 4 (2002) 659.

79. J. Niedziolka, E. Rozniecka, J. Stafiej, J. Siriex-Plenet, L. Gaillon, D. Di Caprio, M. Opallo, *Chem. Commun.* (2005) 2954.

80. I. Noviandri, K.N. Brown, D.S. Fleming, P.T. Gulyas, P.A. Lay, A.F. Masters, L. Phillips, *J. Phys. Chem. B*. 103 (1999) 6713.

81. F. Scholz (Ed.), *Electroanalytical Methods. Guide to Experiments and Applications*, Springer 2005.

82. C. Shi, F.C. Anson, *Anal. Chem.* 70 (1998) 3114.

83. C. Shi, F.C. Anson, *J. Phys. Chem. B* 102 (1998) 9850.

84. C. Shi, F.C. Anson, *J. Phys. Chem. B* 103 (1999) 6283.

85. H. O. Shafer, T.L. Derback, C.A. Koval, *J. Phys. Chem. B* 104 (2000) 1025.

86. J. Chen, O. Ikeda, K. Aoki, *J. Electroanal. Chem.* 496 (2001) 88.

87. J. Yoshida, J. Chen, K. Aoki, *J. Electroanal. Chem.* 553 (2003) 117.

88. M.C. Buzzeo, R.G. Evans, R.G. Compton, *Chem. Phys. Chem.* 5 (2004) 1106.

89. B.M. Quinn, Z. Ding, R. Moulton, A.J. Bard, *Langmuir* 18 (2002) 1734.

90. J.D. Wadhawan, U. Schroder, A. Neudeck, S.J. Wilkins, R.G. Compton. F. Marken, C.S. Consorti, R.F. de Souza, J. Dupont, *J. Electroanal. Chem.* 493 (2000) 75.

91. J.C. Myland, K.B. Oldham, *Electrochem. Commun.* 2 (2002) 541

92. M. Lovric, F. Scholz, *J. Electroanal. Chem.* 540 (2003) 89.

93. T.J. Davies, B.A. Brookes, R.G. Compton, *J. Electroanal. Chem.* 566 (2004) 193.

94. T.J. Davies, A.C. Garner, S.G. Davies, R.G. Compton, *J. Electroanal. Chem.* 570 (2004) 171.

95. M. Lovric, S. Komorsky-Lovric, R.G. Compton, *Electrochim. Acta* 50 (2005) 1377.

96. A.C. Pierre, *Introduction to Sol-Gel Processing,* Kluwer Academic Publisher 1998.

97. J.D. Wright, N.A.J.M. Sommerdijk, *Sol-Gel Materials Chemistry and Applications*, OPA 2001.

98. J.P. Flory, *Disc. Faraday Soc*. 57 (1974) 7.

99. H. Dislich, *J. Non-Cryst. Solids* 73 (1985) 599.

100. C.J. Brinker, G. W. Scherer, *Sol-Gel Science,* Academic Press 1990.

101. M.D. Petit-Dominguez, H. Shen, W.R. Heinemen, C. Seliskar, *Anal. Chem.* 69 (1997) 703.

102. G. Shustak, S. Marx, I. Turyan, D. Mandler, *Electroanalysis* 15 (2003) 398.

103. H. Schroeder in *Physics of Thin Films*, ed. G. Hass, Vol.5 Academic Press, New York 1969.

104. L.W. Hrubesh, R.W. Pekala, in *Sol-Gel Processing and Applications,* Plenum Press, New York 1994, p. 363.

105. D.S. Hagberg, D.A. Payne, in *Sol-Gel Processing and Applications,* Plenum Press, New York 1994, p. 97.

106. B.J. Scott, G. Wirnsberger, G. Stucky, *Chem. Mater*. 13 (2001) 3140.

107. C. Moreno-Castilla, F.J. Maldonado-Hodar, *Carbon* 43 (2005) 455.

108. J.P. Chen, W.S. Lin, *Enzyme Microbial Technol*. 32 (2003) 801.

109. R. Gvishi, G. Ruland, P.N. Prasad, *Optics Commun*. 126 (1996) 66.

110. Y.H. Lee, Y.B. Shim, S.B. Park, *Anal. Chem*. 76 (2004) 6150.

111. Y.A. Attia, M.S. Ahmed, M. Zhu in *Sol-Gel Processing and Applications,* Plenum Press, New York 1994, p. 311.

112. F. Gelman, J. Blum, D. Avnir, *J. Am.Chem. Soc*. 122 (2000) 11999.

113. O. Lev, Z. Wu, S. Bharathi, V. Glezer, A. Modestov, J. Gun, L. Rabinovich, S. Sampath, *Chem. Mater*. 9 (1997) 2354.

114. M. Tsionsky, G. Gun, V. Glezer, O. Lev, *Anal. Chem*. 66 (1994) 1747.

115. C.C. Hsueh, M.M. Collinson, *J. Electroanal. Chem*. 420 (1997) 243.

116. W. Kim, S. Chung, S.B. Park, S.C. Lee, C. Kim, S.D. Sung, *Anal. Chem.* 69 (1997) 95.

117. P. Audebert, G. Cerveau, R.J.P. Corriu, N. Costa, *J. Electroanal. Chem*. 413 (1996) 89.

118. J. Wang, V.A. Pamidi, D.S. Park, *Anal. Chem*. 68 (1996) 2705.

119. L. Rabinovich, O. Lev, *Electroanalysis* 13 (2001) 265.

120. J.A. Cox, K.S. Alber, *J. Electrochem. Soc*. 143 (1996) L126.

121. M. Tsionsky, O. Lev, *Anal. Chem*. 67 (1995) 2409.

122. L. Rabinovich, V. Glezer, Z. Wu, O. Lev, *J. Electroanal. Chem*. 504 (2001) 146.

123. P.W. Wu, S.R. Holm, A.T. Duong, B. Dunn, R.B. Kaner, *Chem. Mater*. 9 (1997) 1004.

124. M. Opallo, J. Kukulka, *Electrochem. Commun.* 2 (2000) 394.

125. M. Opallo, J. Niedziolka, M. Saczek-Maj, G. Shul, E. Utzig, J. Mrowiec-Bialon, J. Stygar, W. Wieczorek, *Electrochim. Acta* 48 (2003) 4149.

126. J. Livage, G. Guzman, *Solid State Ionics* 84 91996) 205.

127. M.A. Aegerter, C.O. Avellaneda, A. Pawlicka, M. Atik, *J. Sol-Gel Sci. Technol*. 8 (1997) 689.

128. M. Guglielmi, *J. Sol-Gel Sci. Technol*. 8 (1997) 443.

129. S. Sampath, O. Lev, *Anal. Chem*. 68 (1996) 2015.

130. J. Gun, M. Tsionsky, L. Rabinovich, Y. Golan, I. Rubinstein, O. Lev, *J. Electroanal. Chem.* 395 (1995) 57.

131. G. Oskam, P. Searson, *J. Phys. Chem. B* 102 (1998) 2464.

132. I. Svancara, K. Vytras, J. Barek, J. Zima, *Crit. Rev. Anal. Chem.* 31 (2001) 311.

133. J. Janata, M. Josowicz, P. Vanysek, D.M. DeVaney, *Anal. Chem.* 70 (1998) 179R.

134. J.M. Zen, A.S. Kumar, D.M. Tsai, *Electroanalysis* 15 (2003) 1073.

135. A.J. Downard, *Electroanalysis* 12 (2000) 1085.

136. G. Gun, M. Tsionsky, O. Lev, *Anal. Chim. Acta* 294 (1994) 261.

137. I. Svancara, K. Vytras, J. Barek, J. Zima, *Crit. Rev. Anal. Chem.* 31 (2001) 311.

138. M. Tsionsky, O.Lev, *J. Electrochem. Soc.* 142 (1995) 2132.

139. P. Wang, X. Wang, Y. Yuan, G. Zhu, *J. Non-Cryst. Solids* 277 (2000) 22.

140. J. Li, L.S. Chia, N.K. Goh, S.N. Tan, *J. Electroanal. Chem.* 460 (1999) 234

141. J. Gun, O. Lev, *Anal. Chim. Acta* 336 (1996) 95.

142. A. Salimi, R. Hallaj, M.K. Amini, *Anal. Chim. Acta* 534 (2005) 335.

143. A. Salimi, R. Hallaj, M. Ghadermazi, *Talanta* 65 (2005) 888.

144. R.N. Adams, *Anal. Chem.* 30 (1958) 1576.

145. A.J. Bard, L.R. Faulkner, *Electrochemical Methods. Fundamentals and Applications*, John Wiley & Sons, INC 2001.

146. J. Wang, *Analytical Electrochemistry*, VCH 1994.

147. R. Greef, *Instrumental Methods in Electrochemistry,* J. Wiley & Sons, 1985.

148. Z. Galus, *Teoretyczne Podstawy Elektroanalizy Chemicznej*, PWN 1997.

149. J.W.S. Hearle, J.T. Sparow, P.M. Cross, *The Use of the Scanning Electron Microscope*, Pergamon Press, 1972.

150. "*Practical Scanning Electron Microscopy. Electron and Ion Microprobe Analysis*", Ed. By J.I. Goldstein, H. Yakowitz, Plenum Press, 1975.

151. http://mse.iastate.edu/microscopy/path2.html

152. M.A. Murphy, G.D. Wilcox, R.H. Dahm, F. Marken, *Electrochem. Commun.* 5 (2003) 51.

153. S.J. Stott, K.J. McKenzie, R.J. Mortimer, C.M. Hayman, B.R. Buckley, P.C. Bulman Page, F. Marken, G. Shul, M. Opallo, *Anal. Chem.* 76 (2004) 5364.

154. Z. Samec, J. Langmaier, A. Trojanek, *J. Electroanal. Chem.* 409 (1996) 1.

155. http://www.sigmaaldrich.com/catalog/search/ProductDetail/ALDRICH/237825

156. L. Murtomaki, M.H. Barker, J.A. Manzanares, K. Kontturi, *J. Electroanal. Chem.* 506 (2003) 95.

157. http://en.wikipedia.org/wiki/Ferrocene

158. D.S.H. Wong, J.P. Chen, J.M. Chang, C.H. Chou, *Fluid Phase Equilibr.* 194-197 (2002) 1089.

159. J.G. Huddleston, A.E. Visser, W.M. Reichert, H.D. Willauer, G.A. Broker, R.D. Rogers, *Green Chem.* 3 (2001) 156.

160. C. Wakai, A. Oleinikova, M. Ott, H. Weingartner, *J. Phys. Chem. B* 109 (2005) 17028.

161. R.G. Evans, O.V. Klymenko, C. Hardacre, K.R. Seddon, R.G. Compton, *J. Electroanal. Chem*. 556 (2003) 179.

162. S. Wilke, T. Zerihum, *J. Electroanal. Chem*. 515 (2001) 52

163. *Liquid Interfacial in Chemical, Biological, and Pharmaceutical Applications* Ed. by A.G. Volkov, Marcel Dekker, Inc. 2001.

164. Y. Marcus, *Ion Solvation*, John Wiley & Sons Ltd., 1985.

165. F. Marken, M.I. Gerrard, I.M. Mellor, R.J. Mortimer, C.E. Madden, S. Fletcher, K. Holt, J.S. Ford, R.H. Dahm, F. Page, *Electrochem. Commun*. 3 (2001) 177.

166. K.J. McKenzie, J. Niedziolka, C.A. Paddon, F. Marken, E. Rozniecka, M. Opallo, *Analyst*, 129 (2004) 1181.

167. P. Zanello, *Inorganic Electrochemistry*, RSC, London, 2003.

168. J.R. Pladziewicz, J.H. Espenson, *J. Am. Soc*. 95 (1973) 56.

169. W.R. Fawcett, M. Opallo, *Angew. Chem. Int. Ed. Engl*. 33 (1994) 2131.

170. P.W. Atkins, *Chemia Fizyczna*, PWN, 2001.

171. N.M. Alpatova, E.V. Ovsyannikova, *Electrochim. Acta* 36 (1991) 435.

172. T. Kuwana, W.G. French, *Anal. Chem*. 36 (1964) 241.

173. G. Shul, K.J. McKenzie, J. Niedziolka, E. Rozniecka, B. Palys, F. Marken, C.M. Hayman, B.R. Buckley, P.C. Bulman Page, M. Opallo, *J. Electroanal. Chem.* 582 (2005) 202.

174. E. Szabo, J. Szabon, *Acta Chim. Acad. Sci. Hungar*. 48 (1966) 299.

175. *Poradnik Fizykochemiczny*. WNT, 1974.

176. C.P. Andrieux, P. Hapiot, J-M. Saveant, Chem. Rev. 90 (1990) 723.

177. J. Heinze, *Angew. Chem. Int. Ed. Engl*. 32 (1993) 1268.

The results presented in this PhD thesis are partially published in following papers:

1. *"Electroactive ceramic carbon electrode modified with hydrophobic polar solvent"* G. Shul, M. Saczek-Maj, M. Opallo, *Electroanalysis*, 16 (2004) 1254-1261.

2. *"Ceramic carbon electrode modified with redox probe and salt solution in hydrophobic polar solvent"* G. Shul, M. Opallo, *Polish J. Chem.* 78 (2004) 1449-1456.

3. *"Liquid / liquid ion-transfer processes at the dioctylphosphoric acid (N,N-didodecyl-N',N'-diethylphenylenediamine) / water (electrolyte) interface at graphite and mesoporous TiO₂ substrates"* S.J. Stott, K.J. McKenzie, R.J. Mortimer, C.M. Hayman, B.R. Buckley, P.C. Bulman Page, F. Marken, G. Shul, M. Opallo, *Anal. Chem.* 76 (2004) 5364-5369.

4. *"Characterisation of biphasic electrodes based on the liquid N,N-didodecyl-N',N'-diethylphenylenediamine redox system immobilised on porous hydrophobic silicates and immersed in aqueous media"* G. Shul, K.J. McKenzie, J. Niedziolka, E. Rozniecka, B. Palys, F. Marken, C.M. Hayman, B.R. Buckley, P.C. Bulman Page, M. Opallo, *J. Electroanal. Chem.* 582 (2005) 202-208.

5. *"Ion transfer across liquid / liquid interface coupled to electrochemical redox reaction at carbon paste electrode"* G. Shul, M. Opallo, *Electrochem. Commun.* 7 (2005) 194-198.

6. *"Liquid / liquid interfacial processes at hydrophobic silica carbon composite electrodes: ion transfer at water / nitrobenzene, water / o-nitrophenyloctylether, and at water / o-nitrophenylphenylether interfaces"* G. Shul, M. Opallo, F. Marken, *Electrochim. Acta*, 50 (2005) 2315-2322.

7. *"Electroactive ceramic carbon electrode modified with ionic liquid"* E. Rozniecka, G. Shul, J. Siriex-Plenet, L. Gaillon, M. Opallo, *Electrochem. Commun.* 7 (2005) 299-304.

8. *"Effects of carbon nanofiber composites on electrode processes involving liquid/ liquid ion transfer"* G. Shul, M.A. Murphy, G.D. Wilcox, F. Marken, M. Opallo, *J. Solid State Electrochem.* 9 (2005) 874-881.

134